Automated Off-Line Cardiorespiratory Event Detection and Validation

Ahmed Aoude
110137216

Master of Engineering

Department of Biomedical Engineering

McGill University

Montreal,Quebec

January 2007

A thesis submitted to McGill University
in partial fulfillment of the requirements of the degree
of Master of Biomedical Engineering

Your file Votre référence
ISBN: 978-0-494-32577-3
Our file Notre référence
ISBN: 978-0-494-32577-3

ACKNOWLEDGEMENTS

With gratitude I wish to thank my supervisors Dr. Robert E. Kearney and Dr. Henrietta L. Galiana, as well as Dr. Karen A. Brown and Dr. Alexis L. Motto. I would like to thank Dr. Kearney and Dr. Galiana who encouraged and guided this work to its completion; Dr. Brown for her help in introducing me to the hospital environment, her guidance and her patience in spending many hours scoring data essential for this thesis; Dr. Motto for his help and mentoring which allowed me to understand all the relevant concepts of the project; without his help and patience this thesis would not have been possible. I would also like to thank all my colleagues in the REKLAB and Dr. Ross Wagner for their great attitude and help which made my time at McGill very pleasant. Many thanks also go to the families who have volunteered themselves for the study of apnea. This work was supported by a grant from the Natural Sciences and Engineering Research Council of Canada.

ABSTRACT

Sleep apnea is a condition where breathing unexpectedly stops during sleep. This condition is a common medical problem affecting infants that can result in serious complications if left untreated. Anesthesia can increase episodes of post-operative sleep apnea in infants. Therefore, the monitoring of infants after surgery is of utmost importance. The standard for diagnosing apnea events remains the visual scoring of cardiorespiratory data by trained personnel. This process is time consuming and prone to human error. In this thesis, we present automated off-line algorithms for the detection of pauses, asynchrony and movement artifact in cardiorespiratory data. These algorithms were implemented in a new tool intended to replace the visual scoring process. The automated algorithms' effectiveness relative to visual scoring is presented. This comparison was achieved using a new visual scoring tool. Results presented in this thesis demonstrate that the developed methods are comparable to visual scoring, work with uncalibrated respiratory signals and provide quick, reliable and standardized analysis.

ABRÉGÉ

L'apnée du sommeil est un problème médical commun pour les enfants qui peut avoir de sérieuses conséquences si non traîté. L' anesthésie peut accroitre le risque d'apnée du sommeil chez les enfants. Donc, il est très important de surveiller les enfants après une chirurgie. Le standard de diagnostique de ces évènements reste l'analyse visuelle des enregistrements cardiorespiratoires effectuée par un personnel qualifié. Ce processus est sous le joug de l'erreur humaine et prend beaucoup de temps. Dans ce rapport, on présente des algorithmes automatiques pour la détection d'évènements cardiorespiratoires. Ces algorithmes sont appliqués dans un nouveau outil prévu pour remplacer l'analyse visuelle. L'efficacité des algorithmes par rapport à l'analyse visuelle est présentée. Cette comparaison est accomplie avec l'aide d'un nouvel outil dévellopé pour l'analyse visuelle. Les résultats présentés dans ce rapport démontrent que les algorithmes sont comparables à l'analyse visuelle, et fournissent une analyse rapide, fiable et standardisée.

CONTRIBUTIONS OF AUTHORS

The work in the manuscript presented in this thesis (chapter 5) is largely my own. Dr. Kearney, Dr. Galiana, Dr. Brown and Dr. Motto provided me with suggestions and substantial feedback that led to the completion of the work. Dr. Brown provided the clinical expertise in visually scoring all patient data presented in the manuscript. Dr. Motto helped in the algorithm conception. I wrote the manuscript, I implemented the algorithm and I conducted the analysis for the validation of the methods.

LIST OF SYMBOLS

τ^{rc} Threshold for on-line pause detection in the ribcage RIP signal.

τ^{ab} Threshold for on-line pause detection in the abdominal RIP signal.

τ_1 Threshold for on-line movement artifact detection.

τ_2 Threshold for on-line asynchrony detection.

E_1^{rc} Test statistic used for on-line pause detection in the ribcage RIP signal.

E_1^{ab} Test statistic used for on-line pause detection in the abdominal RIP signal.

M^{rc} Test statistic used for on-line movement artifact detection in the ribcage RIP signal.

M^{ab} Test statistic used for on-line movement artifact detection in the abdominal RIP signal.

ϕ_i Test statistic used for on-line asynchrony detection.

$\delta(P)$ Logic signal for on-line pause detection (set to 1 if pause is detected and 0 otherwise).

$\delta(\phi_i)$ Logic signal for on-line asynchrony detection (set to 1 if asynchrony is detected and 0 otherwise).

$\delta(M)$ Logic signal for on-line movement artifact detection (set to 1 if movement is detected and 0 otherwise).

$\mathcal{H}_0^P$ Hypothesis, pause absent (on-line algorithm).

$\mathcal{H}_1^P$ Hypothesis, pause present (on-line algorithm).

$\mathcal{H}_0^M$ Hypothesis, movement artifact absent (on-line algorithm).

$\mathcal{H}_1^M$ Hypothesis, movement artifact present (on-line algorithm).

$\mathcal{H}_0^A$ Hypothesis, asynchrony absent (on-line algorithm).

$\mathcal{H}_1^A$ Hypothesis, asynchrony present (on-line algorithm).

γ^{rc} Threshold for off-line movement artifact detection in the ribcage RIP signal.

γ^{ab} Threshold for off-line movement artifact detection in the abdominal RIP signal.

γ_1^{rc} Threshold for off-line pause detection in the ribcage RIP signal.

γ_1^{ab} Threshold for off-line pause detection in the abdominal RIP signal.

γ_2 Threshold for off-line asynchrony detection.

E_3^{rc} Test statistic used for off-line pause detection in the ribcage RIP signal.

E_3^{ab} Test statistic used for off-line pause detection in the abdominal RIP signal.

T^{rc} Test statistic used for off-line movement artifact detection in the ribcage RIP signal.

T^{ab} Test statistic used for off-line movement artifact detection in the abdominal RIP signal.

ϕ_I Test statistic used for off-line asynchrony detection.

P Logic signal for off-line pause detection (set to 1 if pause is detected and 0 otherwise).

$\delta(\phi_I)$ Logic signal for off-line asynchrony detection (set to 1 if asynchrony is detected and 0 otherwise).

$\delta(T)$ Logic signal for off-line movement artifact detection (set to 1 if movement is detected and 0 otherwise).

$\mathcal{H}_0^p$ Hypothesis, pause absent (off-line algorithm).

$\mathcal{H}_1^p$ Hypothesis, pause present (off-line algorithm).

$\mathcal{H}_0^m$ Hypothesis, movement artifact absent (off-line algorithm).

$\mathcal{H}_1^m$ Hypothesis, movement artifact present (off-line algorithm).

$\mathcal{H}_0^a$ Hypothesis, asynchrony absent (off-line algorithm).

$\mathcal{H}_1^a$ Hypothesis, asynchrony present (off-line algorithm).

$\mathcal{H}_0^{oa}$ Hypothesis, obstructive apnea absent.

$\mathcal{H}_1^{oa}$ Hypothesis, obstructive apnea present.

TABLE OF CONTENTS

LIST OF TABLES

LIST OF FIGURES

CHAPTER 1
Introduction

First described in 1965, sleep apnea is a condition in which there is an interruption or complete cessation of breathing during sleep. In fact, apnea is a Greek word literally meaning 'without breathing'. Apnea is classified into three categories depending on whether respiratory movement is present or not. If no respiratory movement is present, then the episode is classified as central apnea; if respiratory movement is present with obstruction of the airway the episode is classified as obstructive apnea; and if a combination of both central and obstructive apnea is observed, the episode is termed mixed apnea. Irrespective of the difference in the root cause of each, in all three, a cessation of functional breathing is observed. Apnea can be life threatening and affects adults, children and infants alike. To diagnose and treat apnea-related disorders, it is important to distinguish among the three types of apnea.

Polysomnography (PSG) is normally used to diagnose, assess and monitor apnea-related disorders [10,11]. PSG is the simultaneous recording of brain activity, eye movement, blood oxygen levels, respiration, and muscle activity [12]; these variables are recorded via electroencephalogram (EEG), electrooculogram (EOG), electrocardiogram (ECG), electromyogram (EMG), nasal airflow (NAF), abdomen and thoracic movement, and blood oxygen saturation. PSG monitoring requires continuous supervision of the patient by trained personnel because of the complexity of the recording. Thus, due to the numerous signals and equipment required in PSG monitoring, cardiorespiratory monitoring is more practical for use in the recovery room or at home [13]. Cardiorespiratory monitoring records a subset of the PSG signals (respiratory movement and pulse oximetry) and so requires fewer connections to the patient.

Cardiorespiratory monitoring is robust and allows for the determination of a patient's cardiorespiratory state by manual review of the data [14–16]. Although manual review of the data

classifies apnea events for diagnosis and treatment, it is time consuming and prone to human error. Consequently, the development of automated procedures for the detection of cardiorespiratory events would be advantageous.

Automated on-line methods for the detection of cardiorespiratory events were developed by A. L. Motto at McGill University in [5] and [6]. These on-line methods were modified for off-line use in this thesis. These methods detect the lack of breathing effort, asynchronous breathing and movement artifact in respiratory inductance plethysmography data. This thesis will present these new procedures and demonstrate their effectiveness when applied to real data acquired from infants post-operatively in the recovery room at the Montreal Children's Hospital (MCH).

To validate the methods, it was important to acquire precise visual coding of off-line infant data records. Thus, a graphical tool was developed to visually score data. A second graphical tool was also developed to run and present the automated off-line analysis. Both tools were developed to be user friendly for the clinician. A full description of these tools is presented in this thesis and its appendices.

This thesis is organized as follows: Chapter 2 presents some background information on respiratory physiology and apnea, as well as a summary of the automated on-line methods developed by A. L. Motto; Chapter 3 presents the graphical tools used for visual scoring and automated off-line cardiorespiratory event detection; Chapter 4 presents the automated off-line segmentation method and provides some results based on simulated and real infant data; Chapter 5 presents the overall method and the results obtained for the automated off-line detection of pause, asynchrony and movement artifact; Chapter 6 presents possible future work and some concluding remarks. The manuals for the graphical tools, a conference paper, and extended results can be found in the appendices.

CHAPTER 2
Background

According to the National Institutes of Health (NIH), sleep apnea, which is characterized by an unexpected absence of breathing during sleep, is a common and serious disorder affecting 12 million Americans. Moreover, other studies have shown that this disorder also affects between 1%-3% of children [17–20]. A better understanding of apnea would lead to advancements in the treatment and prevention of Obstructive Sleep Apnea Syndrome (OSAS), Sudden Infant Death Syndrome (SIDS), Postoperative Apnea (POA) and Apnea of Pre-maturity.

2.1 Physiology of Respiration

The primary function of the human respiratory system is continuous gas exchange, supplying oxygen (O_2) to the blood and removing carbon dioxide (CO_2). This process is efficient, reliable and essential for survival. Oxygen is acquired from the external environment via the respiratory tract, an airway that extends from the nasal cavity to the trachea, the bronchioles, and finally the alveoli as shown in Fig. 2–1. Gas exchange between the air and the blood is achieved by simple diffusion at the alveolar capillary interface; a thin gas-blood barrier between the alveolar space and the pulmonary capillaries allowing for rapid gas exchange (depicted in Fig. 2–2).

During breathing, the lungs expand and contract allowing air to enter and leave the lungs. This active process of inhalation and exhalation requires the contraction of skeletal muscles [3]. The primary respiratory muscles for inspiration are the diaphragm and the external intercostal muscles [3]. As shown in Fig. 2–3, the contraction of the diaphragm and the external intercostal muscles causes an increase in the dimension of the thoracic cavity which reduces the pressure in the lungs causing air to flow into the lungs [3]. Similarly, when the diaphragm and the external intercostal muscles relax, the ribs and sternum return to resting position resulting in increased lung pressure which causes air to flow out of the lungs [3].

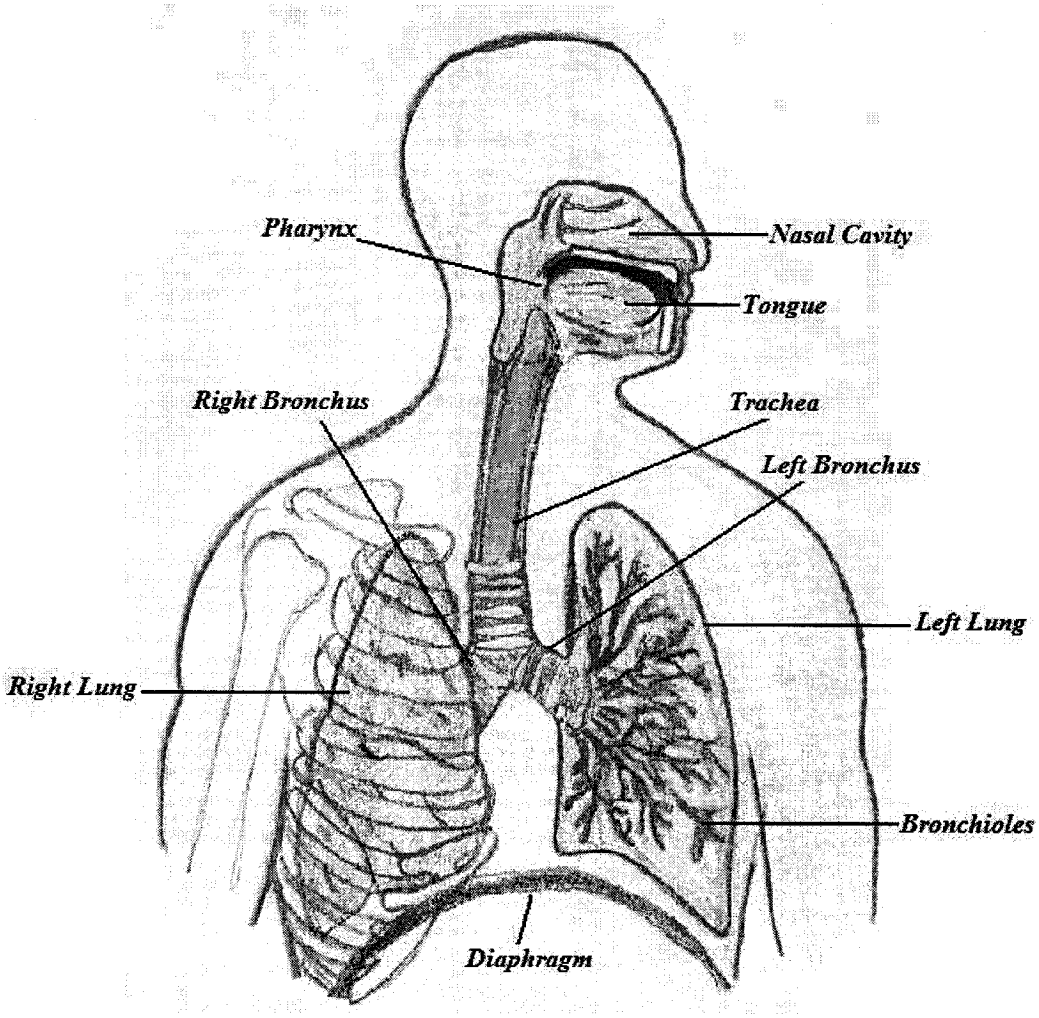

Figure 2–1: The human respiratory tract (Modified from [1]).

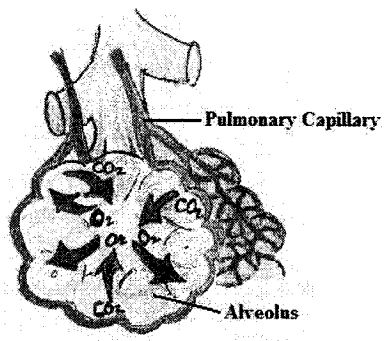

Figure 2–2: Gas exchange at the alveolar capillary interface (Modified from [2]).

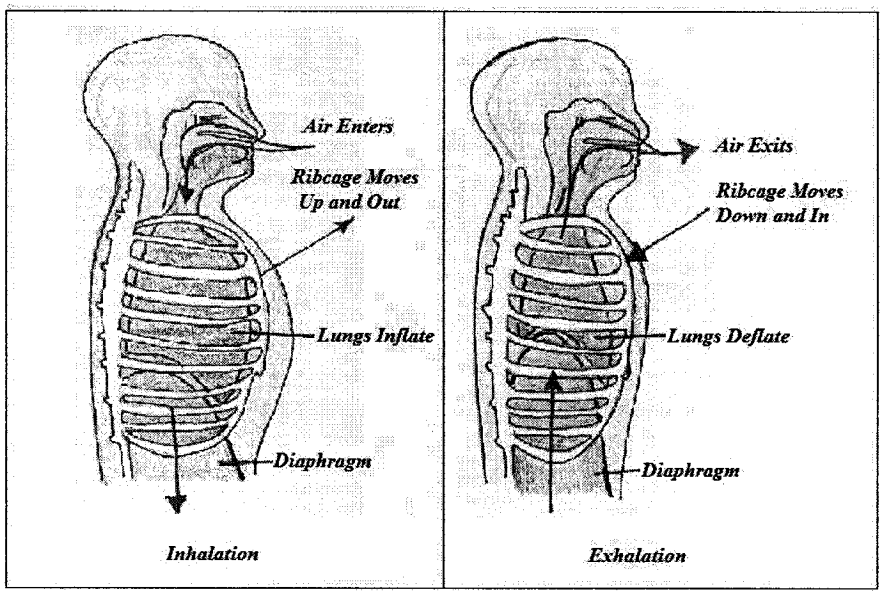

Figure 2–3: Breathing Mechanics (Modified from [3]).

Respiratory rate is important for adequate oxygen supply to the body. Respiratory rate is controlled automatically by the rhythmicity center of the medulla oblongata or voluntarily during consciousness [3]. Spontaneous breathing is generated by the firing of I and E neurons located in the lower part of the brain and in the neck [3]. I neurons excite respiratory muscles during inspiration while E neurons inhibit I neurons during expiration [3]. These neurons are stimulated by the apneustic and the pneumotaxic centers located in the pons (refer to Fig. 2–4). In addition, chemoreceptors located in the aorta, carotid arteries and medulla help regulate respiratory rates [3]. If blood CO_2 level increases or O_2 level decreases, these chemoreceptors stimulate the brain respiratory center to increase the respiratory rate and return O_2 and CO_2 levels back to normal [3]. This automatic process is most important during sleep when a subject is unconscious.

A better understanding of respiratory physiology is crucial for patient safety after surgery since anesthesia can compromise regular respiratory function [21]. In particular, infants have highly irregular breathing patterns during sleep which can be disrupted further after anesthesia [22, 23].

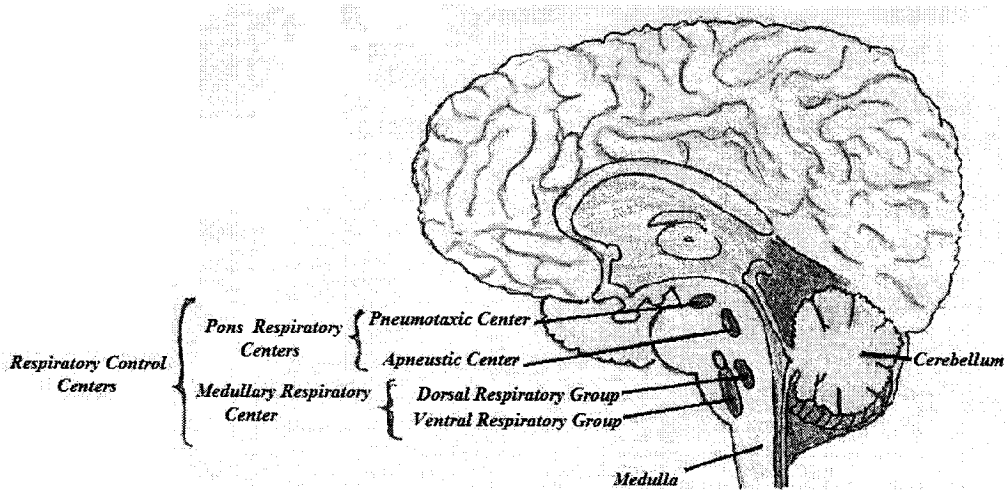

Figure 2–4: The respiratory control centers of the brain (Modified from [4]).

2.2 What is Apnea?

Apnea is a word with Greek etymology meaning temporary absence or cessation of breathing. This Greek word is a clinical term referring to a period of time when respiratory airflow unexpectedly stops. There are three types of apnea: central apnea, obstructive apnea and mixed apnea.

2.2.1 Central Sleep Apnea

Central sleep apnea (CSA) is characterized by an extended period of time with no thoracic or abdominal respiratory movements. The duration of the respiratory pause is used to define CSA. However, this duration is still controversial but is typically greater than 5 s long. Thus, respiratory movement signals can be used to detect CSA events by simply identifying periods when there is no respiratory abdominal and ribcage movement of adequate duration.

The lack of respiratory effort during CSA is due to a lack of respiratory muscle activity, caused by reduced communication between the respiratory centers of the brain and the respiratory muscles [24]. CSA occurs often in children and has been shown to increase with the use of anesthesia [22]. Thus, it is important to monitor children after surgery for the detection and prevention of CSA events.

2.2.2 Obstructive Sleep Apnea

Obstructive Sleep Apnea (OSA) is a disorder characterized by an extended period of upper airway obstruction during sleep. When an individual is awake, muscles keep the upper airway open, once asleep these muscles relax and the airway becomes narrower. During OSA, these muscles relax so much that complete or partial obstruction of the airway occurs, impeding airflow [25]. Some morbidities that can increase the risk of OSA are: neuromuscular disease, craniofacial abnormalities, Down's syndrome, and premature birth [19,26,27].

Research has shown that OSA causes growth delays in children, aggressiveness, poor school performance, hyperactivity, tiredness and neurocognitive deficits [26,28,29]. Therefore, the diagnosis, detection, and monitoring of OSA in children is extremely important.

One of the most common symptoms of OSA is snoring, and OSA is unlikely to be present without snoring. However, OSA cannot be adequately diagnosed based on snoring alone [30–34]. Moreover, adenotonsillar hypertrophy occurs most frequently between 4 and 8 years of age when the hypertrophy relative to the upper-airway is at peak size [12,28]. During this time, enlarged tonsils or adenoids can be a direct cause of OSA. Even so, research has shown that the size of tonsils and adenoids are not related to the presence or severity of OSA [35, 36]. Despite these results, adenotonsillectomy is the treatment of choice in children with OSA [37–40].

Many studies have linked asynchrony between the ribcage and abdomen to airway obstruction in infants [41–43]. Obstruction of the airway causes increased airway resistance and breathing effort, resulting in asynchronous abdominal and thoracic movements [44]. During complete airway obstruction the abdominal and ribcage movements are completely out of phase since lung volume is maintained. As a result, asynchrony between the ribcage and abdomen is commonly used to detect and assess OSA severity.

2.2.3 Postoperative Apnea

Infants that have had anesthesia during surgery are at increased risk of having apnea episodes. Some studies have shown than between 11% and 13% of infants 2 months of age or younger have noticeable apnea episodes after surgery [45,46]. Moreover, children with severe OSA and children younger than 3 years of age are at an increased risk of perioperative problems [26,47]. Therefore, it

is important to closely monitor postoperative children for apnea [48]. Episodes of apnea that occur in the postoperative period are termed postoperative apnea (POA). The pathophysiology of POA is still unknown.

2.3 Cardiorespiratory Monitoring

Cardiorespiratory monitoring is used at the MCH for the study of POA. The cardiorespiratory monitoring acquired at the MCH consists of four recordings: abdomen and thoracic movement from Respiratory Inductance Plethysmography (RIP), pulse oximetry, and finger plethysmography. This thesis will deal with algorithms that are applied to the acquired RIP signals. (Note that in this thesis, *manual review of the data* or *manual scoring* will be used interchangeably with the term *visual scoring*).

2.3.1 Respiratory Inductance Plethysmography (RIP)

Many different noninvasive respiratory monitors are currently used in medical care. These devices detect respiratory movement, gas volume exchange, and air flow. One technique used for respiratory monitoring is Respiratory Inductance Plethysmography (RIP). RIP was introduced in 1977 and detects thoracic and abdominal movement noninvasively. RIP is ideal for use in the recovery room or at home since it quantifies changes in thoracic and abdominal cross sectional area with the help of two noninvasive inductive bands placed around the infant's abdomen and ribcage with no connection at the patient's airway (refer to Fig. 2–5).

The inductive bands are composed of elastic bands containing Teflon-coated wires placed in a sinusoidal or zigzag pattern. These bands are connected to an oscillator that oscillates at approximately 300kHz with small amplitude (approximately 20mV). Changes in the band circumference from respiratory movement, changes the self inductance of the bands which is used to quantify cross sectional area changes of the abdomen and chest.

RIP quantifies changes in the cross sectional area of the abdomen and chest with the help an electromagnetic method proposed by Goldberg and Goldberg [49]. This method has been developed as inductance plethysmography. To understand how inductance plethysmography is useful for determining small variations in area such as during quiet breathing, Martinot-Lagarde *et al.* [50] considered the formulae for self-inductance of a coil of rectangular or circular shape without zigzag

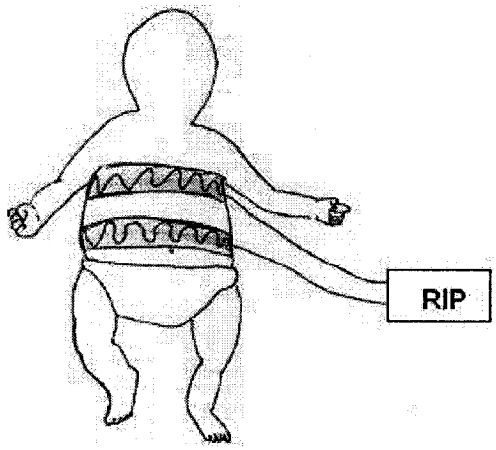

Figure 2–5: Illustration of RIP bands on a patient.

or wavy patterns. These shapes were considered since, as reported in [50], human cross sections are between ellipses and smoothed rectangles. Moreover, more complex shapes with zigzag patterns such as those used in RIP devices use the same concepts.

The self-inductance of a circular loop of radius R with a wire of radius r, is given by [50]:

$$L = \mu_0 R[\ln(8R/r) - 7/4] \;\; if \;\; R >> r \tag{2.1}$$

Where μ_0 is the permeability of the medium.

Equation (2.1) can be rewritten in terms of the area A ($A = \pi R^2$) as follows [50]:

$$L = \mu_0 \sqrt{A/\pi}[\ln(8\sqrt{A/\pi}/r) - 7/4] \tag{2.2}$$

Similarly, for a rectangular loop with sides of length a, width b and diagonal d, the self-inductance equation is given by [50]:

$$L = \mu_0/\pi[a\ln(2ab/r(a+d)) + b\ln(2ab/r(b+d)) + 2d - 7/4(a+b)] \tag{2.3}$$

Equation (2.3) can be rewritten in terms of the area A ($A = ab$) and the ratio $\rho = a/b$ as [50]:

$$\begin{aligned} L &= \mu_0/\pi\sqrt{A}[(\sqrt{\rho}+1/\sqrt{\rho})\ln(2\sqrt{A}/r) - \sqrt{\rho}\ln(\sqrt{\rho}+\sqrt{\rho+1/\rho}) \\ &\quad -1/\sqrt{\rho}\ln(1/\sqrt{\rho}+\sqrt{\rho+1/\rho}) + 2\sqrt{\rho+1/\rho} - 7/4(\sqrt{\rho}+1/\sqrt{\rho})] \end{aligned} \tag{2.4}$$

As seen in the equations above, it is possible to determine the area of given coil shape from its self-inductance. The relationship between area and self-inductance is almost linear with a shape-dependant sensitivity [50]. Thus, as noted by Goldberg and Goldberg [49] these methods only approximate the area changes. The simple rectangular and circular forms presented above can be extended for more complex shapes and coils such as those present in RIP bands.

2.3.2 RIP Feasibility for Respiratory Analysis

In [51], the accuracy of RIP for the analysis of respiratory waveforms was examined. RIP was compared to body plethysmography and pneumotachography. Measurements of respiratory movement obtained by RIP were comparable to both body plethysmography and pneumotachography; frequency responses were comparable for all three techniques. Thus, Carry *et al.* [51] concluded that RIP is accurate for analysis of respiratory waveforms. Moreover, Watson *et al.* [52] showed that RIP accurately reflects changes in cross sectional area and confirmed the baseline stability of RIP for physiological shapes. Therefore, it can be concluded that RIP performs well in situations where continuous noninvasive respiratory monitoring is required.

Since both obstructive apneas and central apneas occur during sleep in infants [53], the comfort of the infants being monitored is important. Folke *et al* [54] stated that a clinically relevant monitor must allow for natural movement and breathing through the nose and mouth. Since RIP is noninvasive and does not hinder infant movement or breathing, it has numerous potential applications for infants, including postoperative respiratory monitoring. In fact, RIP is the most widely accepted method for qualitative and quantitative respiratory measurements [50].

RIP is not only tolerable for the patient but also permits estimation of both respiratory rate and tidal volume. Many studies have examined the accuracy of RIP in lung volume estimation, for example in a newborn animal model [55]. The study showed a good correlation between lung volumes measured with RIP and injected gas volumes [55].

To accurately assess lung volume, RIP must be calibrated. Many different methods for calibration have been used, including the isovolume manoeuvre presented by Konno *et al.* [56] in 1967, the least squares method proposed by Chadha *et al.* [57] in 1982, and the Qualitative Diagnostic Calibration (QDC), introduced by Sackner *et al.* [58] in 1989. The choice of the calibration method depends on experimental and clinical conditions [59]. However, Brown *et al.* [60] showed that the QDC method used to estimate tidal volume in anaesthetized infants was inaccurate if measurement conditions or the pattern of breathing changed. Thus, it would be advantageous to use uncalibrated RIP signals since this would eliminate the need for calibration which has been shown to be inaccurate during real recordings.

RIP is commonly used in cardiorespiratory monitors. The current standard for diagnosis using cardiorespiratory monitoring is the manual scoring of records by trained personnel. However, manual scoring of numerous cardiorespiratory records is time consuming and costly. In addition, the possibility of human error is high and the results are subjective [61]. Reliable automated monitoring systems would require less time for analysis, and provide consistent and standardized analysis. Therefore, fully automated monitoring systems would be ideal but clinicians are still cautious about their use in a clinical environment.

2.4 Methods for automated Cardiorespiratory Monitoring

As reported in [62], RIP can be used to determine the phase relationship between the thoracic and abdomen signal and thus, can be used to distinguish between central and obstructive apnea. Therefore, RIP can be used for the detection of obstructive breathing episodes which have been associated with life-threatening events such as SIDS [53, 63, 64].

In [44], an automated method to determine thoracoabdominal asynchrony was used to examine obstructive apnea episodes in ten full-term infants. Results showed that 79.3% of obstructive apnea events had thoracoabdominal asynchrony while only 10.9% of the events scored as obstructive apneas were true obstructive apneas [44]. De Groote *et al.* [44] determined thoracoabdominal asynchrony using a 'mirror index' method. The 'mirror index' was calculated for each respiratory period; a respiratory period was defined as the data between two successive maxima or minima. A

normalized sum (S) of the thorax and abdominal signals was calculated as follows,

$$S = \frac{ab + rc}{AB + RC} \tag{2.5}$$

where ab and rc are the abdominal and ribcage RIP signals respectively, and where AB and RC are the maximum amplitude of each RIP signal in a respiratory period.

Next, the area under the sum curve was determined. This area is large when the two signals are in phase and small when the two signals are out of phase (asynchronous). Finally, a 'mirror index' between 1 and 0 was obtained by dividing the area by the length of the respiratory period. Phase opposition, or obstructive apnea events were defined by a 'mirror index' below a threshold of 0.15 reflecting significant increase in asynchrony during the apnea [44]. Although the method is robust, many false alarms were observed perhaps because De Groote *et al.* [44] did not eliminate movement artifact or noisy signals from the phase analysis. De Groote *et al.* [44] also obtained similar results using an artificial neural network method.

Many other automated methods for detecting apnea have been presented in the literature. Including: hidden Markov models [65], artificial neural networks [44,66], recursive least squares [7], fuzzy logic systems [67] , and many other techniques [?,68–70]. These automated, off-line techniques function well under controlled circumstances but generate large numbers of false alarms when applied to clinical data where movement artifact is present. Thus, alternative automated techniques are needed to overcome these flaws.

2.5 On-Line Automated Cardiorespiratory Event Detection Developed at McGill University

As previously mentioned many methods have been developed to allow for automated cardiorespiratory event detection. Some of these new methods have been developed by Motto *et al.* at McGill University to directly detect pauses, asynchrony, and movement artifact. These on-line methods form the basis from which the automated off-line methods presented in thesis were developed. Pauses and asynchronies are detected since central and obstructive apnea events are characterized by these signal attributes. Moreover, movement artifact is detected to improve the performance of the detectors as described in the following sections.

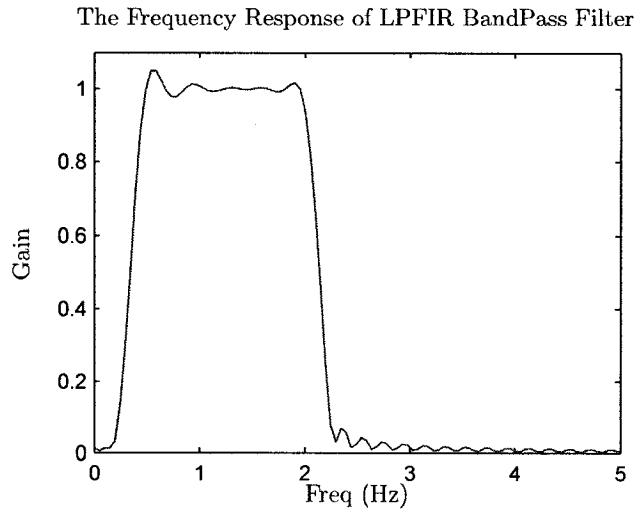

Figure 2–6: The magnitude frequency response of the LPFIR bandpass filter used to increase the signal-to-noise ratio of the RIP signals.

2.5.1 On-Line Pause Detection Algorithm

Motto *et al.* developed a pause detection algorithm to detect periods without respiratory movement in uncalibrated RIP data. The presence of a pause (a constant 'flat' period) in both RIP signals indicates that the abdomen and ribcage areas were constant for a period in time. Thus, a pause in both RIP signals indicates a lack of breathing effort which is associated with central apnea. The algorithm used to detect pauses is described next.

In the first step of the pause detection algorithm, a linear-phase, finite-duration, impulse response (LPFIR) band-pass filter is used to increase the signal-to-noise ratio of the thoracic and abdominal signals. This filter was designed by Motto *et al.* [5] on the basis of the Fourier analysis of quiet breathing segments in 22 infants, previously reported by Brown *et al.* [7]. This analysis showed that for frequencies outside [0.4, 2.0] Hz the power-spectral densities of quiet breathing were small. This led to the hypothesis that thoracoabdominal movement signals during quiet breathing are bandpass signals within [0.4, 2.0] Hz. The LPFIR band-pass filter frequency response is shown in Fig. 2–6 [5].

Next, the root mean square (RMS) of the filtered RIP signals over a window of length N_1 centered at each sample n is computed as:

$$E_1^{ab}[n, N_1] = \sqrt{\frac{1}{N_1} \sum_{k=n-N_1/2+1}^{n+N_1/2} ab_f^2[k]} \tag{2.6a}$$

$$E_1^{rc}[n, N_1] = \sqrt{\frac{1}{N_1} \sum_{k=n-N_1/2+1}^{n+N_1/2} rc_f^2[k]} \tag{2.6b}$$

where, ab_f and rc_f are the bandpass-filtered abdominal and ribcage signals respectively.

The outputs of the energy functions ($E_1^{ab}[n, N_1]$ and $E_1^{rc}[n, N_1]$) are then compared to a threshold value τ to determine if a pause is present for each RIP signal. These comparators are defined by:

$$\bar{p}_{ab}[n] = \begin{cases} 1 & if E_1^{ab}[n, N_1] \geq \tau^{ab} \\ 0 & if E_1^{ab}[n, N_1] < \tau^{ab} \end{cases} \tag{2.7}$$

$$\bar{p}_{rc}[n] = \begin{cases} 1 & if E_1^{rc}[n, N_1] \geq \tau^{rc} \\ 0 & if E_1^{rc}[n, N_1] < \tau^{rc} \end{cases} \tag{2.8}$$

The values $\bar{p}_{ab}[n]$ and $\bar{p}_{rc}[n]$ are the abdominal and ribcage decision flags that indicate wether or not a pause is present in each RIP signal.

To determine if a pause is present in both the ribcage and abdomen signals, the outputs of the comparators ($\bar{p}_{ab}[n]$ and $\bar{p}_{rc}[n]$) are fed to a NOR-gate. The output of the NOR-gate ($\delta(P[n])$) is 1 if both the abdominal and ribcage signals have pauses and 0 otherwise.

$$\delta(P[n]) = \begin{cases} 1 & \text{, if } \bar{p}_{ab}[n] = 0 \text{ and } \bar{p}_{rc}[n] = 0 \\ 0 & \text{, otherwise} \end{cases} \tag{2.9}$$

Thus, $\delta(P[n])$ reflects the following hypotheses:

$$\begin{gathered} \mathcal{H}_0^P\text{: Pause absent } (\delta(P[n]) = 0) \\ \text{vs.} \\ \mathcal{H}_1^P\text{: Pause present } (\delta(P[n]) = 1) \end{gathered} \tag{2.10}$$

2.5.2 On-Line Movement Artifact Detection Algorithm

Movement artifact is common in infant RIP data. This artifact arises when an infant moves or is being moved. It is assumed that apnea episodes are very unlikely during movement. In fact, it is routine for a nurse to move an infant during an apnea episode to stop it. Thus, the ability to automatically detect movement artifact in RIP is advantageous since movement artifact segments could be rejected for automated apnea detection analysis, thereby reducing the rate of false apnea detection.

An on-line segmentation algorithm was developed to segment cardiorespiratory data into regions with and without movement artifact [6]. This method uses linear filters, an energy function, and a comparator to determine if an artifact is present. Since it was determined that movement artifacts had high energy and were predominantly of low bandwidth ([0, 0.4]Hz), the test statistic used to detect artifact is defined as the energy ratio:

$$M^{ab}[n, N_2] = \frac{E_1^{ab}[n, N_2]}{E^{ab}[n, N_2]} \tag{2.11a}$$

$$M^{rc}[n, N_2] = \frac{E_1^{rc}[n, N_2]}{E^{rc}[n, N_2]} \tag{2.11b}$$

where, E_1^{ab} and E_1^{rc} are defined as in equation (2.6), and where E^{ab} and E^{rc} are defined as:

$$E^{ab}[n, N_2] = \sqrt{\frac{1}{N_2} \sum_{k=n-N_2/2+1}^{n+N_2/2} ab^2[k]} \tag{2.12a}$$

$$E^{rc}[n, N_2] = \sqrt{\frac{1}{N_2} \sum_{k=n-N_2/2+1}^{n+N_2/2} rc^2[k]} \tag{2.12b}$$

where, ab and rc are the raw abdominal and ribcage signals respectively, and N_2 is the window length. The energy values E_1^{ab} and E_1^{rc} are the RMS values of the bandpass filtered ([0.4, 2]Hz) RIP signals, while E^{ab} and E^{rc} are the RMS values of the raw RIP signals.

These ratios are compared to a threshold (τ_1) to determine if an artifact is present. The comparator used is defined by:

$$\delta(M[n]) = \begin{cases} 1 & \text{if } M^{ab}[n, N_2] < \tau_1 \text{ and } M^{rc}[n, N_2] < \tau_1 \\ 0 & \text{otherwise} \end{cases} \tag{2.13}$$

Thus, $\delta(M[n]) = 1$ if both the RIP signals have most of their energy at lower frequencies, indicating that movement artifact is present. Conversely, $\delta(M[n]) = 0$ if at least one of the RIP signals has most of its energy at frequencies in the expected breathing range, indicating movement artifact is absent. Thus, $\delta(T[n])$ reflects the following hypotheses:

$$\begin{gathered} \mathcal{H}_0^M\text{: Movement artifact absent } (\delta(M[n]) = 0) \\ \text{vs.} \\ \mathcal{H}_1^M\text{: Movement artifact present } (\delta(M[n]) = 1) \end{gathered} \tag{2.14}$$

2.5.3 On-Line Phase Estimation Algorithm

The ability to automatically detect asynchronous breathing in RIP data is important since asynchrony between thoracic and abdominal movement is associated with obstructive apnea. Thus, Motto *et al.* [5] developed an automated algorithm to estimate the phase between thoracic and abdominal RIP signals. The algorithm uses linear filters, binary converters, and an XOR-gate as depicted in Fig. 2–7. The algorithm works as follows:

Step 1: The LPFIR band-pass filter described in section 2.5.1 is used to increase the signal-to-noise ratio of the thoracic and abdominal signals without distorting their phase relationship.

Step 2: The filtered signals are passed through a binary converter rendering the abdominal and ribcage signals amplitude independent. The binary conversion is done as follows for both the ribcage and abdomen signals [5]:

$$\tilde{s}[n] = \begin{cases} 1 & if \hat{s}[n] \geq 0 \\ 0 & if \hat{s}[n] < 0 \end{cases} \tag{2.15}$$

This conversion allows the method to use uncalibrated RIP signals.

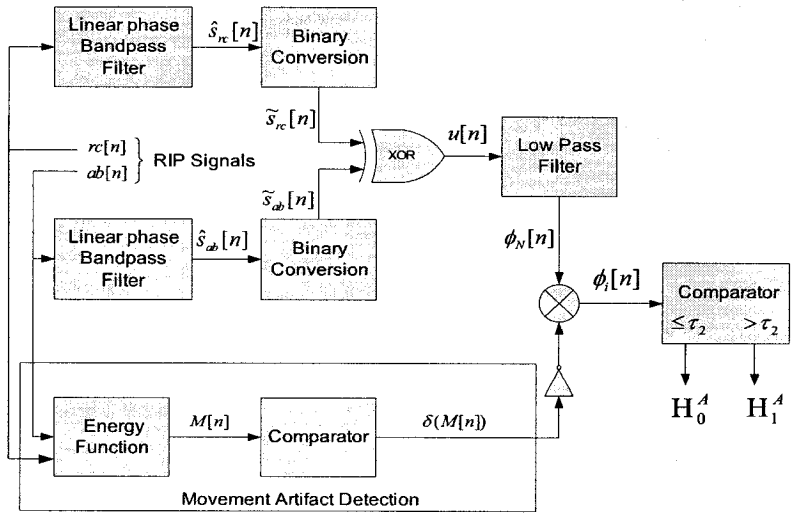

Figure 2–7: Block diagram of phase estimation algorithm as described in [5] and the movement artifact detection described in [6]. The improved phase estimate ϕ_i is used to choose the hypotheses $\mathcal{H}_0^A$ (asynchrony absent) or $\mathcal{H}_1^A$ (asynchrony present) [6].

Step 3: The binary outputs ($\tilde{s}[n]$) for the ribcage and abdomen signals are fed into an XOR-gate which outputs $u[n] = 1$ when the signals are different and $u[n] = 0$ when the signals are the same. The XOR output is then used to determine the phase between the two signals. Assuming that the signals have a constant phase difference over a given window, the phase can be estimated by the amount of time the signals are different over the window length. Since the phase and frequency of spontaneous breathing are in general time-varying, the phase between the thoracoabdominal signals can only be estimated. This estimate of the phase is given by [5]:

$$\hat{\phi} = \frac{\tilde{\tau}}{\tilde{T}} \tag{2.16}$$

where $\tilde{\tau}$ is the amount of time the signals are different ($u[n] = 1$) and $\tilde{T}$ is the time period. The choice of time period $\tilde{T}$ must satisfy: $\tilde{T} >> 1/0.4 = 2.5$ seconds, since as previously mentioned, the respiration of infants was found to be in the range of [0.4, 2.0] Hz. Therefore, 2.5 seconds was chosen since it is the largest expected respiration period. The ratio in equation (2.16), which estimates the phase, is computed by low-pass filtering the output of the XOR-gate over a window of length N (the number of samples in $\tilde{T}$). This is equivalent to taking the average amount of time (samples)

the output of the XOR-gate is 1 over a window of length N. The result is a value between 1 and 0 representing an estimate of the phase, where 1 is π radians out of phase and 0 means in phase. The phase difference is given by [5]:

$$\phi_N[n] = \pi\phi[n] \tag{2.17}$$

This phase estimate is then improved following Motto *et al.* in [6] by using the movement artifact detector described in section 2.5.2. The majority of apnea misclassifications were due to movement artifact [6], so the ability to detect them will improve the performance of phase estimation algorithms used for apnea detection.

Step 4: The phase estimate ϕ_N is improved by multiplying it with $\delta(M[n])$ as [6]

$$\phi_i[n] = \phi_N[n](1 - \delta(M[n])) \tag{2.18}$$

Remember that $\delta(M[n]) = 1$ if movement artifact is present and $\delta(M[n]) = 0$ if movement artifact is absent. The product sets the phase estimate to zero if movement artifact is detected. Thus, using ϕ_i to estimate the degree of asynchrony between the RIP signals avoids problems with movement artifact.

Step 5: In the final step, a comparator chooses between the hypotheses asynchrony present ($\mathcal{H}_1^A$) or asynchrony absent ($\mathcal{H}_0^A$). This is done by comparing the phase estimate ϕ_i to a threshold value (τ_2); if the phase is smaller or equal to the threshold, the signals are labeled as in phase ($\mathcal{H}_0^A$), and if the phase is larger than the threshold, the signals are labeled as asynchronous ($\mathcal{H}_1^A$). This can be written as

$$\text{If } \phi_i[n] \leq \tau_2 \Longrightarrow \mathcal{H}_0^A$$
$$\text{If } \phi_i[n] > \tau_2 \Longrightarrow \mathcal{H}_1^A$$

The comparator step is very important, since in clinical terms, the threshold value τ_2 determines whether asynchrony is present or not, and in turn, determine if obstructive apnea is present.

The method developed by Motto *et al.* [5] is more advantageous than other methods such as [7], [?] and [71] since it is easily implemented, works with *uncalibrated* RIP signals, does not require breath detection, and provides *quantitative* phase estimates.

2.6 Thesis Objectives

Visual scoring of cardiorespiratory data is time consuming, costly, and susceptible to human error [61]. Despite these drawbacks, visual scoring is the method of choice for the evaluation of a patient's cardiorespiratory state. Moreover, visual scoring is necessary for the evaluation of the automated procedures that are intended to replace it. The development of reliable automated methods to replace visual scoring for cardiorespiratory event detection would permit for rapid, standardized and repeatable analysis. These methods would permit the analysis of a large number of files, and so lead to a better understanding of the pathophysiology of respiratory events such as postoperative apnea.

The first objective of this thesis was to develop reliable off-line methods for cardiorespiratory event detection to replace the visual scoring process. Thus, the on-line algorithms used for pause, asynchrony and movement artifact detection were modified and improved for off-line use. Off-line detection can be expected to provide better detection performance than on-line detection since the methods are not limited to real time algorithms. The new off-line methods are intended to be integrated into the off-line option of the cardiorespiratory monitor reported in [72].

To assess the off-line methods' performance relative to visual scoring, it was necessary to acquire precise visual scoring data. The visual scoring previously obtained at the Montreal Children's Hospital only stored the epoch (10s segment) at which an event was identified. This was inadequate since the exact start/end time of each event was not stored. Improved precision was necessary to correctly compare the automated method results to the visually scored equivalent. Thus, the second objective of this thesis was to develop a tool to allow for precise visual scoring of cardiorespiratory data. The tool was used on data acquired in the recovery room of the Montreal Children's Hospital and permits for exact start and end time storage.

The third objective of this thesis was to compare the effectiveness of the off-line methods relative to visual scoring with the visual scoring tool developed as part of this thesis.

The final objective of this thesis was to develop a fully automated tool capable of analyzing and presenting the off-line cardiorespiratory event detection.

CHAPTER 3
Tools for Visual Scoring and Automated Scoring of Cardiorespiratory Events

The following steps were required to complete the thesis objectives:

1. Develop automated off-line algorithms for cardiorespiratory event detection
2. Develop a new visual scoring tool to obtain precise visual scoring of the infant database acquired at the MCH
3. Compare the off-line algorithms performance relative to visual scoring
4. Develop a tool to display and automatically analyze cardiorespiratory data using the new automated off-line algorithms

This chapter will present the two tools used for off-line cardiorespiratory visual scoring and automated off-line cardiorespiratory event detection; that is the tools used to attain points 2 and 4 above. A description of the new automated off-line algorithms (point 1) and their effectiveness relative to visual scoring (point 3) is presented in chapter 4, chapter 5, and Appendix D.

3.1 Off-line Cardiorespiratory Visual Scoring

Visual scoring is the annotation of off-line cardiorespiratory data by trained personnel to identify cardiorespiratory events and respiratory problems for diagnosis and treatment. The automated methods presented in this thesis were developed to automate the visual scoring process. These methods are validated in comparison to visual scoring in chapter 5 and Appendix D, since there is no consensus on the definitions of the cardiorespiratory events being detected [73, 74]. The precise visual scoring of data files was a prerequisite to assess the methods' effectiveness.

Visual scoring is normally performed at the MCH by analyzing data records in 10s segments (epochs). Each epoch is examined visually by a trained scorer and categorized as to its cardiorespiratory event. Each visually scored event is stored with the epoch where it occurred, the exact start and end times of events are not stored. This lack of precision motivated the development of a new

tool to acquire precise visual scoring. This new tool is named *ApneaScore* and can be used on any PC-compatible computer with a basic Matlab 7.0 (The Mathworks, Inc, Natick, MA) installation. The *ApneaScore* tool was developed using Matlab's GUIDE (Graphical User Interface Development Environment) and provides an interactive graphical user interface (GUI).

3.1.1 The ApneaScore Graphical User Interface

The *ApneaScore* application was designed to be a simple, user-friendly tool for the visual identification of events. Fig. 3–1 shows the overall structure of the *ApneaScore* tool, as presented to the user through the interface. The tool supports analysis of off-line cardiorespiratory data stored in the Labdat format (RHT-InfoDat, Montreal) used at the MCH. Visual scoring of events is performed in the main window of the application (Figure 3–2). This window permits:

1. The display of the cardiorespiratory data
2. The selection and classification of the events
3. Data Storage

Cardiorespiratory data displayed in the main window includes: ribcage, abdominal, finger plethysmography and oxygen saturation signals. These data are presented to the scorer in 30s epochs. The tool permits the user to store the type and exact timing of an event with three mouse clicks. To score an event, the user positions two cursors on the data to select the event start and end times respectively. All data in the selected time interval are then highlighted, allowing the scorer to visualize the selection. If satisfied with the selection, the user then clicks the appropriate event button in the main window. The exact timing and type of the event is then stored. For more information refer to Appendix A.

The visually scored data is stored in a Matlab file (*.mat format) by default but can also be saved as an excel file (*.xls format). Data storage and the cardiorespiratory events considered in the tool are discussed next.

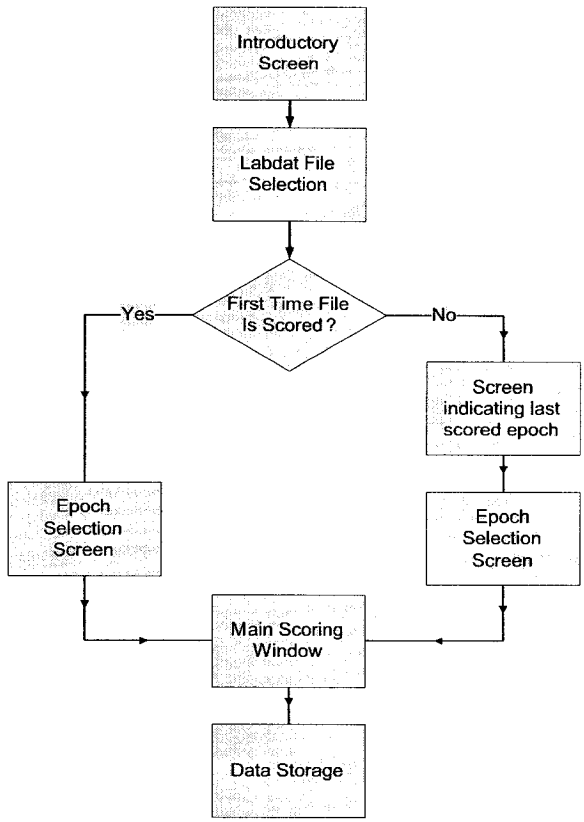

Figure 3–1: Overall structure for the *ApneaScore* GUI. The application notifies the user of the last epoch that was scored if the user had previously started scoring the data record. The user can then select the epoch at which to start visual scoring and start the analysis in the main window.

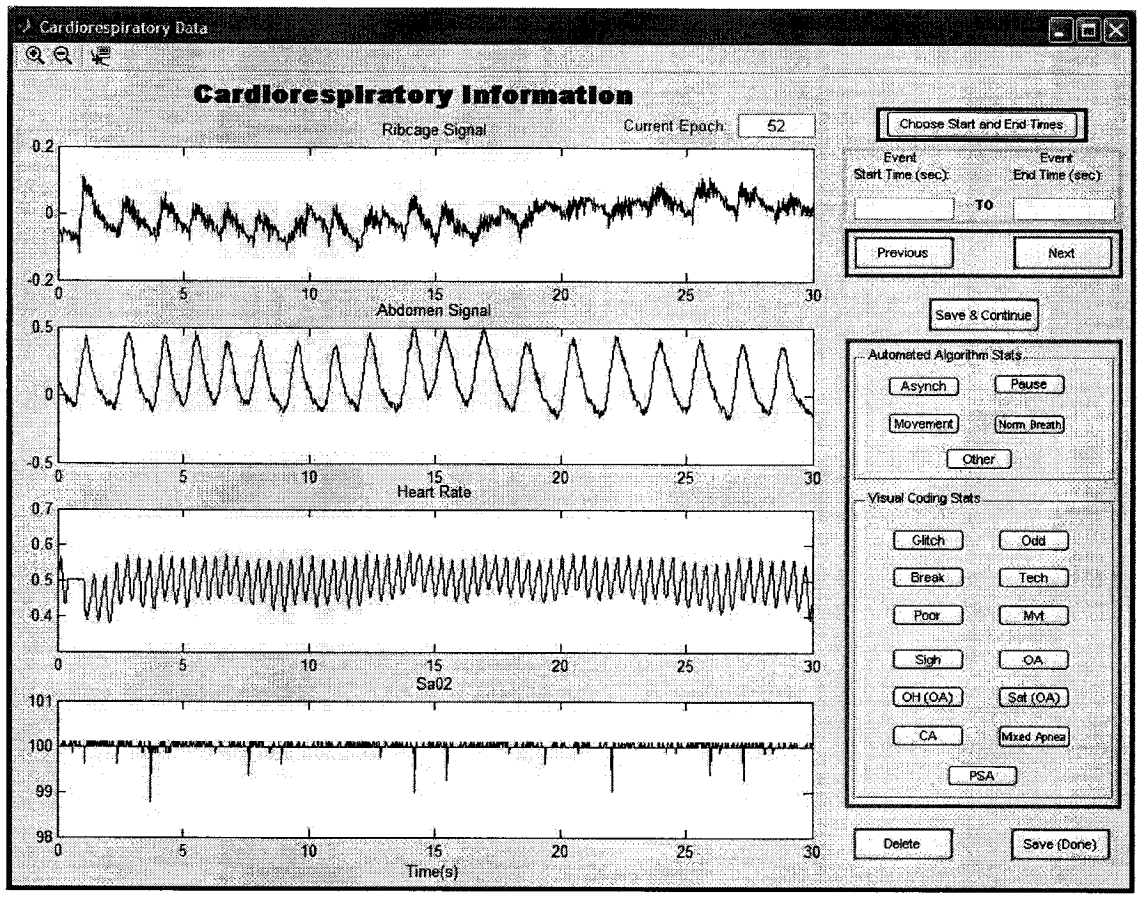

Figure 3–2: Main window for *ApneaScore* visual scoring tool. The user can scroll through the data, identify events, and store data in Microsoft Excel or Matlab format.

3.1.2 Cardiorespiratory Events Considered

The cardiorespiratory events for visual scoring in the GUI are enumerated below (these events are the exact events found in the button group of Figure 3–2):

1. *Asynchrony*: Periods when abdomen and ribcage signals are asynchronous.
2. *Pause*: Periods when the ribcage or abdomen signals are deemed 'flat'.
3. *Movement*: Periods corrupted by movement artifact.
4. *Norm Breath*: Periods of normal breathing (sinusoidal like signals).
5. *Glitch*: Sudden shift in the baseline of either the ribcage or abdomen signals.
6. *Odd*: Non-sinusoidal breathing pattern.
7. *Poor*: Poor quality signal in either the ribcage or abdomen signals.
8. *None*: Presently not being used.
9. *Break*: Non-sinusoidal breathing pattern, characterized by slow exhalation.
10. *Tech*: Technical problems. (broken leads, leads off, filter off etc.)
11. *Sigh*: Large tidal breaths, sigh.
12. *OA*: Obstructive apnea episodes.
13. *OH (OA)*: Obstructive Hypopneas.
14. *Sat (OA)*: Decrease in 5% or more of oxygen saturation.
15. *Mixed Apnea*: Mixed apnea episodes.
16. *CA*: Central apnea episodes.
17. *PSA*: Post sigh apnea episodes.
18. *Other*: Anything not specified by the rest of the buttons.

Note that the events numbered 5 to 18 above are mutually exclusive, while events 1 to 4 are not since they can occur during other events. For example, pause and asynchrony occur together during obstructive apnea.

These eighteen events enumerated are distinguished by a trained clinician. Four events are most important: pauses, asynchrony, normal breathing and movement artifact since our automated algorithms were developed to determine these events specifically. Moreover, these events are the constituents of apnea events to be determined.

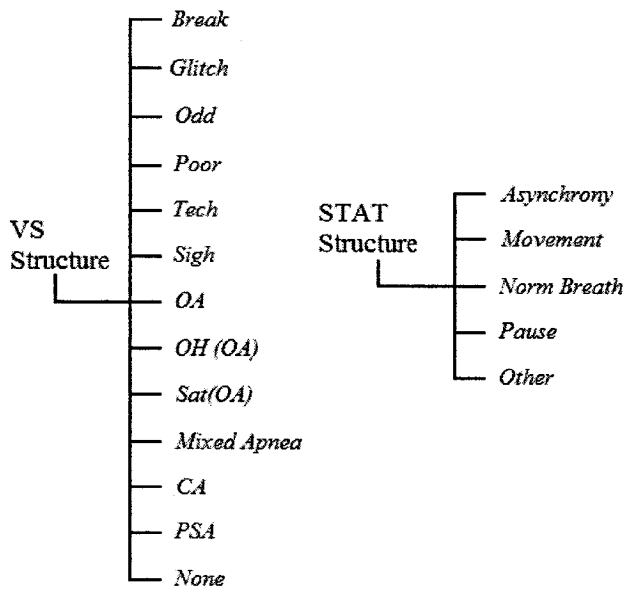

Figure 3–3: Events in the VS and STAT structures. The events in the STAT structure are used to determine the automated algorithms effectiveness while, the VS structure contains all remaining events normally visually scored at the MCH.

The data considered in this thesis was visually scored by K. A. Brown (MD, Anesthesiologist), Anesthesia Department, Montreal Childrens Hospital/ McGill University Health Center (MCH/MUHC), Montreal, QC, Canada. Visual scoring was obtained using *ApneaScore* to allow for accurate segment annotation. The event definitions given above are general and were determined by Dr. Brown in accordance with standard practice at the Montreal Children's Hospital.

3.1.3 Scored Data Storage

The visually scored data is stored in a MATLAB file (*.mat format) as two structures: VS and STAT (representing the two button groups on the GUI). Each structure contains an array for each scored respiratory event. Fig. 3–3 shows the events stored in each structure.

In both structures, each event is stored in an array format. The array for each event contains the start and end times. A maximum of 6 occurrences for each event is stored per 30s epoch since it is assumed that the same event cannot occur more that 6 separate times in a single epoch. The scored data is stored by sample number, allowing for precise storage.

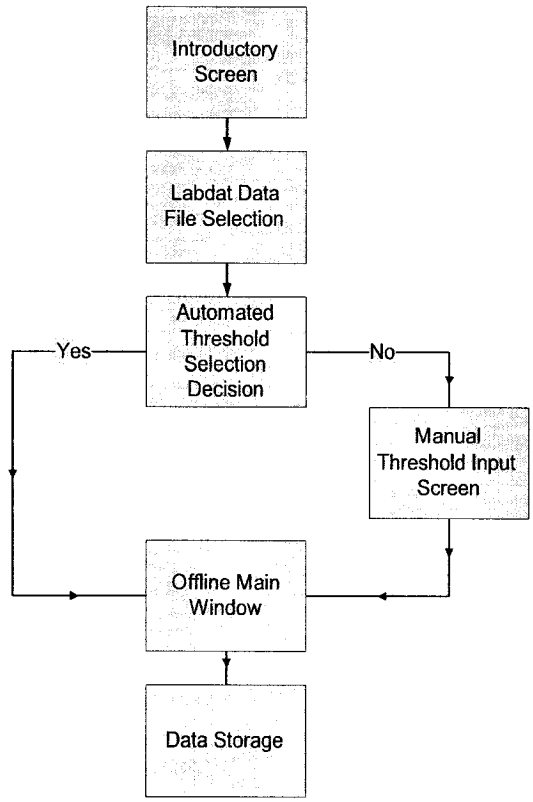

Figure 3–4: Overall structure for the *Offline* GUI. The application allows the user to manually set the threshold for analysis or set them automatically. The analysis results as well as the thresholds used for the analysis are presented to the user in the main window.

The application is also capable of saving the data in an excel file. The excel file contains the type of event, start and end times, the initials of the visual scorer and the date the visual scoring was completed (For more detail refer to Appendix A). The next section will present a new tool developed to perform automated off-line cardiorespiratory event detection.

3.2 Off-line Cardiorespiratory Event Detection Tool

A graphical tool was developed to carry out and present the automated off-line cardiorespiratory event detection of infant data. This tool is named *Offline*. *Offline* was developed using Matlab's GUIDE and provides an interactive GUI.

Fig. 3–4 shows the overall structure of the Offline tool, as presented to the user through the interface. The tool supports off-line analysis of cardiorespiratory data acquired at the MCH

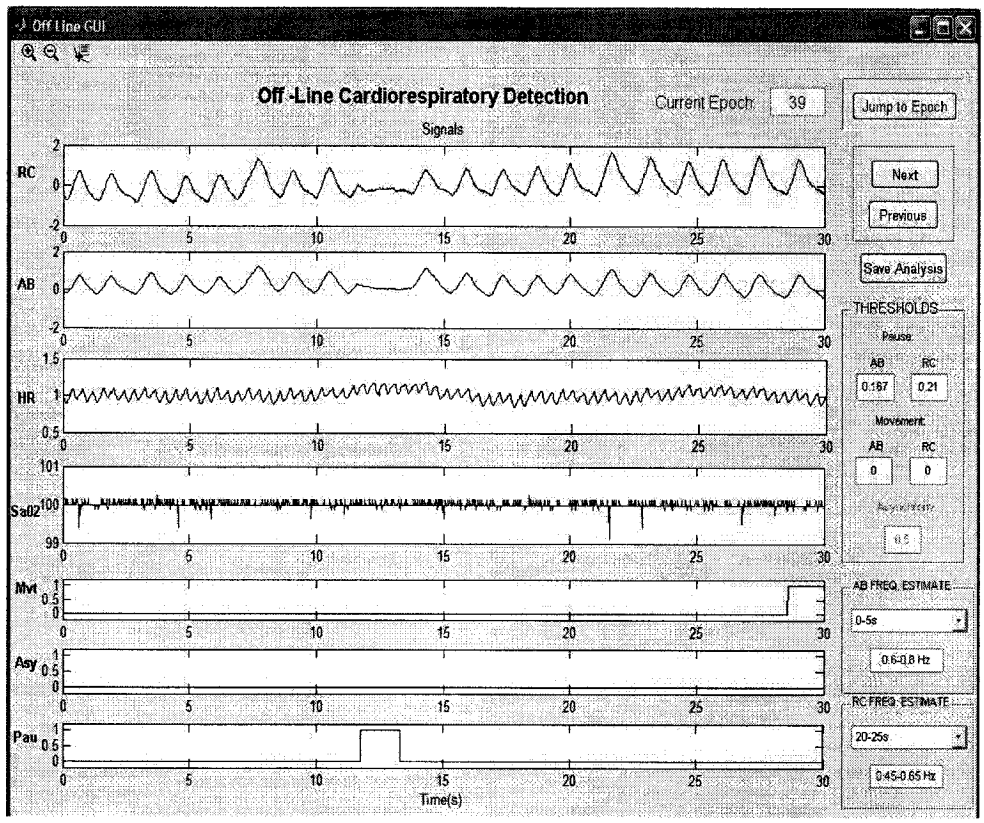

Figure 3–5: Main window for *Offline* GUI tool. The example presented in this figure shows a pause detection in the time interval 10-15s.

stored in the Labdat data format (RHT-InfoDat, Montreal). The GUI was developed to permit the automated detection of pauses, asynchronous breathing and movement artifact segments, as well as to estimate breathing frequency using the automated off-line methods discussed in Chapters 4 and 5. The program displays the automated analysis and the corresponding cardiorespiratory data in 30s epochs. Fig. 3–5 shows the main window of the *Offline* GUI. The data presented in the main window is ordered from top to bottom as follows: ribcage, abdominal, finger plethysmography, oxygen saturation, movement artifact detection, asynchrony detection and pause detection signals. The last three signals are logical signals which are set to one if the event is detected and set to zero otherwise.

The off-line analysis imbedded in the application detects pauses, asynchrony, movement artifact and permits the user to estimate breathing frequency for a data segment. This analysis can be run in

a fully automated manner using the automatic threshold selection techniques described in Chapter 5. Alternatively, the user can manually set thresholds for the analysis if required.

Dr. K. A. Brown used the tool and provided feedback to ensure that the GUI was clinician friendly and simple to use. The analysis of off-line data requires a few minutes compared to the hours required for visual scoring. The tool can be run on any PC-compatible machine with a basic Matlab 7.0 (The Mathworks, Inc, Natick, MA) installation. Once analyzed, the analysis performed by the user can be stored in a MATLAB file (*.mat format). The stored data file contains the thresholds used for the analysis and the three detection signals used to identify pause, asynchrony and movement artifact segments. For more detail, refer to the *Offline* GUI user manual presented in Appendix B.

3.3 Conclusions

The *ApneaScore* application was developed to provide data to assess the accuracy of the automated off-line algorithms relative to visual scoring. The *Offline* application was developed to implement the off-line algorithms and provide clinicians with a tool for automated off-line analysis. In comparison to previous visual scoring used at the MCH, *ApneaScore* requires less time and stores data with greater precision. However, the time required to score an entire data record with the *ApneaScore* tool can still take several hours. This process is time consuming since a single data record can consist of more than 800 epochs, highlighting the need for automated cardiorespiratory event detectors such as the ones used in the *Offline* tool. Subsequent chapters of this thesis present the new automated off-line algorithms and their effectiveness relative to visual scoring.

CHAPTER 4
Power-Based Segmentation and Breathing Frequency Estimation of Respiratory Signals Using Forward-Backward Bank Filtering

This chapter presents the automated off-line algorithm used to detect movement artifact and estimate breathing frequency in RIP data. The introduction, method description and some of the results presented in this chapter were taken from the conference paper entitled: **Power-Based Segmentation of Respiratory Signals Using Forward-Backward Bank Filtering**, accepted by the *28th Annual International Conference of the IEEE Engineering in Medicine and Biology Society (EMBS) held from the August 30 to September 3, 2006 in New York City, USA*. Authors: Ahmed A. Aoude, Alexis L. Motto, Henrietta L. Galiana, Karen A. Brown, and Robert E. Kearney. A copy of the conference paper can be found in Appendix C.

4.1 Introduction

Signal processing procedures that mark the start and end times of "useful data segments" from a record of respiratory and sleep data, or a subset thereof, have an important role in the diagnosis of clinically significant abnormalities. The term "useful data segment" is used here to designate any time interval of respiratory inductance plethysmography (RIP) signals that has a sufficiently high signal-to-noise ratio. A low signal-to-noise ratio arises when either or both ribcage and abdominal channels are corrupted by non-respiratory-induced movements, occurring, for example, when the subject is moving or being moved. For illustration, Fig. 4–1 provides a representative segment of respiratory excursion signals measured by RIP in the recovery room of the Montreal Children's Hospital (MCH) [7]. The first 20s period shows no apparent artifact whereas the following 11s period is corrupted by artifact. This chapter presents a signal processing procedure for the off-line, automated partitioning of RIP signals into segments either with or without artifacts.

The need for the automated segmentation of cardiorespiratory signals has been well recognized. Weese-Mayer *et al.* [75] reported that the performance of automated cardiorespiratory monitoring procedures could be significantly improved if signal segments corrupted with artifacts could be systematically identified. In [5], an automated procedure was proposed to estimate the phase relation between thoracic and abdominal excursions measured by noninvasive RIP. It was noted that the performance of the phase estimator could be improved if it was combined with an automated procedure for partitioning RIP signals into periods with and without artifact corruption. Such an automated signal segmentation procedure would also be useful in the analysis of long off-line records of respiration and sleep data. Furthermore, since RIP signals corrupted by movement artifact can not be used to identify apnea events and, since a large number of apnea misclassification is due to movement artifact [75, 76], the hypothesis "apnea present" was rejected during detected movement in RIP data; thereby improving the performance of automated apnea detectors.

In [6], it was shown that a Neyman-Pearson energy-based detector could be used for the automated detection of artifacts. Reference [6] was mainly concerned with the on-line detection of

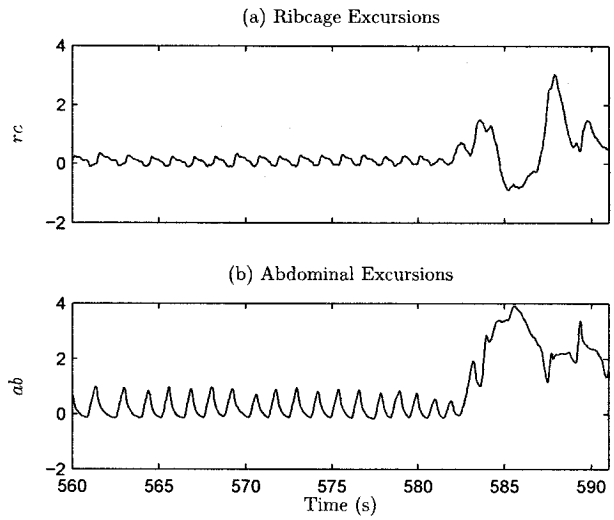

Figure 4–1: A representative segment of infant ribcage and abdominal excursions measured by RIP. The data shown in this figure was obtained from the Montreal Children's Hospital (MCH), from the study identification *SHIF* [7].

artifacts whereas this chapter is concerned with the off-line detection and, therefore, uses forward-backward IIR (infinite impulse response) filters, producing an array of zero-phase filters with narrower pass bands and smaller transition bands. As a by-product, we obtain an estimate of the fundamental frequency of breathing within the narrow band of the filters.

4.2 Algorithm Description

The proposed method was developed to automatically segment thoracic and abdominal signals into periods with artifact present and periods with artifact absent. From our previous study [5], it was observed that:

1. Quiet breathing signals are band limited within [0.4, 2] Hz
2. The energy of sensor noise is negligible compared to quiet breathing components.
3. The energy of movement artifact is generally greater than that of quiet breathing and sensor noise with predominance at lower frequencies ([0, 0.4] Hz).

Using the above observations, we developed a method that uses a bank of IIR filters and average power to automatically segment respiratory data into quiet breathing and movement artifact, and obtain a breathing frequency estimate. In brief, the method uses the frequency content of the RIP

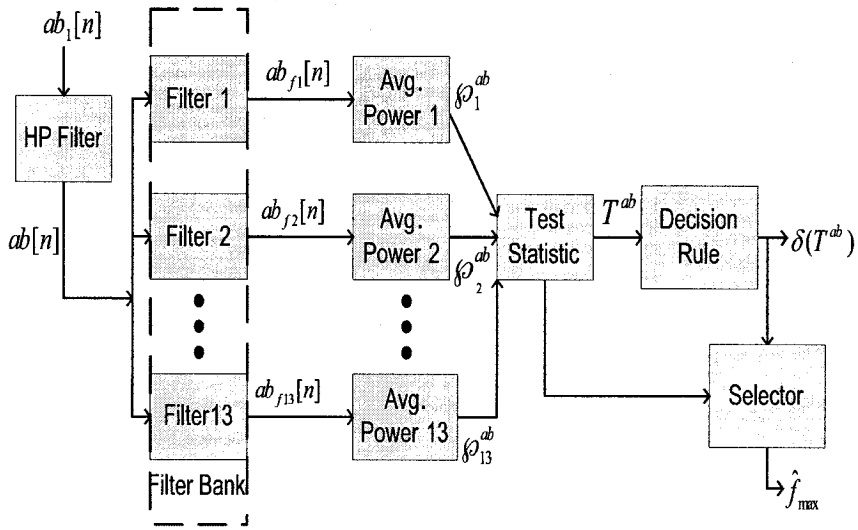

Figure 4–2: Simplified diagram of proposed method for respiratory data segmentation. The figure depicts the process for the abdominal RIP signal ($ab_1[n]$). The same process is also applied to the ribcage RIP signal.

signals to segment the respiratory data; if more than half of the signal power is found in the range [0, 0.4] Hz, the signal is labeled as movement artifact present; otherwise, if more than half of the signal power is found in the range [0.4, 2] Hz, the signal is labeled as quiet breathing. Fig. 4–2 shows a block diagram of the proposed method. Next, we describe the main components of the method.

4.2.1 High Pass Filter (Trend Removal)

A high pass filter with a cut-off frequency equal to 0.05 Hz was used to remove offsets and decays (from AC-coupling) observed in infant data acquired at the MCH. In Fig. 4–2 the original RIP signal is denoted ab_1, and the high pass filtered signal is denoted ab.

4.2.2 IIR Filter Bank

The filter bank used in the method is considered to evaluate the frequency content of the RIP signals and estimate their fundamental frequency. This filter bank consists of 13 filters selected to minimize overlap between adjacent filter passband widths over [0, 2.0] Hz. The 0-2 Hz bandwidth was chosen for two main reasons. Firstly, it covers the range of fundamental frequencies of infant

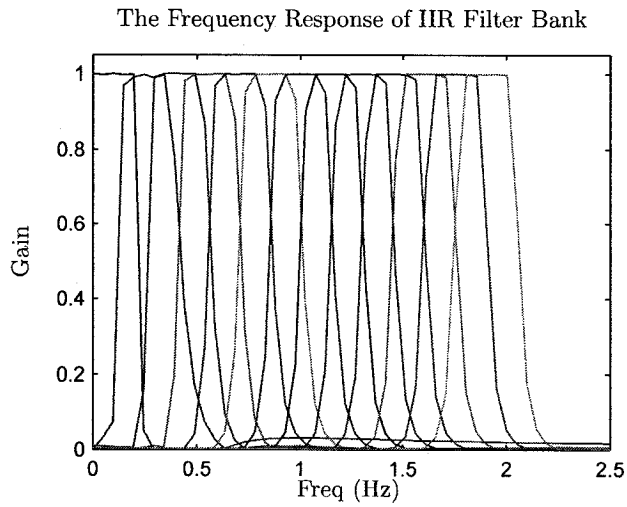

Figure 4–3: The magnitude frequency response of all thirteen filters found in the IIR filter bank with the design specifications enumerated in Table 4–1.

quiet breathing (0.4-2 Hz), as reported in [5]. Secondly, it covers low-frequencies (0-0.4 Hz) that are predominant in RIP artifacts.

The filters were designed with a pass-band width of 0.2 Hz as well as specified pass-band and stop-band ripples (refer to Table 4–1). Forward-backward filtering using IIR filters is used to perform zero-phase digital filtering to prevent distorting the phase relationship between the thoracic and abdominal signals. The IIR filters were chosen to be Cauer (elliptic) digital filters to obtain sharper roll offs and precise filter designs [77]. The optimal filter order was chosen using the elliptic low-pass filter order prediction formula described in [77, p.241] with the Signal Processing Toolbox of Matlab [8].

Table 4–1 enumerates the filters used and the specifications used to design them.

Fig. 4–3 shows the frequency responses of all thirteen filters; they all had sharp roll-offs with a passband gain equal to one as specified in Table 4–1.

4.2.3 Average Power

The average power of the filtered RIP signals over a window length $2L+1$ was used to segment the signals. Let $\wp_i^{ab}[n,N]$ denote the average power value of the filtered abdominal signals over a

Table 4–1: Design specification of IIR filters[1]

Filter number (i)	f_l (Hz)	f_h (Hz)	n	ω_p (dB)	ω_s (dB)
1	0	0.2	7	0.01	50
2	0.15	0.35	3	0.1	30
3	0.3	0.5	4	0.01	40
4	0.45	0.65	4	0.01	40
5	0.6	0.8	4	0.01	50
6	0.75	0.95	4	0.01	50
7	0.9	1.1	4	0.01	50
8	1.05	1.25	4	0.01	50
9	1.2	1.4	4	0.01	50
10	1.35	1.55	4	0.01	50
11	1.5	1.7	4	0.01	50
12	1.65	1.85	4	0.01	50
13	1.8	2.0	4	0.01	50

[1] f_l denotes the filters' low cut off frequency; f_h denotes the filters' high cut off frequency; n denotes the filter order; ω_p denotes the maximum pass-band ripple level; ω_s denotes the minimum stop-band ripple attenuation level.

window $N = 2L + 1$, then

$$\wp_i^{ab}[n, N] = \frac{1}{N} \sum_{k=n-L}^{n+L} ab_{fi}^2[k], \text{ for } i = 1, 2, ...13 \tag{4.1}$$

Where $ab_{fi}[n]$ represents the i^{th} filtered abdominal signal from the filter bank (refer to Fig. 4–2). The ribcage power, $\wp_i^{rc}[n, N]$ is similarly defined.

4.2.4 Segmentation Test Statistic

It is assumed that infant quiet breathing is between [0.4, 2] Hz and that artifacts are at lower frequencies. Let $\mathcal{I}$ and $\mathcal{J}$ denote the index sets of the IIR bandpass filters covering the quiet breathing and artifact frequency ranges, respectively; that is $\mathcal{I} = \{3, 4, ..., 13\}$ and $\mathcal{J} = \{1, 2\}$. Then, we can define the test statistic for the abdomen, T^{ab} as

$$T^{ab}[n] = \frac{\max\limits_i \{\wp_i^{ab}\}_{i \in \mathcal{I}} - \max\limits_j \{\wp_j^{ab}\}_{j \in \mathcal{J}}}{\max\limits_i \{\wp_i^{ab}\}_{i \in \mathcal{I}} + \max\limits_j \{\wp_j^{ab}\}_{j \in \mathcal{J}}}, \tag{4.2}$$

where we use the convention $\frac{0}{0} = 1$. The test statistic for the ribcage, T^{rc} can be similarly defined.

4.2.5 Decision Rule

The test statistic T^{ab} can then be used, together with a Neyman-Pearson threshold γ [78], for deciding

$$\delta(T^{ab}) = \begin{cases} 1, \text{if } T^{ab} \leq \gamma \\ 0, \text{if } T^{ab} > \gamma \end{cases} \tag{4.3}$$

This decision rule states that the hypothesis $\mathcal{H}_0^m$ is chosen if $T^{ab} \leq \gamma$ and the hypothesis $\mathcal{H}_1^m$ is chosen if $T^{ab} > \gamma$. Where the hypotheses are:

$$\begin{gathered} \mathcal{H}_0^m\text{: Artifact Absent} \\ \text{vs.} \\ \mathcal{H}_1^m\text{: Artifact Present} \end{gathered} \tag{4.4}$$

4.2.6 Selector

The selector in Fig. 4–2 yields an estimate of the breathing frequency to within 0.2 Hz, $\hat{f}_{max}$:

$$\hat{f}_{max}[n] = \delta[n] \min\{\arg\max_{i \in \mathcal{I}} \wp_i^{ab}[n]\}. \tag{4.5}$$

Equation (4.5) states that $\hat{f}_{max}[n] = 0$ if there is *artifact present*; otherwise, $\hat{f}_{max}[n]$ is the index of a filter whose average power is maximum among the relevant filters ($\mathcal{I}$ = 3-13). The operation min ensures that $\hat{f}_{max}[n]$ is a singleton if multiple filters have similar average power.

In other words, when we decide *artifact absent*, the output $\hat{f}_{max}$ of Fig. 4–2 is an integer value representing a filter number of Table 4–1. Thus, the $\hat{f}_{max}$ value is representative of the respiratory frequency in the band $[f_l, f_h]$ Hz, where f_l and f_h are the low and high cut off frequencies of filter number $\hat{f}_{max}$.

4.3 Simulated Data

Simulated data was considered first since the correct result is known and can be used to test the new method directly. Simulated data was used to verify that the frequency estimation and data segmentation methods were valid, given the underlying assumptions of Section 4.2 are correct.

4.3.1 Simulated Data for the Frequency Estimation Analysis

Piecewise-linear frequency modulated signals where used to simulate normal breathing RIP signals. Simulated ribcage ($s_1(t)$), and abdominal ($s_2(t)$) signals, were used to test the frequency estimates obtained with the method. These signals were defined as,

$$s_1(t) = A_1 \cos(2\pi\sigma(t)t) + e^{-0.02t} \tag{4.6a}$$

$$s_2(t) = A_2 \cos(2\pi\sigma(t)t + \phi_0) + e^{-0.02t} \tag{4.6b}$$

where,

$$A_1 = 1, A_2 = 2, \phi_0 \in [0, \pi] \tag{4.6c}$$

$$\sigma(t) = \begin{cases} 0.1, & \text{if } t \leq 8s \\ 0.7, & \text{if } 8s < t \leq 14s \\ 1.75, & \text{if } 14s < t \leq 20s \\ 1.15, & \text{if } 20s < t \leq 26s \\ 0.3, & \text{if } 26s < t \leq 32s \\ 0.85, & \text{if } 32s < t \leq 38s \\ 1.0, & \text{if } 38s < t \leq 44s \\ 0.55, & \text{if } 44s < t \leq 50s \\ 1.3, & \text{if } 50s < t \leq 56s \\ 1.45, & \text{if } 56s < t \leq 62s \\ 1.6, & \text{if } 62s < t \leq 68s \\ 0.4, & \text{if } 68s < t \leq 76s \\ 1.9, & \text{if } 76s < t \leq 80s \end{cases} \tag{4.6d}$$

Note that ϕ_0 was set to zero for the simulated analysis and that $e^{-0.02t}$ was used to model decaying trends observed in real RIP data.

An accurate representation of real RIP signals must account for electronic and sensor noise as well as movement artifact. These noise processes are nondeterministic and must be modeled with stochastic processes. It was assumed that these noise processes were additive and that electronic or sensor noise can be modeled as additive Gaussian white processes. The noise processes are similar to ones used in [5]. To first demonstrate the effectiveness of the method in estimating breathing frequencies in quiet breathing, movement artifacts were omitted (quiet breathing signals are defined to be movement artifact free). Thus, the virtual breathing signals were predominantly corrupted by white Gaussian additive noise denoted $n_1(t)$, $n_2(t)$, respectively.

All random numbers were generated using the pseudonormally distributed random number generator in Matlab 7.0 (Mathworks Inc., Natick, MA). The state of the random generator was set to 5 and 2 for $n_1(t)$, $n_2(t)$, respectively.

The simulated thoracic and abdominal RIP signals with noise were defined as follows.

$$y_1(t) = \rho_{11} s_1(t) + \rho_{12} n_1(t) \tag{4.7}$$

$$y_2(t) = \rho_{21} s_2(t) + \rho_{22} n_2(t) \tag{4.8}$$

where $\rho_{11}, \rho_{12}, \rho_{21}, \rho_{22} \in [-1, 1]$. Fig. 4–4 shows a plot of the signal y_2.

4.3.2 Simulated Data for the Segmentation Analysis

Simulated data was also used to test the method for cardiorespiratory data segmentation. Here the simulated process used to model RIP signals for segmentation purposes had to include a process with prominent low frequency components representing movement corruption. This was modeled with a stochastic diffusion process, called *mean reverting Itô processes* (e.q.,see [79]) [5]. In brief, mean reverting Itô processes can be generated by the stochastic differential equation: $d\tilde{n}(t) = \mu(\tilde{n}, t)dt + \sigma dW(t)$ where, $W(t)$ is a standard Wiener process, and $\mu(\tilde{n}, t) = \tilde{c}(\tilde{\mu} - \tilde{n}(t))$ for real constant $\tilde{\mu}$ and positive constant $\tilde{c}$ [5]. For more detail, the main concepts and derivations of the simulated breathing and additive noise signals used for the segmentation analysis can be found in [5, pp.617-618].

4.4 Simulated Data Results

4.4.1 Representative Results for the Frequency Estimation Analysis

To assess the effectiveness of estimating breathing frequencies, the method was applied to simulated ribcage and abdominal RIP signals (section 4.3.1). Recall that the $\hat{f}_{max}$ values obtained for artifact free segments indicate the breathing frequency estimates obtained (refer to section 4.2.6).

Fig.4–4 shows that our method correctly estimates the breathing frequency in the simulated data. For clarity, Fig.4–4 only shows the results for the simulated abdominal signal, the results for the simulated ribcage signal were similar. In fact, the simulated abdominal signal is labeled with the correct $\hat{f}_{max}$ values; the expected $\hat{f}_{max}$ values for each segment in order is {1, 5, 12, 8, 2, 6, 7, 4, 9 , 10, 11, 3, 13} (refer to equation (4.6) and table 4–1). The delays in the change of some $\hat{f}_{max}$ values can be attributed to the use of non-ideal filters which are not exact shifted replicas of one another; causing some filters to have slightly higher average power. These delays (< 2.5 s) are acceptable since real RIP data is assumed to have constant breathing frequencies for long periods in time, making the slight delays negligible in comparison.

4.4.2 Representative Results for the Segmentation Analysis

To assess the effectiveness of the segmentation method, a simulated RIP signal was generated. This signal was composed of four segments: the first and third segments were predominantly composed of normal breathing (simulated breathing + slight movement) while, the second and fourth segments were predominantly composed of movement (simulated movement + slight breathing) as per section 4.3.2. All segments also had additive electronic noise. Note that the first and third segments were simulated with a 17.72 dB signal-to-noise ratio (one forth of the noise process was movement and the rest was electronic noise); while, the second and fourth segments were simulated with a -26.29 dB signal-to-noise ratio (one seventh of the noise process was electronic noise and the rest was movement).

Fig. 4–5 shows that our method correctly distinguished the artifact corrupted and normal breathing segments. The normal breathing segments were labeled with $\hat{f}_{max}$ values equal to 5 and 4, which are the correct values since they correspond to breathing frequencies in the ranges [0.6, 0.8] Hz and [0.45, 0.65] Hz (the simulated frequencies were 0.7 Hz and 0.5 Hz respectively).

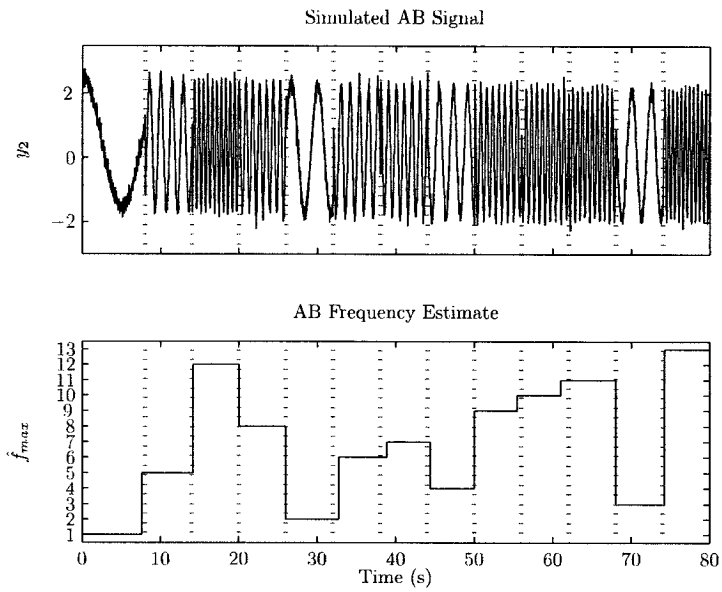

Figure 4–4: Analysis of a 80s simulated segment of infant abdominal RIP signal modeled as a piece-wise linear frequency modulated sinusoidal signal derived from equation (4.6). The signal is corrupted by additive noise with a signal-to-noise ratio = 22.5 dB. The dotted vertical lines indicate the transition points where frequencies changed. As expected, the frequency indices obtained were accurate (the expected $\hat{f}_{max}$ values for each segment in order is: {1, 5, 12, 8, 2, 6, 7, 4, 9, 10, 11, 3, 13}).

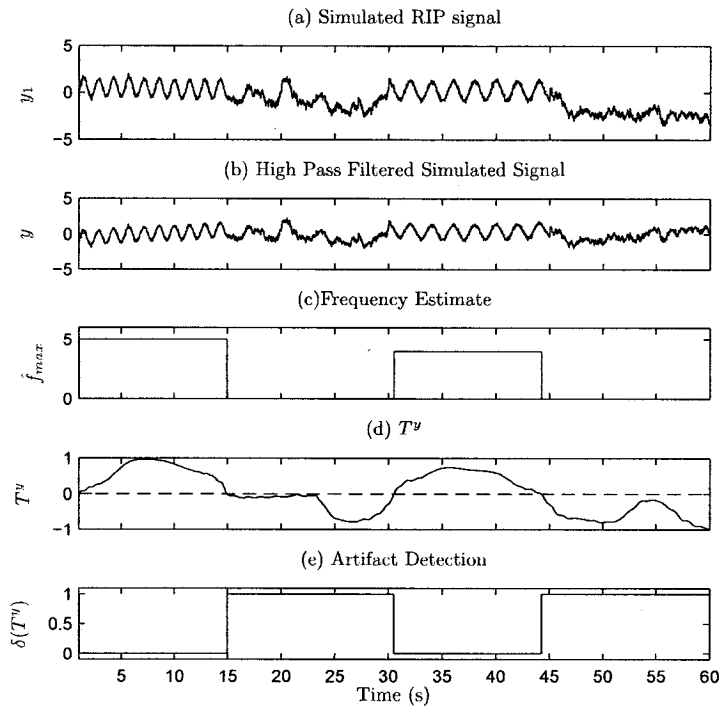

Figure 4–5: Segmentation analysis of a 60s simulated segment of infant RIP signal. Note that for the simulated RIP signal a 0.7 Hz noise corrupted signal was used for the first 15s and a 0.5 Hz noise corrupted signal was used for time 30s to 45s. Time 15s to 30s and the last 15s of the simulated signal was predominantly composed of simulated movement artifact. (a) is the original signal, (b) is the high pass filtered signal, (c) is a plot of the frequency estimate $\hat{f}_{max}$, (d) is a plot of the movement artifact detector test statistic T^y (dashed line: $\gamma = 0$), and (e) is the decision indicating if movement artifact is present $\delta(T^y)$. As expected, the method detects the artifact corrupted segments ($\delta(T^y) = 1$).

4.5 Infant Data Results

To demonstrate the method on infant data, segments of cardiorespiratory data acquired at the MCH were considered. This data was previously reported by Brown *et al.* [7] as part of another study with appropriate ethics approval. The continuous-time ribcage and abdominal signals (NIMS^{TM}, Respitrace Plus, North Bay Village, Florida), were amplified and filtered with 15Hz 8-pole Bessel filters (Frequency Devices, Haverhill, MA), and sampled at 50 Hz with a 12-bit analog-to-digital converter (Data Translation, Marlborough, MA). This data was stored on a computer using LABDAT^{TM} data acquisition software (RHT-InfoDat, Montreal). No attempt was made to calibrate the signals in absolute terms.

4.5.1 Breathing Frequency Estimate Examples

The frequency estimation method was evaluated with real data segments from infant data acquired at the MCH by comparing the breathing frequencies obtained with the automated method to those obtained with a manual analysis (peak detection or cycles/second). Fig. 4–6 shows that the method correctly determined the breathing frequency of a quiet breathing segment within a narrow band (0.2 Hz). The breathing frequency of the segment was approximately 0.6 Hz (6 breaths in 10s), therefore the $\hat{f}_{max}$ value of 4 is correct since it indicates a breathing frequency between 0.45 and 0.65 Hz.

Fig. 4–7 shows that the method also correctly estimated breathing frequencies in a quiet breathing segment with a decaying trend. Here peak detection provided a visual estimate of breathing frequency of 0.8 Hz and 1 Hz respectively, for the first and second half of Fig. 4–7. The automated method estimated the corresponding breathing frequencies of $\hat{f}_{max} = 6$ and 7 which correspond to [0.75, 0.95] Hz and [0.9, 1.1] Hz.

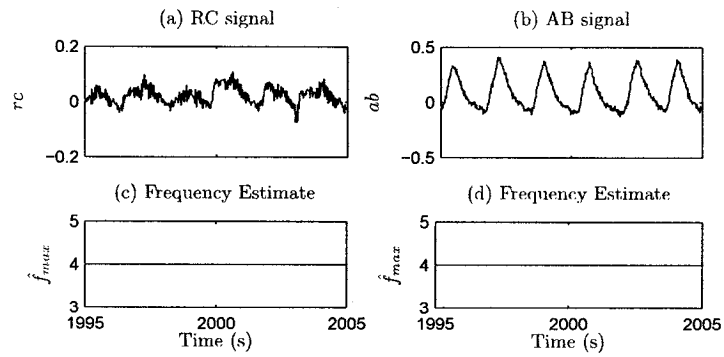

Figure 4–6: Analysis of a 10s segment of ribcage ($rc[n]$) and abdominal ($ab[n]$) breathing excursions measured by inductance plethysmography of an infant (47 weeks old weighing 4.8 kg, study identification: *ARC*). Note that for both the RIP signals a quasi-sinusoidal breathing signal is observed. As expected, the $\hat{f}_{max}$ values ((c) and (d)) obtained with the method correctly estimated frequency, visually estimated at 0.6 Hz ($\hat{f}_{max} = 4 \Rightarrow [0.45, 0.65]Hz$). Note that this figure was generated with a filtering window of 251 samples and $\gamma = 0$.

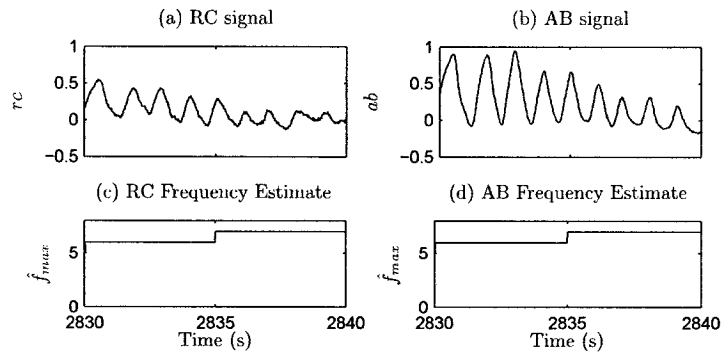

Figure 4–7: Analysis of a 10s segment of ribcage ($rc[n]$) and abdominal ($ab[n]$) breathing excursions measured by inductance plethysmography of an infant (42 weeks old weighing 3.9 kg, study identification: *SHIF*). Note that for both the RIP signals a quasi-sinusoidal breathing signal with a trend is observed. As expected, the $\hat{f}_{max}$ values ((c) and (d)) obtained with the method correctly estimated frequency, visually estimated as 0.8 Hz and 1 Hz for the early and later segments respectively ($\hat{f}_{max} = 6 \Rightarrow [0.75, 0.95]Hz$, $\hat{f}_{max} = 7 \Rightarrow [0.9, 1.1]Hz$). Note that this figure was generated with a filtering window of 251 samples and $\gamma = 0$.

4.5.2 Segmentation Examples

The segmentation obtained with the method was demonstrated using two signal segments representative of normal breathing and artifact corruption in post-operative infants. Fig. 4–8 shows a segment of infant data consisting of normal breathing followed by artifact corruption. Fig. 4–9 shows a segment of infant data but consisting of artifact corruption followed by quasi-sinusoidal breathing with a time-varying trend. In both examples, the test statistic T^{ab} was close to one for the breathing segments and close to negative one for the movement corrupted segments. Thus, $\delta(T^{ab})$ was equal to 1 for the artifact corrupted segments in both figures, while for the breathing segments $\delta(T^{ab})$ was 0. It is evident that the choice of γ is important for correct segmentation; $\gamma = 0$ was used in this example since it is the mid-point of test statistic T^{ab}. Thus, any T^{ab} value above zero indicates that the majority of the signal power is in the expected breathing band, while any T^{ab} value below zero indicates that the majority of the signal power power is in the expected movement artifact band. Note that Fig. 4–8 and Fig. 4–9 were generated using a window length (N) equal to 251 samples or 5 seconds.

4.6 Conclusion

The segments included in figures 4–6 to 4–9 are intended to demonstrate the results obtained with the method on real data segments. The methods' effectiveness on infant data was also considered relative to visual scoring obtained with the *ApneaScore* tool. The conference paper in appendix C presents the results obtained for 8 infant data records relative to visual scoring. These results are not present in this chapter since Chapter 5 presents similar results for the entire infant database acquired at the MCH (21 infant data records). The next chapter also presents the automated off-line methods developed for pause and asynchrony detection. A comparison between all automated methods and visual scoring is included.

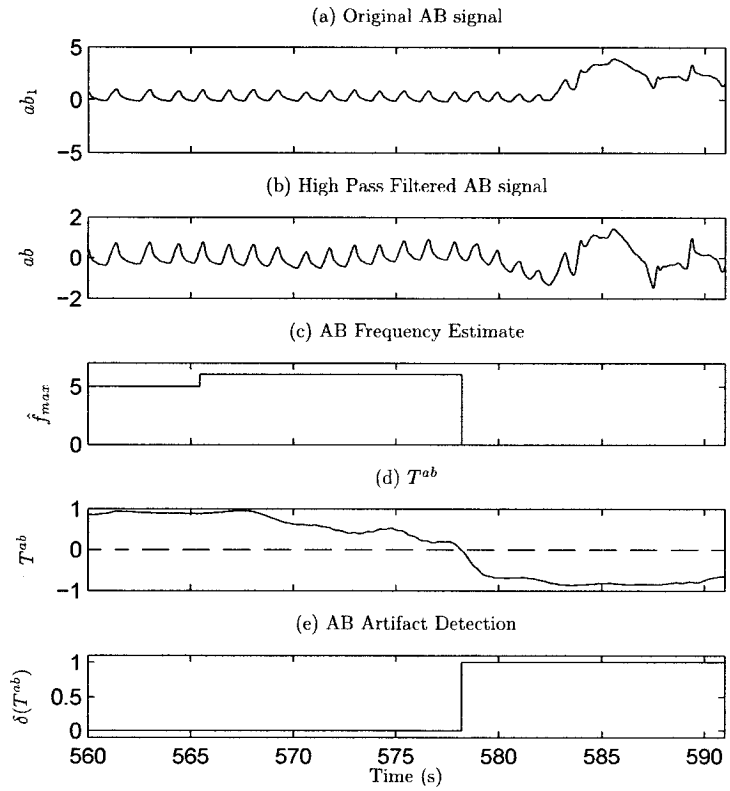

Figure 4–8: Segmentation analysis of a 31s segment of abdominal ($ab_1[n]$) breathing excursions measured by inductance plethysmography of an infant (42 weeks old weighing 3.9 kg). Note that a quasi-sinusoidal breathing signal is observed for the first 20s followed by 11s of artifact corruption. (a) is the original RIP signal, (b) is the high pass filtered signal, (c) is a plot of of the frequency estimate $\hat{f}_{max}$, (d) is a plot of the test statistic used to detect movement artifact T^{ab} (dashed line: $\gamma = 0$), and (e) is the movement artifact decision $\delta(T^{ab})$ (set to 1 if movement artifact is detected). Note that for the interval 577.5s to 582s the signal is composed of both, low frequency artifact and quiet breathing; since the power of the low frequency component is higher ($T^{ab} < 0$), the method labeled this segment as having artifact corruption.

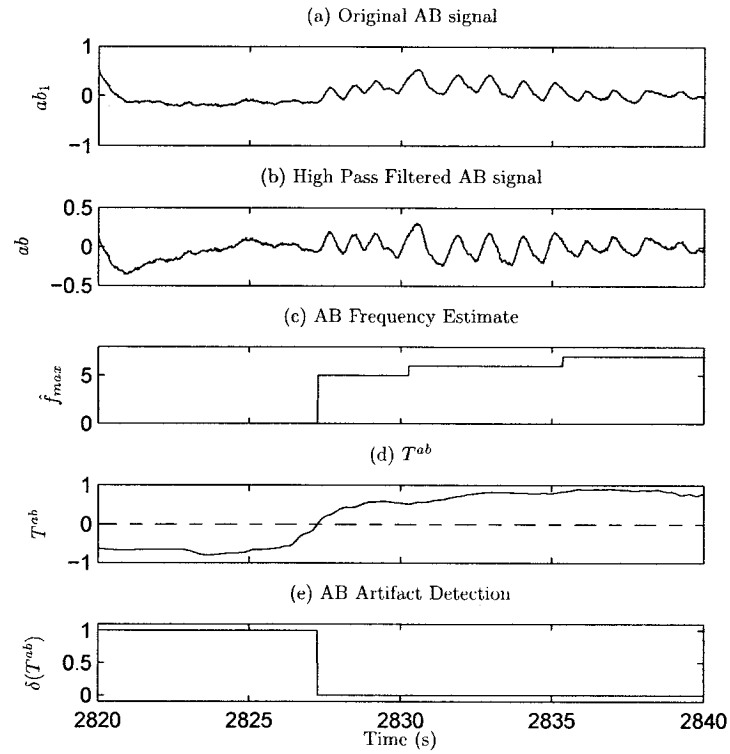

Figure 4–9: Segmentation analysis of a 20s segment of abdominal ($ab_1[n]$) breathing excursions measured by inductance plethysmography of an infant (42 weeks old weighing 3.9 kg). Note that artifact corruption is observed for the first 7.5s followed by 12.5s a quasi-sinusoidal breathing signal with a trend. (a) is the original RIP signal, (b) is the high pass filtered signal, (c) is a plot of the frequency estimate $\hat{f}_{max}$, (d) is a plot of the test statistic used to detect movement artifact T^{ab} (dashed line: $\gamma = 0$), and (e) is the movement artifact decision $\delta(T^{ab})$ (set to 1 if movement artifact is detected).

CHAPTER 5
Automated Off-Line Cardiorespiratory Event Detection

This chapter presents the overall automated off-line event detection process used to identify pause, asynchrony and movement artifact segments in RIP data. The effectiveness of the methods relative to Dr. K. A. Brown's visual scoring for all infant data acquired at the MCH is also presented. This chapter is in the format of a journal paper submitted to IEEE Transactions on Biomedical Engineering.

Automated Off-Line Cardiorespiratory Event Detection

Ahmed A. Aoude, Alexis L. Motto, Henrietta L. Galiana, Karen A. Brown, and Robert E. Kearney

To be submitted to: IEEE Transactions on Biomedical Engineering

5.1 Abstract

In [5] and [9] we presented methods for automated phase estimation and movement artifact detection in respiratory inductance plethysmography (RIP) signals. In the present paper, we combine and improve these methods to develop a method for the automated off-line detection of asynchrony, pauses and movement artifacts. Examples of applications include home and sleep laboratory studies of cardiorespiratory data. The new procedure was successfully applied to cardiorespiratory signals acquired post-operatively from infants in the recovery room. A comparison between event detection obtained with the automated method and visual scoring is presented. The method provides the following advantages: 1) fully automated; 2) less time consuming than visual scoring; 3) repeatable and standardized analysis; and 4) applicable to uncalibrated RIP signals. It is also amenable to on-line detection once statistics on large databases become available.

5.2 Introduction

Respiratory inductive plethysmography (RIP) is the most widely accepted method for qualitative and quantitative respiratory measurements [50,80]. In fact, RIP is a common cardiorespiratory monitor used in sleep laboratories and in the home [81]. These monitors are noninvasive, robust, well tolerated by patients and recommended for diagnostic testing. Therefore, we suggest that cardiorespiratory monitors can be used to study respiration in infants at risk of postoperative apnea (POA). Infants are at increased risk of developing respiratory problems such as POA after receiving anesthesia and so require monitoring after surgery [82]. Consequently, we have applied cardiorespiratory monitoring for the study of POA.

Visual scoring of cardiorespiratory data is commonly used to identify cardiorespiratory events because, to date, no reliable automated method has been presented [14–16]. Episodes of central and obstructive apnea are identified as part of this visual scoring. Although visual scoring is the standard for determining respiratory disorders, the likelihood of human error in visual coding is high and the results may be subjective [61]. Thus, the development of a reliable automated method to detect respiratory events would allow for a more systematic and less time consuming process when compared to visual scoring. Automated methods for the analysis of cardiorespiratory data exist. Some of these methods include: hidden Markov models [65], artificial neural networks [44,66],

recursive least squares [7], fuzzy logic systems [67] , and others. Although these methods perform well on simulated data, they encounter difficulties when applied to clinical data sets where movement artifact is prominent.

The need for the automated segmentation of cardiorespiratory signals has been well recognized. Weese-Mayer *et al.* [75] reported that the performance of automated cardiorespiratory monitoring procedures could be significantly improved if signal segments corrupted with artifacts could be systematically identified. Such automated signal segmentation procedures would also be useful in the analysis of long records of off-line respiratory data acquired during sleep. Moreover, since RIP signals corrupted by movement artifact can not be used to identify apnea events and, since a large number of apnea misclassification is due to movement artifact [75, 76], the hypothesis "apnea present" was rejected during detected movement in RIP data; thereby improving the performance of automated apnea detectors.

A comprehensive automated method must be comparable to visual scoring in detecting obstructive and central apnea events as well as movement artifacts which occur during sleep in infants. Obstructive sleep apnea (OSA) is characterized by reduced or absent airflow with some degree of asynchrony (or paradoxical motion) between the thorax and abdomen; central sleep apnea (CSA) is characterized by an extended period with no thoracic or abdominal respiratory effort. Our approach distinguishes between central and obstructive events by analyzing RIP signals for pauses and asynchrony.

We previously presented methods for phase estimation in [5] and movement artifact detection in [6]. The segmentation method was modified and improved for off-line use in [9]. In the present paper, we propose a comprehensive off-line method to detect pauses, estimate the phase between the RIP signals, and detect movement artifact corrupted segments. The *combination* of these methods can also be used to determine central and obstructive apnea events.

The remaining sections are organized as follows. Section 5.3 describes the methods developed for automated detection of pauses, movement artifact corruption and phase estimation. Section 5.4 gives some quantitative results based on the application of the new methods to infant respiration signals. Section 5.5 provides some concluding remarks.

5.3 Methods

Fig. 5–1 shows a block diagram of the proposed method, with it's main components: pause, asynchrony and movement artifact detection. The sections below provide more details.

5.3.1 Movement Artifact Detection and Breathing Frequency Estimation

Movement Artifact Detection

The off-line method used to detect data segments corrupted by movement artifact is described in [9]. In brief, the method uses a bank of infinite impulse response (IIR) filters, a power function, a test statistic, and a comparator to decide if the artifact is present or not. Table C-1 presents the IIR filters used.

It was determined that infant quiet breathing is between [0.4, 2.0] Hz while movement artifacts are at lower frequencies [5]. Thus, we defined the test statistic, T^{ab} as

$$T^{ab}[n] = \frac{\max\limits_{i}\{\wp_i^{ab}\}_{i\in\mathcal{I}} - \max\limits_{j}\{\wp_j^{ab}\}_{j\in\mathcal{J}}}{\max\limits_{i}\{\wp_i^{ab}\}_{i\in\mathcal{I}} + \max\limits_{j}\{\wp_j^{ab}\}_{j\in\mathcal{J}}}, \tag{5.1}$$

where $\mathcal{I}$ and $\mathcal{J}$ denote the index sets of the IIR bandpass filters covering the quiet breathing and artifact frequency ranges, respectively; that is $\mathcal{I} = \{3, 4, ..., 13\}$ and $\mathcal{J} = \{1, 2\}$. $\wp_i^{ab}$, the average power over a window $N = 2L + 1$ is defined as,

$$\wp_i^{ab}[n, N] = \frac{1}{N}\sum_{k=n-L}^{n+L} ab_{fi}^2[k], \text{ for } i = 1, 2, ...13 \tag{5.2}$$

Where ab_{fi} represents the i^{th} filtered abdominal signal from the filter bank; that is ab_{fi} is the abdominal RIP signal filtered by filter number i of Table C-1. Note that T^{rc} is similarly defined for the ribcage signal.

The test statistic T^{ab} is then used, together with the threshold γ^{ab}, to decide

$$\delta(T^{ab}) = \begin{cases} 1, \text{if } T^{ab} \leq \gamma^{ab} \\ 0, \text{if } T^{ab} > \gamma^{ab} \end{cases} \tag{5.3}$$

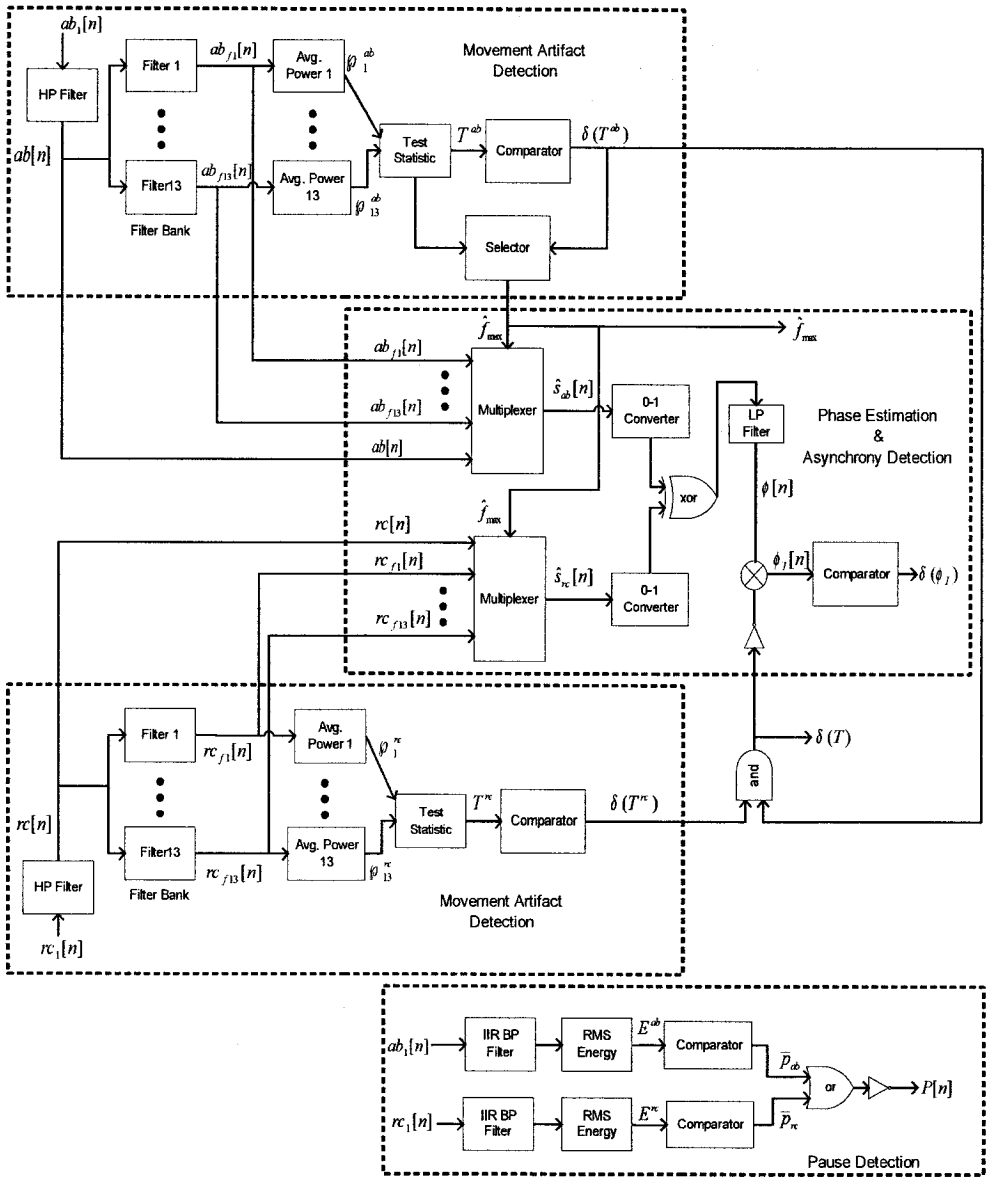

Figure 5–1: Procedure for the automated detection of asynchrony, pauses and movement artifact in RIP data. The outputs $\delta(\phi_I)$, $\delta(T)$ and $P[n]$ are the decisions used to automatically detect asynchrony, movement artifact and pauses respectively. In addition $\hat{f}_{max}$ yields an estimate of the breathing frequency up to a narrow band. Note that the procedure was implemented using the Signal Processing Toolbox of Matlab [8] (refer to [9] for more detail on the movement artifact components).

Table 5–1: Design specification of IIR filters[1]

Filter number (i)	f_l (Hz)	f_h (Hz)	n	ω_p (dB)	ω_s (dB)
1	0.00	0.20	7	0.01	50
2	0.15	0.35	3	0.10	30
3	0.30	0.50	4	0.01	40
4	0.45	0.65	4	0.01	40
5	0.60	0.80	4	0.01	50
6	0.75	0.95	4	0.01	50
7	0.90	1.10	4	0.01	50
8	1.05	1.25	4	0.01	50
9	1.20	1.40	4	0.01	50
10	1.35	1.55	4	0.01	50
11	1.50	1.70	4	0.01	50
12	1.65	1.85	4	0.01	50
13	1.80	2.00	4	0.01	50

[1] f_l denotes the filters' low cut off frequency; f_h denotes the filters' high cut off frequency; n denotes the filter order; ω_p denotes the maximum pass-band ripple level; ω_s denotes the minimum stop-band ripple attenuation level.

The comparator in equation (5.3) selects the hypothesis $\mathcal{H}_1^m$ if $T^{ab} \leq \gamma$ or the hypothesis $\mathcal{H}_0^m$ if $T^{ab} > \gamma$. Where the hypotheses are:

$$\begin{gathered} \mathcal{H}_0^m\text{: Artifact Absent} \\ \text{vs.} \\ \mathcal{H}_1^m\text{: Artifact Present} \end{gathered} \tag{5.4}$$

Thus, the test statistic and comparator of equation (5.3) detect movement artifact if more than half of the signal power is at lower frequencies, or detect quiet breathing if more than half of the signal power is in the quiet breathing frequency range.

Breathing Frequency Estimation

A breathing frequency estimate, $\hat{f}_{max}$, is obtained as a by-product of the method. This estimate is obtained with the selector in Fig. 5–1 which estimates the breathing rate up to a narrow band (0.2 Hz) as,

$$\hat{f}_{max}[n] = \delta[n] \min\{\arg\max_{i \in \mathcal{I}} \wp_i^{ab}[n]\}. \tag{5.5}$$

The output $\hat{f}_{max}$ of Fig. 5–1 is an integer value representing one of the 13 filter numbers of Table C-1. Thus, the $\hat{f}_{max}$ value is representative of a breathing frequency estimate in the band $[f_l, f_h]$ Hz, where f_l and f_h are the low and high cut off frequencies of filter number $\hat{f}_{max}$ of Table C-1. $\hat{f}_{max}$ is also used to generate an adaptively filtered version of the RIP signals used in the phase estimation algorithm of Section 5.3.3.

5.3.2 Pause Detection

We developed an automated pause detection algorithm to identify periods without respiratory movements in RIP data. In the first step of the pause detection algorithm, the RIP signals are bandpass filtered ([0.4, 2.0]Hz) using an IIR bandpass filter to increase their signal-to-noise ratio. Next, the root mean square (RMS) of signals over a window of length N_1 is computed. The RMS value of the abdominal signal is given by:

$$E_3^{ab}[n, N_1] = \sqrt{\frac{1}{N_1} \sum_{k=n-N_1/2+1}^{n+N_1/2} ab_f^2[k]} \tag{5.6}$$

where, ab_f is the bandpass filtered abdominal signal. Note that E_3^{rc}, is similarly defined.

The test statistic E_3^{ab} is then used, together with the threshold γ_1^{ab}, to decide

$$\bar{p}_{ab}[n] = \begin{cases} 1 & if E_3^{ab}[n, N_1] \geq \gamma_1^{ab} \\ 0 & if E_3^{ab}[n, N_1] < \gamma_1^{ab} \end{cases} \tag{5.7}$$

The comparator output ($\bar{p}_{ab}$) is 0 when a pause is detected and 1 otherwise. Thus, we choose $\mathcal{H}_1^p$ if $E_3^{ab} < \gamma_1^{ab}$ and we choose $\mathcal{H}_0^p$ if $E_3^{ab} \geq \gamma_1^{ab}$. Where hypotheses are:

$$\begin{gathered} \mathcal{H}_0^p\text{: Pause absent} \\ \text{vs.} \\ \mathcal{H}_1^p\text{: Pause present} \end{gathered} \tag{5.8}$$

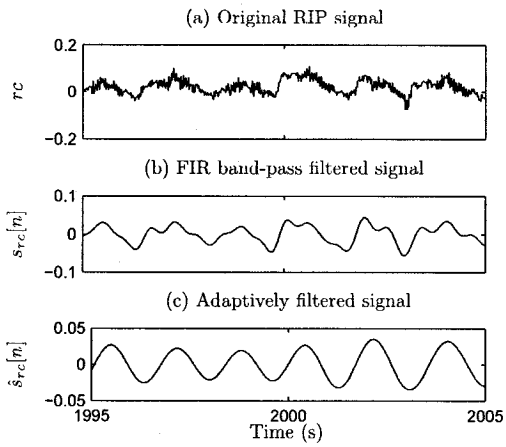

Figure 5–2: Example segments of an RIP signal obtained from a 47 weeks old infant weighing 4.8 kg. (a) is the original RIP signal, (b) is the same RIP signal filtered with the filter described in [5], and (c) is the adaptively filtered version of the RIP signal obtained with the new method. The adaptively filtered version of the signal clearly has the highest signal-to-noise ratio.

5.3.3 Phase Estimation Algorithm and Asynchrony Detection

Phase Estimation Algorithm

A prerequisite for the automated detection of obstructive apnea using RIP is a robust procedure for estimating the phase difference between thoracic and abdominal signals. This phase estimate can be used to determine if asynchrony is present and, in turn, determine if an obstructive event is present. Thus, we developed an automated phase estimation algorithm in [5]. This phase estimation method has the advantage of working with uncalibrated RIP measurements and providing a quantitative phase estimate (ϕ) in the 0 to 180 degree range.

The method presented in [5] is used in this paper with a slight modification. In the first step of the algorithm, an adaptively filtered version of the RIP signals replaces the band-pass filtered RIP signals. The adaptively filtered signals are used because they have a higher signal-to-noise ratio when compared to the band-pass filtered RIP signals used in [5] (the adaptively filtered signals were filtered with narrower band-pass filters which increased their signal-to-noise ratio, Fig. 5–2 shows an example). A description of the adaptive filtered signals is given below.

In the remaining steps of the algorithm, a binary converter, a logic gate and a low pass filter (used to take the average value over a window of size N) are used to generate a phase estimate in the 0 to 180 degree range (refer to [5] for more detail).

Asynchrony Detection

Following [5], an improved phase estimate $\phi_I[n]$ is obtained by correlating $\phi[n]$ with the movement detector output $\delta(T)$; this correlation can be written as,

$$\phi_I[n] = \phi[n](1 - \delta(T)) \tag{5.9}$$

Equation (5.9) states that any phase estimate is set to zero, and not considered, if movement artifact is detected ($\delta(T) = 1$). Once the phase estimate $\phi_I[n]$ is obtained it is used to determine if the RIP signals are asynchronous. Hence, $\phi_I[n]$ and the threshold γ_2, are used to decide

$$\delta(\phi) = \begin{cases} 1, \text{if } \phi_I > \gamma_2 \\ 0, \text{if } \phi_I \leq \gamma_2 \end{cases} \tag{5.10}$$

The comparator of equation (5.10) chooses the hypothesis $\mathcal{H}_1^a$ if $\phi_I[n] > \gamma_2$ or the hypothesis $\mathcal{H}_0^a$ if $\phi_I[n] \leq \gamma_2$. Where the hypotheses are:

$$\begin{gathered} \mathcal{H}_0^a\text{: Asynchrony Absent} \\ \text{vs.} \\ \mathcal{H}_1^a\text{: Asynchrony Present} \end{gathered} \tag{5.11}$$

Adaptive Filtering

The multiplexer in Fig. 5–1 is used to adaptively filter the RIP signals as follows: the n^{th} sample of $\hat{s}_{ab}$ is generated by selecting the n^{th} sample of ab_{fi}, where i is chosen according to the $\hat{f}_{max}$ value at the n^{th} sample. If the $\hat{f}_{max}$ value is zero at a given sample, indicating artifact presence, then the high passed RIP signal ab is used to generate $\hat{s}_{ab}$.

$$\hat{s}_{ab}[n] = \begin{cases} ab[n], \text{ if } \hat{f}_{max}[n] = 0 \\ ab_{fi}[n], \text{ if } \hat{f}_{max}[n] \neq 0, \text{ where } i = \hat{f}_{max}[n] \end{cases} \tag{5.12}$$

Thus, at each sample, $\hat{f}_{max}$ (the breathing frequency estimate) determines which filter output to select to generate the signals $\hat{s}_{rc}[n]$ and $\hat{s}_{ab}[n]$, the adaptively filtered versions of the ribcage and abdominal signals respectively. Note that to remove offsets and exponential decays observed in real infant data, a high pass filter with a cut-off frequency equal to 0.05 Hz was used to generate *ab* (refer to Fig. 5–1).

5.3.4 Combining the Detectors

Fig. 5–1 shows the overall block diagram including all three detectors. The outputs $\delta(\phi_I)$, $\delta(T)$, and $P[n]$ are the decisions used to automatically detect asynchrony, movement artifact and pauses respectively.

Note that $\delta(T)$ is set to one (i.e. true) if both the ribcage and abdomen signals have artifact present (achieved by using an AND-gate on the decisions $\delta(T^{ab})$ and $\delta(T^{rc})$); similarly, the pause output $P[n]$ is true if both the ribcage and abdomen signals are deemed to be 'flat' (achieved by using a NOR-gate on the decisions $\bar{p}_{ab}[n]$ and $\bar{p}_{rc}[n]$).

5.4 Method Validation: Application to Infant Data

5.4.1 Description of Infant Data

We now consider segments in breathing periods from 19 infants (21 data files) aged 44 $\pm$ 5 weeks (postconceptional age), weighing 4.0 $\pm$ 1.5 Kg (refer to Table 5–2). These data were previously reported by Brown *et al.* [7]. The infants had undergone elective hernioraphy with general and/or caudal anesthesia. Data were obtained following written informed parental consent and appropriate Institutional Ethics Review Board approval. Nineteen data sets were obtained from infants immediately after surgery, and two data sets were obtained from 2 infants less than 24 hours after surgery. The measured continuous-time ribcage and abdominal signals (NIMS^{TM}, Respitrace Plus, North Bay Village, Florida), were amplified, low-pass filtered at 15Hz with 8-pole Bessel filters (Frequency Devices, Haverhill, MA), and sampled at 50 Hz with a 12-bit analog-to-digital converter (Data Translation, Marlborough, MA). Data were stored on a computer using LABDAT^{TM} data acquisition software (RHT-InfoDat, Montreal). No attempt was made to calibrate the signals in absolute terms.

5.4.2 Analysis of Infant Data

The visual scoring of the 21 infant data sets was considered to determine the methods' effectiveness on clinical data. Note that the asynchrony and movement artifact detectors were tested on simulated data in [5] and [9]; the studies showed that the detectors correctly flag artifacts and asynchronies.

The data were visually scored by K. A. Brown (MD). Respiratory events were defined as:

1. Pauses: Periods with little or no respiratory movement in both the ribcage and abdominal signals.
2. Quiet Breathing: Periods with quasi-sinusoidal breathing patterns in both the ribcage and abdominal signals.
3. Asynchronous Breathing: Periods with asynchronous movement between the ribcage and abdominal signals.
4. Movement Artifact Corruption: Periods with non-sinusoidal like signals typical of movement corruption.
5. Obstructive Apnea: Periods with at least one breath of asynchronous breathing followed and/or proceeded by a pause.

Fig. 5–3 shows representative segments of each of these events. The definitions enumerated above are general, the events are ultimately defined by the visual scorer in accordance to regular clinical practice.

Visual scoring of the data sets was achieved as follows. Four signals were recorded for each subject, namely, the ribcage and abdomen signals by Respitrace (NIMS^{TM}, Respitrace Plus, North Bay Village, Florida), blood oxygen saturation and pulse rate signals by Nellcor N-200 (Nellcor Inc., Hayward, CA). The data were examined using a visual scoring tool that allowed the investigator to mark the start and end times of pauses, asynchronous breathing, movement, quiet breathing and obstructive apnea segments. The visual scoring tool was developed using Matlab 7.0 (The Mathworks, Inc, Natick, MA) to provide a convenient graphical user interface to facilitate the marking of event type and timing. Event start and end times were selected by the scorer by positioning 2 cursors. Once this selection was completed, the data within the selection was highlighted, allowing

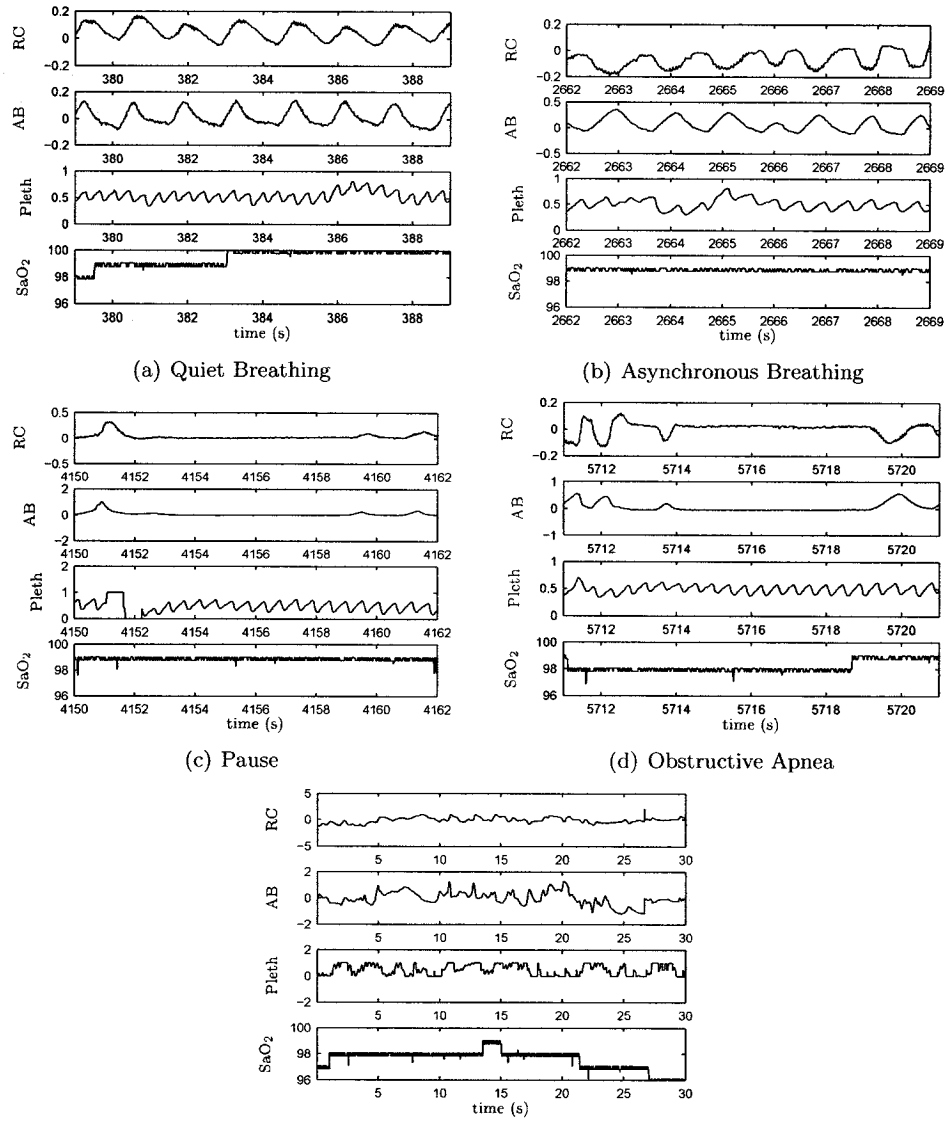

(a) Quiet Breathing

(b) Asynchronous Breathing

(c) Pause

(d) Obstructive Apnea

(e) Movement Artifact

Figure 5–3: Example segments from the visual scoring of infant data. The examples shown are from a 49 weeks old infant (postconceptional age), weighing 5.9 kg. (a) Quiet Breathing segment, (b) Asynchronous breathing segment, (c) Pause Segment, (d) Obstructive apnea segment and (e) Movement artifact segment. Note that the ribcage (RC) and abdominal (AB) RIP signals were obtained by Respitrace (NIMS^{TM}, Respitrace Plus, North Bay Village, Florida); the blood oxygen saturation (SaO_2) and pulse rate (Pleth) signals were obtained with the Nellcor N-200 (Nellcor Inc., Hayward, CA).

the scorer to visualize the selection. If satisfied with the selection, the scorer associated the selection with a respiratory event which automatically stored the event start and end times with 0.02 second precision. The data were scored in 30 second windows (epochs); any visual marking that spanned more than one epoch was concatenated into a single event.

Database Content

The number of visually scored segments in the database is given in Table 5–3.

Breathing Frequency Estimation Accuracy

To determine the effectiveness of the breathing frequency estimate $\hat{f}_{max}$, 429 quiet breathing segments were analyzed using ANADAT version 5.2 (RHT-InfoDat, Montreal, 1995) and ABREATH (RHT-InfoDat, Montreal, 1994). These segments were obtained from a previous analysis preformed at MCH. The analysis was conducted as follows: 429 segments were isolated with ANADAT and then inputted as volume signals in the ABREATH software, which identified the inspiratory and expiratory times of each breath in the segments. This breath identification was visually examined by the scorer; if the breath identification was adequate, the average breathing frequency for each segment was stored.

Next, the average breathing frequency obtained using the ABREATH analysis was compared to the average breathing frequency estimate ($\hat{f}_{max}$) obtained with our method for each of the 429 segments. 90.0% of the segments were in agreement for both methods; that is, for each segment, the frequency estimate obtained with the ABREATH analysis was within the frequency range $\hat{f}_{max}$ for 90.0% of the segments. The remaining 10.0% of the segments were slightly different (just out of the frequency range $\hat{f}_{max}$). This demonstrates that the $\hat{f}_{max}$ values can be used to determine the breathing frequency of infant quiet breathing segments. The new methods permits for fully automated, less time consuming, objective, and repeatable analysis when compared to the ABREATH method and visual scoring.

Comparison to Visual Scoring

Movement Artifact Detection: We now present the probability density functions (pdf) of the test statistic used in the segmentation of cardiorespiratory data relative to visual scoring. The segmentation test statistic (T^{ab}) is normalized and denotes the same power ratio for all data; that

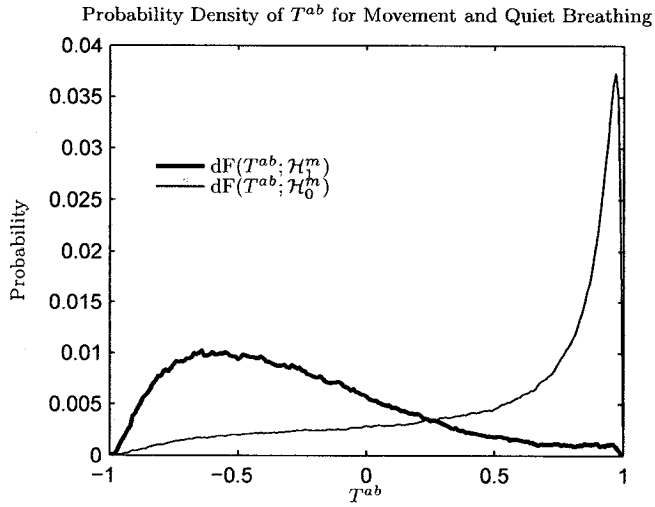

Figure 5–4: Pdf of the movement artifact detector test statistic (T^{ab}) for all 21 data files under the hypotheses $\mathcal{H}_0^m$ (movement artifact absent) and $\mathcal{H}_1^m$ (movement artifact present). The T^{ab} values were calculated using a window size of N = 251 samples (i.e. 5 seconds at 50 Hz).

is, T^{ab} is always a value in the range [-1, 1] representing the amount of signal power in the expected movement artifact range relative to the amount of the signal power in the expected breathing frequency range.

Fig. 5–4 shows the pdf of T^{ab} over segments visually identified as quiet breathing and gross body movement for all 21 data files; that is under $\mathcal{H}_0^m$ and $\mathcal{H}_1^m$, respectively. We derived the hypotheses $\mathcal{H}_0^m$ and $\mathcal{H}_1^m$ from the visual scoring done by K. A. Brown. The figure shows that the pdf is fairly spread out with little overlap, indicating that the test statistics T^{ab} can be used reliably to identify movement artifact in real infant data.

The performance of the proposed artifact detector, compared to visual scoring, is summarized in the receiver operating characteristic (ROC) for the test statistics T^{ab}. The ROC plot is presented in Fig. 5–5.

Note that P_{FA} denotes the probability of false alarm, and P_D denotes the probability of detection. From the pdf of T^{ab} shown in Fig. 5–4, P_D and P_{FA} for a given threshold γ can be found by solving,

$$P_D = \int_{-1}^{\gamma} dF(T^{ab}, \mathcal{H}_1^m),\ P_{FA} = \int_{-1}^{\gamma} dF(T^{ab}, \mathcal{H}_0^m) \tag{5.13}$$

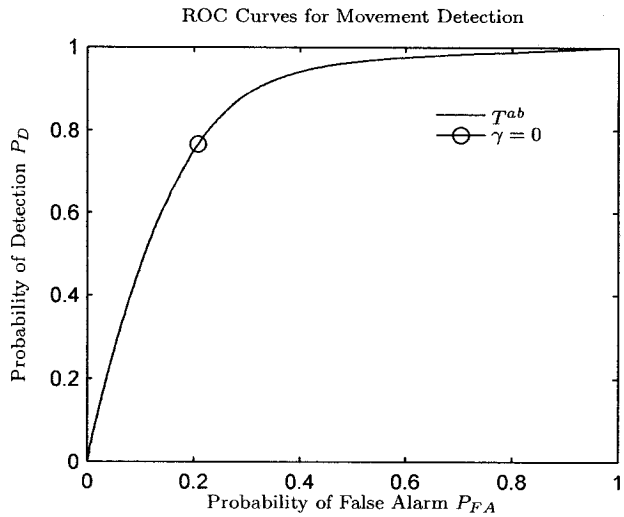

Figure 5–5: Receiver operating characteristic for the movement artifact detection in all 21 infant data sets. The circle indicates the probabilities for $\gamma = 0$.

Each P_D and P_{FA} pair in the ROC plot is obtained for a unique threshold value. Thus, the choice of threshold determines the trade off between P_D and P_{FA}.

Asynchronous Breathing Detection: Similar to the movement artifact detector test statistic, the test statistic used to detect asynchronous breathing (ϕ) is normalized and denotes the same phase estimate for all data; that is, ϕ is always a value in the range [0, 1] representing the degree of asynchrony between the ribcage and abdominal signals.

Fig. 5–6 shows the pdf of ϕ over segments visually identified as quiet breathing and asynchrony for all 21 data files; that is under $\mathcal{H}_0^a$ and $\mathcal{H}_1^a$, respectively.

Note that the pdf of the asynchrony detector did not show as much separation as obtained for the movement artifact detector. This can be attributed to the fact that the phase estimate obtained with the automated method is more precise, less biased and more consistent than a phase estimate obtained with the 'eyeball' approach used in visual scoring.

The performance of the proposed asynchrony detector, compared to visual scoring, is summarized in the receiver operating characteristic (ROC) for the test statistics ϕ shown in Fig. 5–7.

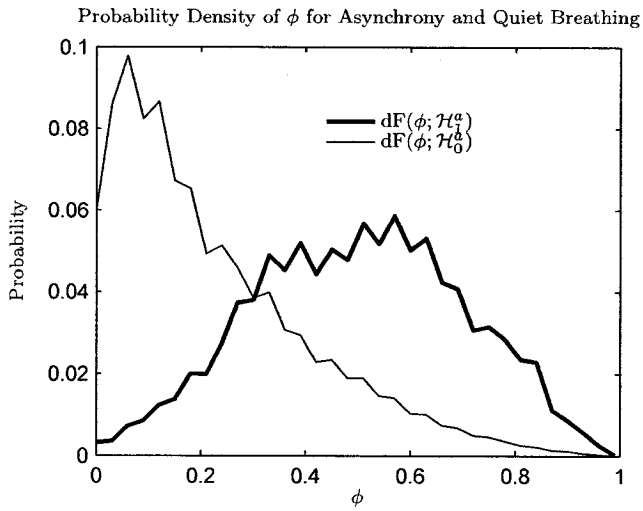

Figure 5–6: Pdf of the asynchrony detector test statistic (ϕ) for all 21 data files under the hypotheses $\mathcal{H}_0^a$ (asynchrony absent) and $\mathcal{H}_1^a$ (asynchrony present). The ϕ values were calculated using a window size of N = 251 samples (i.e. 5 seconds at 50 Hz).

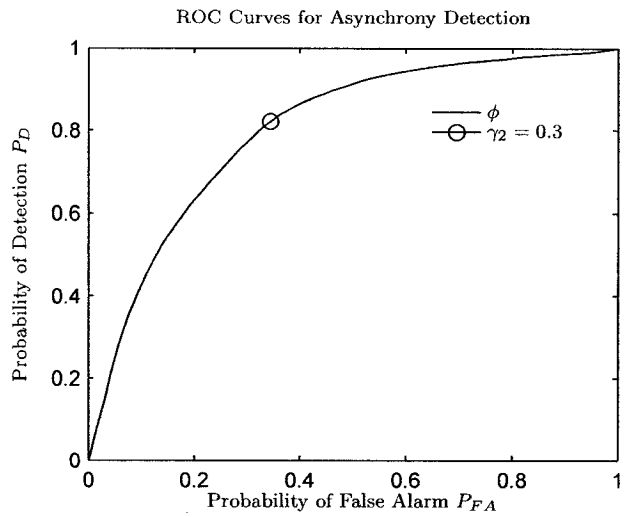

Figure 5–7: Receiver operating characteristic for asynchrony detection in all 21 infant data sets. The circle indicates the probabilities for $\gamma_2 = 0.3$ (54 degrees).

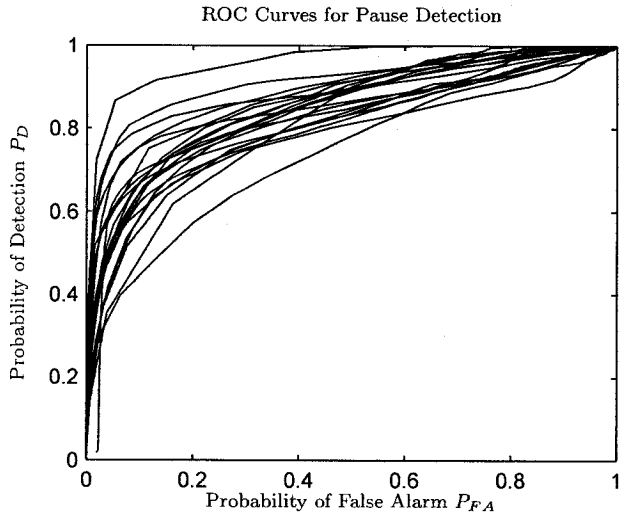

Figure 5–8: Receiver operating characteristic for pause detection for each of the 21 infant data sets. The test statistic used was $E_3^{ab}[n, N_1]$ with a window size $N_1 = 51$ samples.

Similar to equation (5.13), the P_D and P_{FA} pairs plotted in Fig. 5–7 for a given threshold γ_2 can be found by solving,

$$P_D = \int_{\gamma_2}^{1} dF(\phi, \mathcal{H}_1^a),\ P_{FA} = \int_{\gamma_2}^{1} dF(\phi, \mathcal{H}_0^a) \tag{5.14}$$

Pause Detection: The test statistic used for pause detection (E_3^{ab}) is not normalized; that is, the pdf of the RMS energy for each patient differs. Thus, we must consider the ROC plots of each data file separately. Fig. 5–8 shows the performance of the pause detector for the 21 data files. The ROC curves differ for each file due to the quality of the signals in each recording and visual scoring inconsistencies.

Note that for Fig. 5–8, P_D and P_{FA} for a given threshold γ_1 can be found by solving

$$P_D = \int_{0}^{\gamma_1^{ab}} dF(E_3^{ab}, \mathcal{H}_1^p),\ P_{FA} = \int_{0}^{\gamma_1^{ab}} dF(E_3^{ab}, \mathcal{H}_0^p) \tag{5.15}$$

where $dF(E_3^{ab}, \mathcal{H}_1^p)$ and $dF(E_3^{ab}, \mathcal{H}_0^p)$ are the pdfs for the test statistic E_3^{ab} under the hypotheses $\mathcal{H}_1^p$ (*pause present*) and $\mathcal{H}_0^p$ (*pause absent*) respectively.

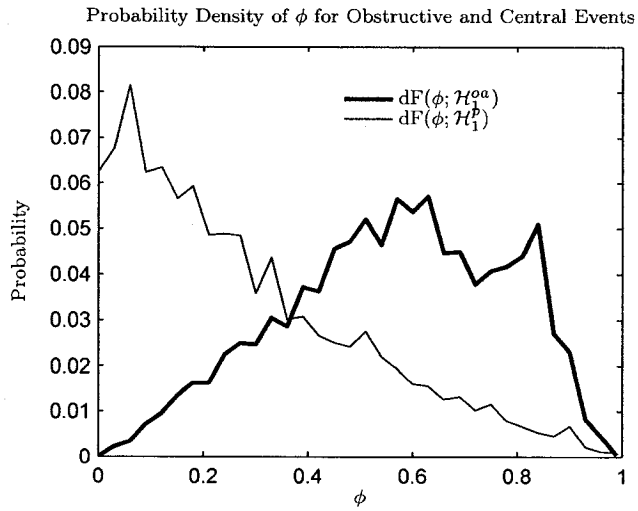

Figure 5–9: Pdf of the asynchrony detector test statistic (ϕ) for all 21 data files. The two density functions shown are for events visually identified as obstructive apnea ($\mathcal{H}_1^{oa}$) and events visually identified as pauses ($\mathcal{H}_1^{p}$). Note that pauses within obstructive apnea events were excluded from $\mathcal{H}_1^{p}$.

Distinguishing between Obstructive and Central Apnea Events: The test statistic ϕ which is used to detect asynchronous breathing can also be used to discriminate between central and obstructive apnea events. Fig. 5–9 shows the pdf of ϕ for obstructive apnea and central pause events (2054 central pause segments and 355 obstructive apnea segments). Although the figure has some overlap, the figure shows that in general, obstructive events have high ϕ values, while the central events have lower ϕ values; indicating that it is possible to use ϕ to distinguish between obstructive and central apnea events.

Note that the high values of ϕ in the pdf of central events can be attributed to visual scoring inconsistencies, as well as, trends and decays observed in the RIP data that affected the phase estimate obtained. On the same note, the lower ϕ values for obstructive events can be attributed to the visual identification of the start and end of theses events. These events consisted of asynchronous breaths followed by or containing pauses; the consideration of pauses in obstructive events lead to lower phase value estimates.

5.4.3 Automated Threshold Selection

The ROC plots above show that it is of great importance to select the appropriate threshold for each detector. This threshold selection can be time consuming and difficult if no prior knowledge of event distributions is known before analysis. Thus, we developed an automated threshold selection technique to provide the user with an estimate of the threshold to use for pause, asynchrony and movement artifact detection.

The thresholds for asynchrony and movement artifact detection can be set to a specific value for all infant data since they are normalized. We are able to obtain a phase estimate using our method, thus to detect asynchrony, we automatically set the asynchrony threshold (γ_2) to 0.3. Using $\gamma_2 = 0.3$ is equivalent to deciding *asynchrony present* if a phase estimate of 54 degrees or greater between the RIP signals is obtained. We choose to use this value from the phase estimate pdf of asynchronous and quiet breathing events (Fig. 5–6). A similar phase value was used to detect asynchrony in [83].

To determine if movement artifact is present, we automatically set the movement artifact threshold (γ) to 0. This 0 value was chosen since it is equivalent to deciding *artifact present* if most of the signal power is in the expected artifact frequency range; otherwise, if most of the signal power is in the expected breathing frequency range we decide *artifact absent.* In addition, Fig. 5–5 shows that $\gamma = 0$ provides a good trade off between P_D and P_{FA}.

It is more difficult to automatically select a threshold γ_1 for pause detection since the test statistic used in the pause detector is not normalized. Hence, each file requires a unique threshold. We will consider the threshold selection for the abdominal RIP signal (an identical process applies for the ribcage signal). To automatically select γ_1^{ab}, we first found optimal thresholds for each of the 21 data sets. These optimal thresholds were chosen using the Neyman-Pearson detection criterion with $\alpha \leq 0.2$ [78], where the criterion is

$$\max_{\gamma_1^{ab}} \{P_D(\gamma_1^{ab}) : P_{FA}(\gamma_1^{ab}) \leq \alpha\} \tag{5.16}$$

and α is a bound on the false alarm probability. Equation (5.16) states that we find the threshold γ_1^{ab} that maximizes P_D while preserving P_{FA} to less than or equal to α (in our case we use $\alpha = 0.2$

or 20%); these values were obtained by finding the threshold that resulted in a $P_{FA} = 0.2$ on the ROC curve for each of the patient files.

To investigate the possibility of setting γ_1^{ab} using the statistical properties of the test statistic E_3^{ab}, a least squares fit between the optimal thresholds and the statistical properties of E_3^{ab} was performed. The mean (μ), standard deviation (σ), maximum value (max) and median (me) of E_3^{ab} for each patient file were used as inputs; the corresponding optimal thresholds were used as desired outputs. This least squares fit provided the following equation to automatically set the threshold γ_1^{ab} for each file,

$$\begin{aligned} \gamma_1^{ab} &= -0.005 - 0.6902\mu + 0.0148max \\ &\quad +0.1284\sigma + 1.1686me \end{aligned} \tag{5.17}$$

The percent variance account for (%VAF) between the optimal thresholds and the automatically set thresholds was found to be 98.62%. Thus, we are able to automatically set γ_1^{ab} for each patient file using the statistical properties of E_3^{ab}. Table 5–4 presents the optimal thresholds for each patient file and the corresponding thresholds obtained using equation (5.17) (second column).

To test the effectiveness of this automated pause threshold selection on new data, a leave one out validation was used. The automated thresholds obtained in the leave one out validation are presented in the third column of Table 5–4. Table 5–4 shows that the thresholds obtained for the leave one out validation and the thresholds obtained using equation (5.17) were similar. The %VAF between the optimal thresholds and the leave one out thresholds was found to be 95.34%. Thus, we can reliably say that equation (5.17) can be used to estimate the pause threshold for new data.

Effectiveness of Automated Threshold Selection

The automated threshold selection technique presented above was applied to all 21 data files to detect pauses, asynchrony and movement artifact segments. We obtained the following probabilities of segment detection (P_D^s) and false alarm (P_{FA}^s) relative to visual scoring:

- Artifact detection: $P_D^s = 80\%$ and $P_{FA}^s = 19.7\%$.
- Pause detection: $P_D^s = 82.1\%$ and $P_{FA}^s = 5.6\%$.
- Asynchrony detection: $P_D^s = 78.8\%$ and $P_{FA}^s = 20.1\%$.

The probabilities given above are the mean values for the entire data set; the probabilities of detection and false alarm for each patient file is given in Table 5–5 and Table 5–6.

The results suggest that it could prove useful to use the three detectors along with the threshold selection technique to detect pauses, asynchrony and movement artifact in real infant data. However, in certain cases, such as files with very noisy data, human intervention may be required to adjust thresholds accordingly.

Note that the probabilities of segment detection (P_D^s) and false alarm (P_{FA}^s) were obtained as follows. As a general rule, the probabilities were determined on a segment by segment basis; a detection was considered if the method detected a segment at least half as long and encapsulated by the visually scored equivalent segment.

5.5 Concluding Remarks

The methods for asynchrony, movement and pause detection perform well for all the infant data studied. These methods provided results that were comparable to the visual scoring, with 80% agreement between the automated method results and visual scoring. The main advantages of these methods are: 1) full automation and simple implementation; 2) less time consuming than visual scoring; 3) repeatable and standardized analysis; and 4) applicable to uncalibrated RIP signals. This last point is of great importance since the Qualitative Diagnostic Calibration method for RIP has been shown to be limited by changes in measurement conditions and breathing patterns [60].

In summary, we have presented a method to allow for the detection of the lack of breathing effort, paradoxical respiratory movement and movement artifact corruption in infant RIP data. The method also generates a breathing frequency estimate and is well suited for the off-line study of long data records such as studies of sleep disordered breathing.

Furthermore, since there is no consensus on the definition of both OSA and CSA for infants [73,74], the presented methods are meant to provide the user with the ability to detect these events relative to their preferred definition. Thus, CSA events can be defined as pauses of a given length, while OSA events can be defined as periods with some degree of asynchrony between the RIP signals for a given amount of time. Future studies will explore the methods' effectiveness in detecting apneas of specific definitions and lengths.

Table 5–2: Patient Files Used in Database

Study ID	Weight (kg)	PCA[1] (weeks)	File Length (hrs)	Gender
ARC	4.8	47	7.48	M
SHIF	3.9	42	7.87	M
BJUT	5.7	48	10.55	M
LACR3	3.6	41	8.08	M
LAMP	4.3	45	3.94	M
MOSS	5.4	45	5.04	M
MUR	5.5	45	4.25	M
CLEM	3.5	48	11.90	F
DIAB	3.8	45	5.22	M
MAX	3.8	44	5.11	M
PETR	2.5	42	12.71	F
BAL2	4.8	48	6.32	M
MICH	5.9	49	3.24	M
CALEB	3.2	45	3.76	M
GAB	3.0	41	23.20	M
GEPL2	4.3	39	11.30	M
LAL3	4.3	44	2.98	M
LOT2	4.5	46	4.88	M
MAR2	2.5	42	2.46	M
GAB2	3.0	41	23.20	M
MART3	2.5	42	2.46	M

[1] PCA is the postconceptional age.

Table 5–3: Database Content

Event	Number of Segments
Pauses	2399
Quiet Breathing	4554
Asynchronous Breathing	1156
Movement Artifact Corruption	2760
Obstructive Apnea	355

[1] The number of segments presented in this table was obtained from visual scoring.

Table 5–4: Automated Pause Threshold Selection for the Abdominal RIP Signal

File Number	Optimal Threshold (γ_1^{ab})	21 File Regression Threshold (γ_1^{ab}) [1]	20 File Regression Threshold (γ_1^{ab}) [2]
1	0.04	0.0603	0.0621
2	0.08	0.0613	0.0510
3	0.14	0.1424	0.1426
4	0.36	0.3438	0.3216
5	0.04	0.0432	0.0435
6	0.19	0.1982	0.1997
7	0.11	0.1156	0.1156
8	0.05	0.0472	0.0469
9	0.08	0.0948	0.2216
10	0.06	0.0975	0.1217
11	0.28	0.2962	0.3033
12	0.25	0.2452	0.2396
13	0.04	0.0342	0.0333
14	0.03	0.0240	0.0232
15	0.04	0.0352	0.0346
16	0.15	0.1628	0.1652
17	0.07	0.0797	0.0807
18	0.23	0.1980	0.1773
19	0.09	0.0976	0.0982
20	0.03	0.0263	0.0259
21	0.10	0.0566	0.0501

[1] Threshold obtained using all 21 files in the least squares fit
[2] Threshold obtained using the other 20 files in the least squares fit

Table 5–5: Automated Pause and Movement Detection Performance for Each Patient

File Number	Pause Detection (P_D^s)	Pause False Alarm (P_{FA}^s)	Movement Detection (P_D^s)	Movement False Alarm (P_{FA}^s)
1	68.75	7.0	53.0	16.4
2	70.9	2.6	81.25	20.0
3	89.6	4.2	92.9	11.2
4	81.5	3.3	73.1	8.0
5	82.5	9.6	81.2	14.3
6	90.0	5.2	89.8	8.3
7	92.6	4.2	87.2	18.5
8	55.5	2.2	77.4	29.5
9	85.7	6.2	75.8	20.8
10	92.4	33.8	80	21.1
11	92.2	4.6	81.7	19.8
12	82.2	5.5	85.3	18.0
13	65.1	1.7	89.6	3.6
14	51.4	0.9	84.3	35.2
15	100.0	0.0	85.7	47.1
16	96.7	10.4	88.7	23.7
17	86.8	2.1	88.3	10.9
18	90.5	4.0	90.0	27.3
19	83.8	5.9	45.5	6.0
20	91.4	3.6	89.7	23.5
21	75.0	1.3	60.0	31.4

Table 5–6: Automated Asynchrony Detection Performance for Each Patient

File Number	Asynchrony Detection (P_D^s)	Asynchrony False Alarm (P_{FA}^s)
1	83.6	36.3
2	84	38.8
3	88.4	46.7
4	61.5	3.4
5	78.1	21.2
6	71.7	7.5
7	73.5	10.1
9	66.7	31.25
10	70.3	11.9
12	83.3	16.9
13	93.8	46.1
16	97.7	6.4
17	100.0	17.4
18	63.6	10.4
19	62.3	40.3
20	84.4	30.5
21	76.5	34.3

[1] Note that not all patients had asynchronous breathing episodes.

CHAPTER 6
Summary and Future Work

The aim of this thesis was to:

1. develop automated off-line methods for the detection of pauses, asynchronies and movement artifacts in cardiorespiratory data
2. develop a tool to facilitate precise visual scoring of cardiorespiratory data
3. validate the off-line methods by comparing them to visual scoring
4. develop a tool for a fully automated off-line analysis of cardiorespiratory data using the off-line algorithms

These aims were met with the completion of this thesis. We presented new automated off-line methods that focus on the analysis of the frequency content of RIP signals to detect pauses, asynchronies and movement artifacts (aim 1). These methods were integrated into a new tool named *Offline* developed to permit fully automated and rapid off-line analysis of cardiorespiratory data (aim 4). We also developed a new tool named *ApneaScore* which acquires precise visual scoring of cardiorespiratory data; this tool was used by Dr. Brown at the MCH to annotate the infant database used (aim 2). The data obtained with *ApneaScore* were then used to assess the new methods effectiveness relative to visual scoring (aim 3).

Method Effectiveness

The new off-line methods were applied to infant data acquired postoperatively at the MCH. A comparison between the detection obtained with the automated methods and visual scoring was presented. This comparison was presented in a point by point evaluation in the ROC curves (Chapter 5 and Appendix D). An overlapping segment comparison was also presented and provided the probabilities of agreement (P_{Agr}) and disagreement (P_{Dis}) between visual scoring and automated detection presented in Table 6–1.

The probabilities presented in Table 6–1 were obtained for the entire MCH infant database. Performance varied from file to file as shown in Appendix D. The differences may be attributed to the natural differences in the breathing patterns of each infant, and most importantly, to the quality of the recorded RIP signals.

The results show that there is 80% agreement between the automated method and visual scoring. We suggest that this amount of agreement is comparable to that between visual scorers. In fact, a comparison between the visual scoring of PSG recordings from OSA patients in 16 different sleep laboratories [84] determined that moderate inter-scorer agreement existed for the detection of arousals during sleep, and relatively low inter-scorer agreement existed for apnea detection. The average inter-scorer agreement was 71.8%. Danker-Hopfe *et al.* [85] also showed that overall inter-scorer agreement was 76.8%. We believe that earlier studies [86–88] that reported as much as 87-95% agreement between scorers were imprecise because inter-scorer agreement was assessed based on scoring of single epochs. Thus, we conclude that the amount of agreement between visual scoring and the new automated method is comparable to inter-scorer agreement, which suggests that the new automated method can be reliably used in the clinical or home environment.

The results also showed that there was approximately 20% disagreement between visual scoring and automated detection of movement artifacts and asynchronies. The disagreement rate was lower (5.6%) for pause detection. The disagreement between visual scoring and automated detection can be explained by:

- Errors in visual scoring; for example, an asynchrony segment with a phase difference only slightly above the asynchrony threshold can be missed by the scorer but detected by the method.
- Errors in the automated scoring; for example, quiet breathing signals with very low energy can be detected as pauses by the method.
- Visual scoring inconsistencies; for example, segments with the same phase difference can be labeled differently by the scorer.

Irrespective of the cause, most of the disagreement between the method and visual scoring occurred in segments that were not significant respiratory events. Perhaps a topic for future work, would

Table 6–1: Performance of On-line and Off-line Detectors Relative to Visual Scoring

	Probability of Agreement (P_{Agr})	Probability of Disagreement (P_{Dis})
On-Line Artifact Detector	89.4%	45.3%
Off-Line Artifact Detector	80.0%	19.7%
On-Line Pause Detector	80.3%	5.7%
Off-Line Pause Detector	82.1%	5.6%
On-Line Asynchrony Detector	81.8%	35.5%
Off-Line Asynchrony Detector	78.8%	20.1%

be to evaluate the method relative to significant respiratory events alone (long pauses, significant asynchronies, etc.). This should lead to higher agreement and lower disagreement between visual scoring and automated detection.

Comparison to On-Line Methods Developed at McGill

A comparison between the off-line methods presented in this thesis and the on-line methods previously developed at McGill were also conducted. In summary, the performance of the off-line asynchrony and pause detectors were similar to their on-line equivalents; the on-line pause detector had slightly lower detection rates while, the on-line asynchrony detector had slightly higher false alarm rates. On the other hand, the new off-line artifact detector provided slightly lower detection performance but significantly reduced the rate of false alarms in comparison to its on-line equivalent. The probabilities of agreement (P_{Agr}) and disagreement (P_{Dis}) between visual scoring and automated on-line detection are presented in Table 6–1. The new off-line methods provide better trade-off between detection and false alarms.

Comparison to Other Methods

A literature review of home diagnosis of sleep apnea conducted by the American Academy of Sleep Medicine, the American College of Chest Physicians, and the American Thoracic Society was presented in [89]. The review reported a total of 49 studies, 16 of which used 7 to 4 channels of PSG recordings (including airflow measurements), and 33 of which used 4 or less signals without airflow measurement. These studies were reported to have sensitivities that ranged from 31-100% and specificities that ranged from 18-100%. Out of all methods, only one used RIP as a secondary

signal and had a sensitivity of 80%. This is similar to the detection agreement between our method and visual scoring which uses the RIP signals alone. This demonstrates that our method obtains results comparable to ones obtained with more complex devices.

Another method using RIP was presented in [44]. The method was most comparable to ours because it used RIP signals from infants to detect obstructive apnea. Results showed that 79.3% of obstructive apnea events were detected but only 10.9% of the detected events were true apneas [44]. Our method is advantageous since it generates similar detection without the high rate of false alarms.

Furthermore, It is important to note that other methods are often used commercially without adequate validation or publication; In [90], only nine out of more than thirty monitoring systems used to detect apnea were found to have published studies in peer-reviewed journals. In addition, a comparison to other methods is not always straight forward because other methods often use a different number of signals and respiratory sensors, and are often validated with adult data. However, we believe that our method is advantageous over others because: it is simple to implement, it is comfortable for the patient (works with RIP signals alone; requires less connection to the patient), it was meticulously validated, and it provides comparable results to those presented in the literature.

Off-Line Method Advantages

We believe that we have presented a novel approach that has been thoroughly validated and shown to be a plausible alternative to visual scoring. The method has the following advantages:

- It automatically detects pauses, asynchronies and movement artifacts
- It uses uncalibrated RIP signals
- It requires less time than visual scoring
- It can distinguish between obstructive and central apnea
- It generates a breathing frequency estimate
- It provides standardized and repeatable analysis

6.1 Future Work

The off-line algorithms presented in this thesis were developed for use with infant cardiorespiratory data. These algorithms can also be used for the analysis of cardiorespiratory data acquired from children. For use with children, the methods must be modified since children, and infants breathe at different rates; i.e. their quiet breathing frequency ranges differ. This would only require adjusting the algorithm filters and bandwidths to operate around the average expected breathing frequency of children. Conceptually the method remains unchanged. The application of the algorithms on adult data may be more complex since adults breath at much slower rates than infants. Thus, further studies are required to determine if the algorithms can be used on data obtained from adults.

The visual scoring of more than one scorer should be used to validate the method. Using segments commonly scored by more than one visual scorer will help distinguish between correct and erroneous scoring, which will allow for a better assessment of the method performance.

The integration of the automated off-line methods into the off-line option of the on-line portable monitor developed in [72] should be completed. A comparison between visual scoring and the automated methods on data acquired with the monitor should be performed. It is likely that the automated monitor will acquire data with fewer trends and decays (better AC-coupling than MCH monitor) which will improve results.

Furthermore, the analysis of the finger plethysmographic heart rate and the $\%SaO_2$ signals should be included to determine if they can be used to improve event detection. A 5% drop in $\%SaO_2$ is often used to detect apnea events in the literature. Although it is a delayed expression, it could be used as an additional factor in confirming potential apnea episodes. In addition, the finger plethysmographic heart rate signal seems to have a corrupted pattern during movement which can be used to confirm movement artifact segments.

There still exists no consensus on the definition of apnea events in children and infants. Reliable automated cardiorespiratory event detectors would be ideal to standardize cardiorespiratory event detection in children and infants. These methods can help reduce the diagnosis time for patients and allow for a better understanding of the pathophysiology of apnea.

Appendix A: ApneaScore GUI User Manual

ApneaScore User Manual

Ahmed Aoude

Department of Biomedical Engineering

McGill University

Motivation

ApneaScore is a graphical user interface (GUI) developed to facilitate precise visual scoring of cardiovascular data. The program permits the visual scoring of cardiorespiratory data by a trained technician. It was developed to acquire the data needed to validate and assess the accuracy of automated algorithms developed by Motto et al. [5, 6] for apnea detection. The lack of precise visual coding of cardiorespiratory data motivated the development of this tool for storage of visually scored data. This tool is used offline and helps generate accurate event statistics of clinically relevant events. The application was developed to allow for easy and accurate scoring of cardiorespiratory data. The application is user friendly with emphasis on the visual identification of events. Once analyzed, the visually scored data is stored in a MATLAB file (*.mat format), a format chosen for future use in MATLAB functions. The user also has the option of storing the data in Microsoft office excel format (*.xls format).

Installation

ApneaScore requires a computer with a basic MATLAB 7.0 R14 suit installation. To use ApneaScore the following steps have to be completed before its first use.

The user must make sure that all the files required for ApneaScore are installed on the computer that will be using the GUI. These files should be saved in a known location under a folder named **'GUI_ApneaScore'**.

The required files are:

1. **ApneaScore.m**
2. **CardiorespData.m**
3. **CardiorespData.fig**

4. **DataSetup.m**
5. **DataSetup.fig**
6. **fisttime.m**
7. **fisttime.fig**
8. **lastEpoch.m**
9. **lastEpoch.fig**
10. **ScorerInitials.m**
11. **ScorerInitials.fig**
12. **Start.m**
13. **Start.fig**
14. **ExcelSave.m**
15. **readlabdat.m**
16. **SortScored.m**

Once these files have been saved on the local machine, it is important to add the **'GUI_ApneaScore'** folder to the MATLAB path. This is done by opening MATLAB and choosing: **File->Set Path.**

Once selected the window in Fig A-1 will appear.

Select Add Folder, then browse to the folder **'GUI_ApneaScore'** and click **OK**. Once the OK button is clicked, the path should be added to the MATLAB search path list in Fig A-1.

For example, if you had saved the ApneaScore files under : **'C: GUI_ApneaScore'** this path would be present in the list as shown in Fig A-2.

Once the path is in the list, select **Save**.

After completing these steps you are ready to launch the ApneaScore application.

How to Use ApneaScore

To start the application type **ApneaScore** in the MATLAB command window and the application will load automatically. A window will open, as is shown in Fig A-3

Click **Start**, after which another window will open. Browse to the file containing the Labdat data. In that file, select the Labdat file to open (*.dat format) and click **Open**. This will load the cardiorespiratory data of that file. An example is shown in the Fig A-4.

If it is the first time you open the file the window in Fig A-5 will appear. Click **OK** to continue.

If it is not your first time opening the file, the window shown in Fig A-6 will appear. This is just a reminder of the last Epoch the user saved.

Click **OK** to continue.

Next, a window will open asking the user at which Epoch (30s segment of data) to start the display of the data. This allows users to continue from a previous save point or start from the beginning of the file. This window is depicted in Fig A-7.

Enter an Epoch integer in the text field to start the reviewing. An error message will appear if the user tries to enter an incorrect value in the Epoch field.

It is important to note that after selecting the starting epoch, the scored information for that epoch will be deleted. Hence re-scoring the first epoch is always necessary. This does not affect any other epochs.

Click **Done** to continue and start visual coding.

Next, the main window for scoring appears. This window displays the cardiorespiratory data, allows for the selection of the start and end time of the events, allows for event classification and allows for scrolling through the data in 30s segments.

To scroll through the data the **Next** and **Previous** buttons are used (shown in a red box in Fig A-8).

Next scrolls to the next 30s of data and, **Previous** scrolls to the previous 30s of data. An error message will appear if the user tries to scroll beyond the file length.

It is important to note that the message shown in Fig A-9 will appear if an epoch ***has already been seen but not necessarily scored***

The user must click **Yes** if he/she would like to re-score the epoch, or if he/she believes the epoch has not been scored, click **No** or **Cancel** otherwise.

Referring to Fig A-8, the button on the top right (**Choose Start and End Times**) is very important (located in the blue square of Fig A-8 above). Once clicked, this button allows for a cursor to be positioned unto the start time. Once positioned on the start time, the user must make one mouse click to select the start time. Next, the user must position the cursor for the end time

and click once. This will display the values of the start and end times in the yellow box of Fig A-8. Moreover, the corresponding plotted data will become red for the selection. If the user is unhappy with the selection, the user can simply re-click the **Choose Start and End Times** button and repeat the same steps until he/she is satisfied with the selection.

Fig A-10 shows an example of a user selected segment.

As shown in Fig A-10, the selection is now in red to help the user visualize his/her selection, and the values for start and end times are displayed in the text fields under the Choose Start and End Times button. If the user selects points outside the time axis an error message will advise him/her of the error.

Next to select the event that has been defined by the start and end times the user must click on the appropriate events present in the purple box of Fig A-8. Clicking any of the buttons stores the start and end times as the event specified by the button name. The user can choose multiple events for the same start and end time selection.

Users must be aware that clicking any button incorrectly will falsify the scoring. Caution has to be taken when selecting the event buttons.

If the user makes an error the **Delete button** (in the brown box of Fig A-8) can be selected. Clicking the **Delete button**, will delete **all** the scored data for the given epoch (30s segment). Hence, if the user decides to delete the information he/she would have to restart the scoring process for that epoch (30s segment). Once the user selects the **Delete** button a message asking the user if he/she is sure about deleting the information is shown. Clicking **Yes** will delete the information, clicking **Cancel** or **No** will not.

Once the user has finished scoring the file, or if the user would like to save the information and exit to continue later on, the user has to select the **Save(Done)** button (located in brown box of Fig A-8). Once selected a message asking the user if he/she is sure he/she wants to save and exit will appear. Clicking **Yes** will save the information, clicking **Cancel** or **No** will not.

Determining Epoch Location

The green box of Fig A-8 is used to determine the Epoch of current viewing.

Alternatively, to determine the current Epoch, just go to the MATLAB command prompt and the current Epoch will be the last epoch displayed in the command window.

Visually Scored Data Storage

The data visually scored by the clinician are stored in a *.mat format under the directory:

`S:\Biomed\REKLAB\Projects\Apnea\Sharing\MCH\DrBrownScoredFiles`.

The data is scored and saved using the GUI tool named ApneaScore.

Scored data is saved with the name scoredNAME.mat, where scored is always appended to the beginning to indicate that the file contains the scored information. The NAME portion of the filename is identical to the patient identification that is used to identify the LABDAT file containing the cardiorespiratory data (the *.DAT filename). An example is: For the ARC.DAT file, the file containing the scored data is named scoredARC.mat.

The visually scored data is stored into two MATLAB structures: VS and STAT (representing the two button groups on the GUI). Each structure contains an array for each scored respiratory event.

The VS structure contains the events: Glitch, Odd, Poor, None, Break, Tech, Sigh, OA, OH (OA), Sat (OA), Mixed Apnea, CA and PSA.

The STAT structure contains the events: Asynchrony, Pause, Movement, Norm Breath and Other.

Each event has its own array with n rows and 12 columns. The n rows are the n epochs (30s segments) of a file. Thus, the n^{th} row contains the data for the n^{th} epoch. There are 12 columns that represent the start and end times for a maximum of 6 occurrences for the same event type in a single epoch. Thus the odd columns (columns 1, 3, 5, 7, 9 and 11), represent the start times of the events and the even columns (columns 2, 4, 6, 8, 10 and 12) represent the end times of the events. The start and end times of a given event are stored in a pair of consecutive columns. Thus, columns 1 and 2 represent the start time and end time respectively for the first event in the epoch, columns 3 and 4 represent the start time and end time respectively for the second event, etc. The start and end times are stored in sample numbers (reminder: sampling frequency is 50Hz).

To view this data in MATLAB simply use the load command and view your workspace. In your workspace there will be two structures STAT and VS as well as a variable called Index_previous. Ignore the variable Index_previous as it is used by the developed GUI for other purposes. Once loaded the structures contain all the relevant data stored as described previously.

Excel Save

Once the user saves his/her data using the ApneaScore tool and finishes, a window will pop-up asking the user if he/she would like to save the data in excel format. If yes is selected a window asking for the scorer's initials then appears. The user enters his/her initials and then the save completes. The excel file is stored under the name: NAME_EVENTS.xls; where _EVENTS is always appended to the file name indicating that the file is the excel file containing the scored information, the NAME portion of the file name is identical to the patient identification that is used to identify the LABDAT file containing the cardiorespiratory data (the *.DAT filename). The data is store in sheet 1 of the excel file where each column is clearly labeled.

The nomenclature of the data file StudyID_EVENTS.XLS was created by A. L. Motto and is presented next. Each row corresponds to an event either scored visually or by means of an automated procedure.

RFILE raw data file associated with event

DATE event date

HH hour(event clock time)

MM minute (event clock time)

SS second (event clock time)

BTIME time elapsed from beginning of recording to beginning of scored event (msec)

ETIME time elapsed from beginning of recording to end of scored event (msec)

TYPE event type: FL-false apnea caused by low amplitude signal; FM-false event caused by movement; FO-false event caused by unspecified factor; GLITCH-sudden shift in the baseline of either the ribcage or abdomen signals; ODD-non-sinusoidal breathing pattern; POOR-poor quality signal in either the ribcage or abdomen signals; MVT- period of movement; BREAK-braking type pattern; TECH-technical problems (that is; broken leads, leads off, filter off

etc.); SIGH-large tidal breaths; OA-obstructive apnea episode; HA-hypopneas; SAT-decrease in 5% or more of oxygen saturation; MA- mixed apnea episode; CA-central apnea episode; PSA-post sign apnea episode;

SCORER scorer initials

POSITION sleep position: SUP-supine; LAT-lateral; PRO-prone; UNK-unknown

RS SP-sigh precedes event; SS-sigh succeeds event

RG quality of respiratory signal: G-good; PM-poor signal due to movement; PA-poor signal due to low amplitude; PO-poor signal due to other cause

RSSH NOSIN-non-sinusoidal or non-quasi-sinusoidal breathing

SQ quality of SaO2 signal: G-good; PM-poor signal due to movement; PA-poor signal due to low amplitude; PO-poor signal due to other cause

SCR_DATE date of scoring

SCR_COMMENT comments, if any

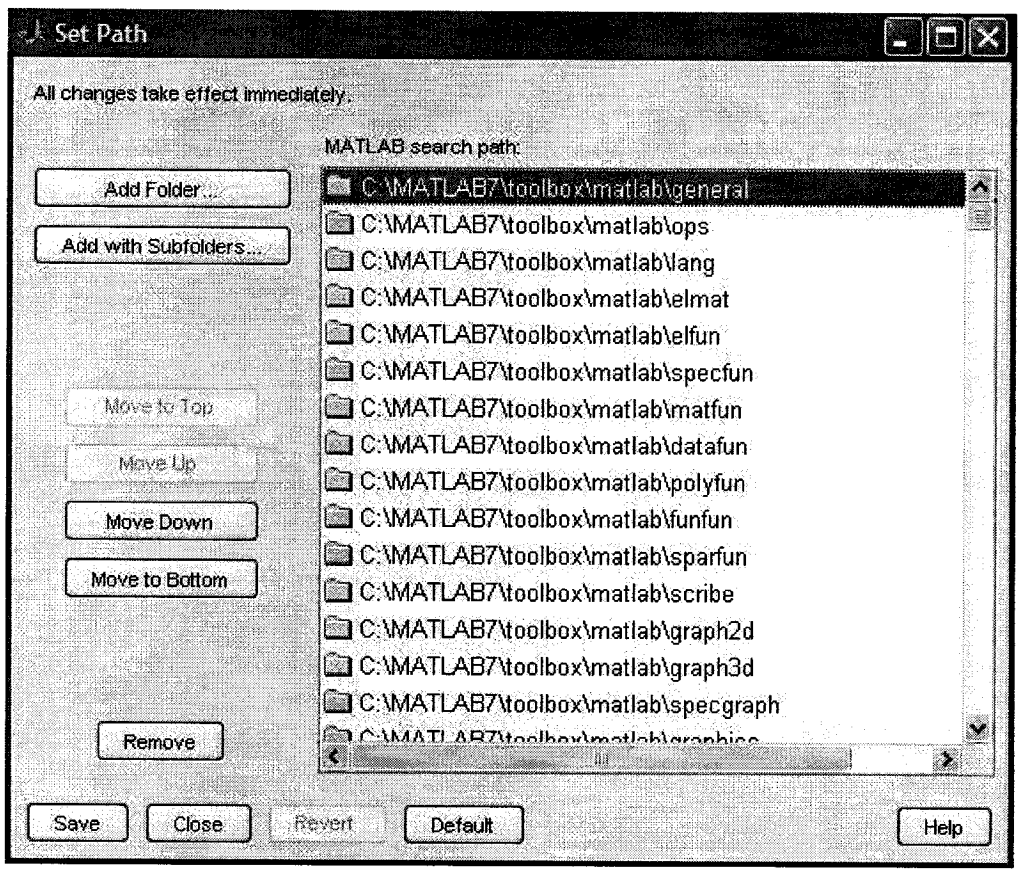

Figure A-1: Matlab set path window.

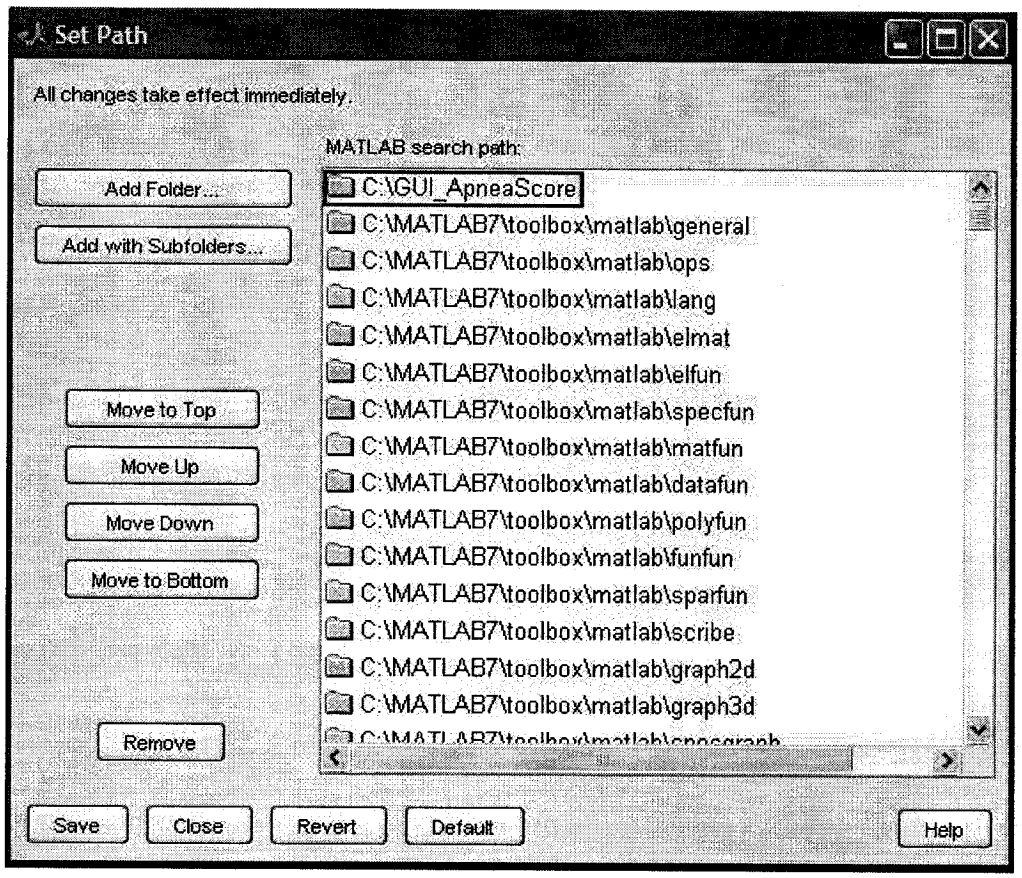

Figure A-2: Example of adding the file 'C: GUI_ApneaScore' in the Matlab set path window.

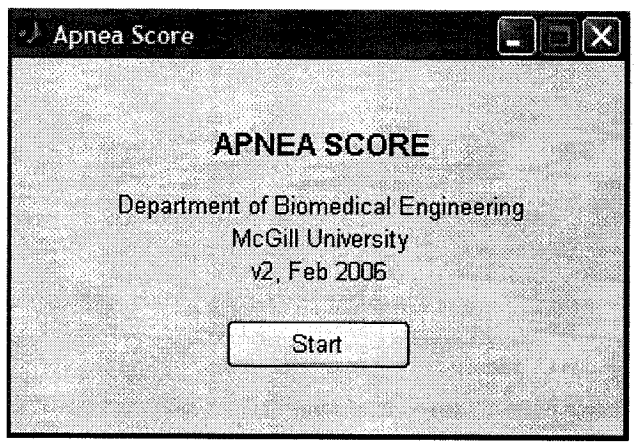

Figure A-3: Opening window of ApneaScore.

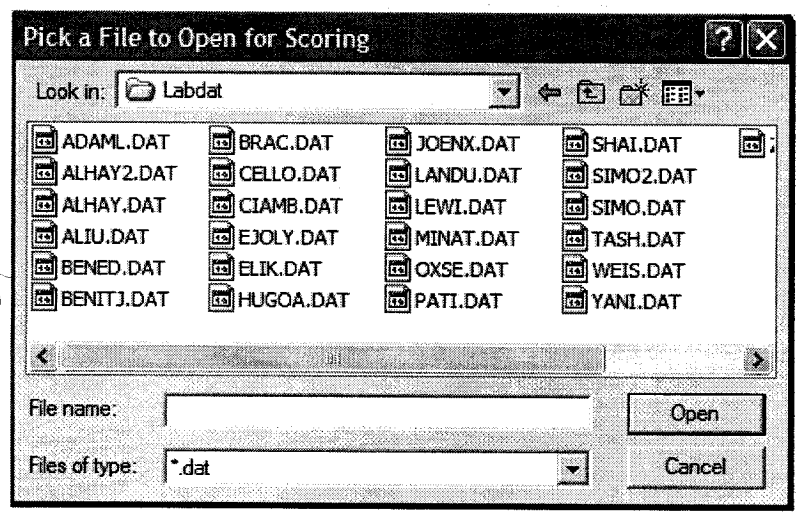

Figure A-4: Labdat file selection example.

Figure A-5: First-time window of ApneaScore.

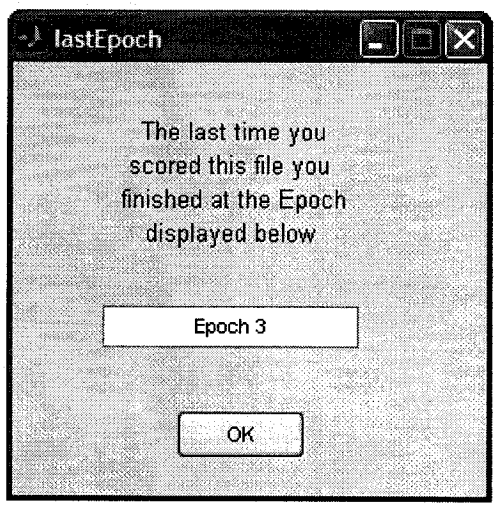

Figure A-6: LastEpoch window of ApneaScore.

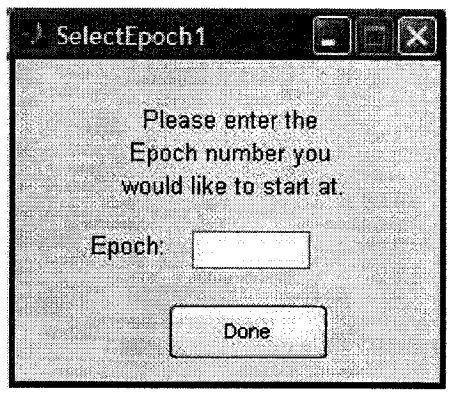

Figure A-7: SelectEpoch window of ApneaScore.

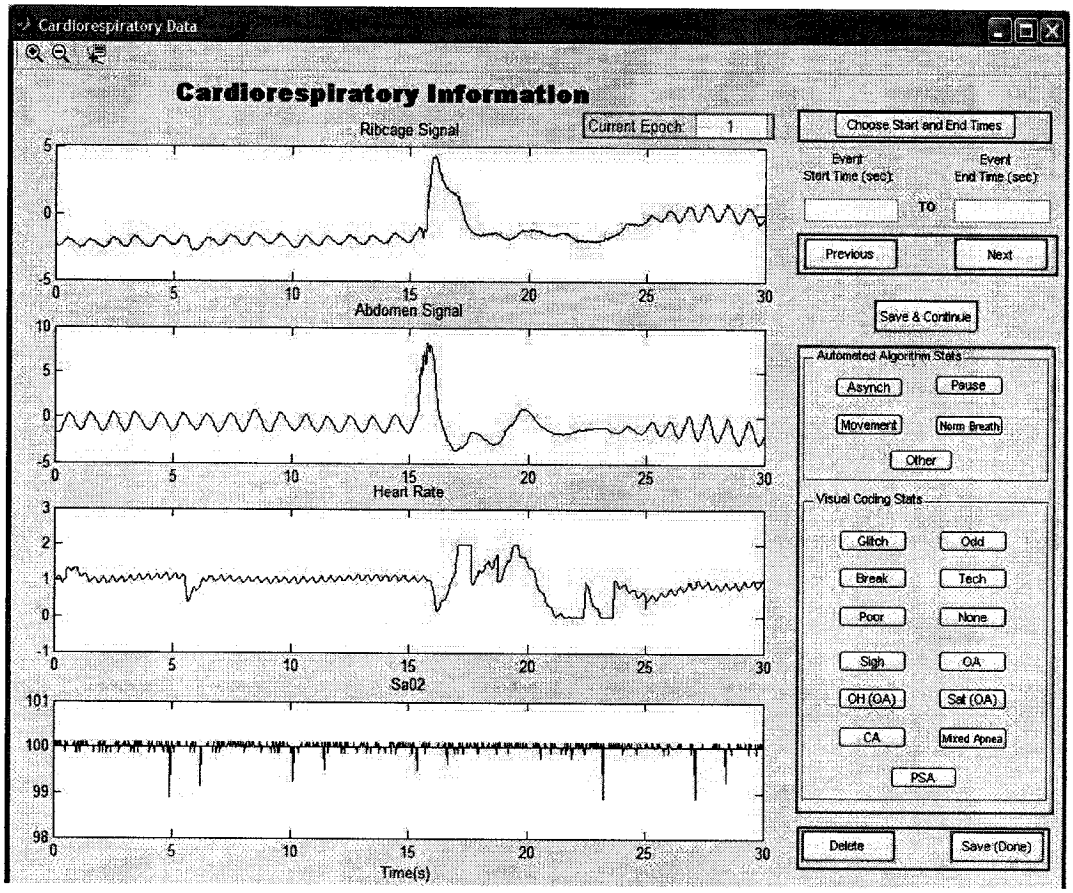

Figure A-8: Main Cardiorespiratory data window

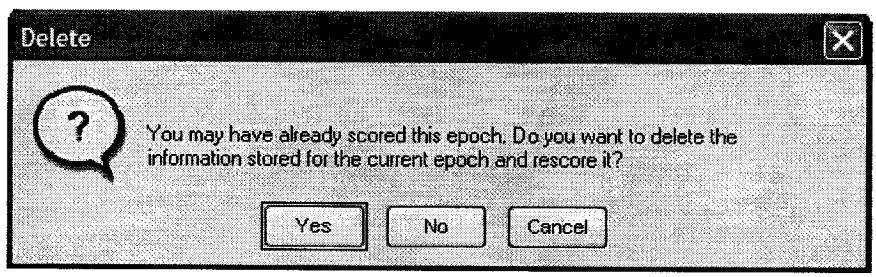

Figure A-9: Message for previously visited epoch.

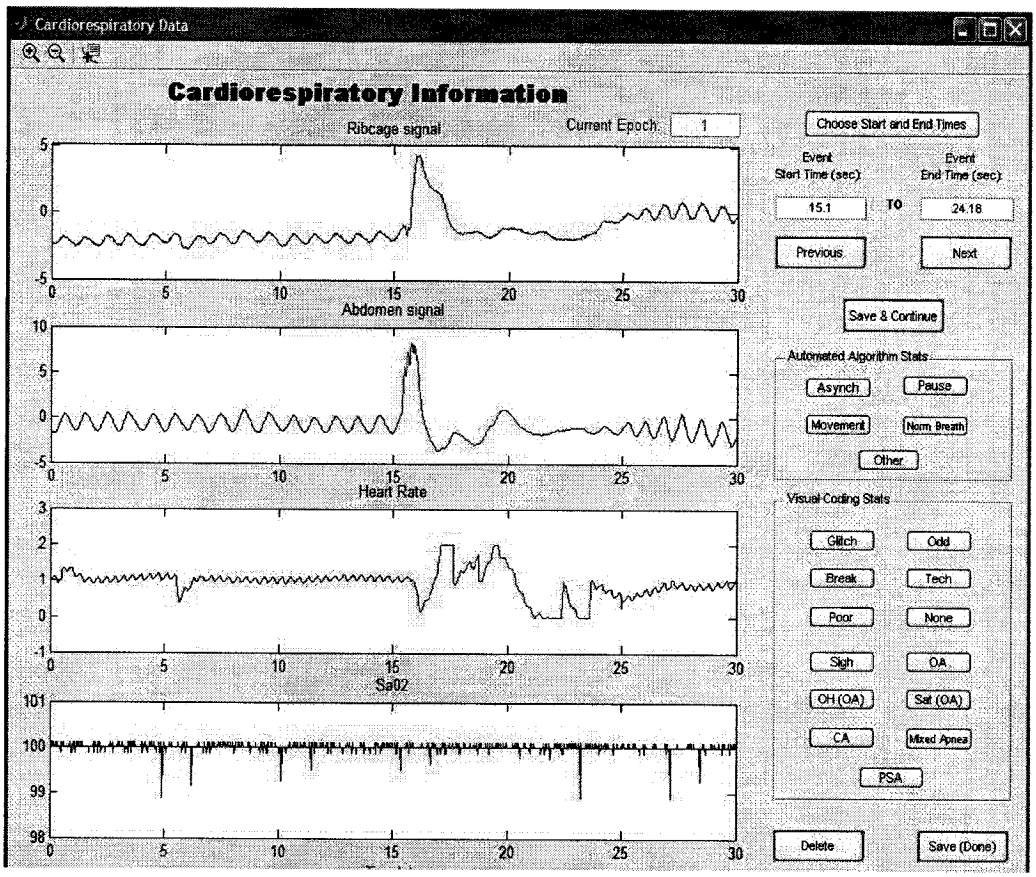

Figure A-10: Example of a user selected segment in ApneaScore.

Appendix B: Offline GUI User Manual

Offline User Manual

Ahmed Aoude

Department of Biomedical Engineering

McGill University

Motivation

Offline is a graphical user interface (GUI) developed for the automated detection of pauses, asynchronous breathing and movement artifact segments using the off-line methods developed at McGill University. The program displays the analysis and corresponding cardiorespiratory data in 30 second epochs. The GUI is user friendly and allows the user to scroll through the data as many times as required. Once analyzed, the analysis is stored in a MATLAB file (*.mat format), this format was chosen for future use in MATLAB functions.

Installation

Offline requires a computer with a basic MATLAB 7.0 R14 installation. To use Offline the following steps have to be completed before its first use.

Make sure that all the files required for Offline are installed on the computer that will run the GUI. These files should be saved in a know location under a folder named **'GUI_Offline'**.

The required files are:

1. **AdaptiveFilter.m**
2. **AutoThres.m**
3. **JumpToEpoch.m**
4. **MultiIIR_T3GUI.m**
5. **Offline.m**
6. **OffLineGUI.m**
7. **SelectThres.m**
8. **CaEnergy.m**
9. **readlabdat.m**

10. **OffLineGUI.fig**

11. **SelectThres.fig**

12. **JumpToEpoch.fig**

13. **AutoThres.fig**

Once you have these file saved on your local machine, it is important to add the **'GUI_Offline'** folder to the MATLAB path. This is accomplished by opening MATLAB and choosing: **File->Set Path**.

Once selected the window shown in Fig A-1 will appear.

Select **Add Folder**, then browse to the folder **'GUI_Offline'** and click **OK**. Once you clicked **OK** the path should be added to the MATLAB search path list.

For example if you had saved the Offline files under : **'C:\GUI_Offline'** this path would be present in the list as shown in Fig B-2.

Once the path is in the list select **Save**.

After completing these steps you are ready to launch the Offline application.

How to Use Offline

To start the application type **Offline** in the MATLAB command window and the application will load automatically. A window will open. Fig A-3 shows a screen shot of this window.

Click **Start** then another window will open. Browse to the file containing the Labdat data. In that file, select the Labdat file to open (*.dat format) and click **Open**. This will load the cardiorespiratory data of that file to analyze. An example is shown in Fig B-4.

Be Patient and the window shown in Fig B-5 will appear.

This allows the user to set the thresholds for pause asynchrony and movement artifact detection or let the program select them automatically. It is recommended that the user let the program select the threshold automatically if it is the first time he/she is analyzing the file. This will give the user an initial estimate of the threshold to use for correct detection. The user must click **Yes** to let the program automatically select the threshold, and click **No** to enter the thresholds manually.

If the user selects **Yes**, the analysis will commence automatically. This may take several minutes so patience is required.

If the user selects **No**, the window shown in Fig B-6 will appear.

This window allows the user to input the desired threshold for each of the detectors. Note that the asynchrony threshold should be a value in the range [0,1], the pause threshold should be in the range [0,inf] and the movement threshold should be in the range [-1,1]. If the user enters a value outside these ranges an error message will pop-up asking the user to re-enter a correct value. Once the user enters the thresholds he/she must click **Analyze** to start the analysis. This may take several minutes so patience is required.

Next, the main window will appear. This widow displays the cardiorespiratory data, allows for scrolling through the data in 30s segments, allows the user to jump to a desired epoch, displays the thresholds used in the analysis (blue box in Fig B-7) and allows the user to view the frequency estimate obtained for a given segment of data within the current epoch (purple box in Fig B-7).

To scroll through the data the **Next** and **Previous** buttons are used (shown in the red box of Fig B-7).

Next scrolls to the next 30s of data and, **Previous** scrolls to the previous 30s of data. An error message will appear if the user tries to scroll beyond the file length.

Referring to Fig B-7, the button on the top right (**Jump To Epoch**) allows the user to jump to the desired epoch he/she wishes to view (located in the green square of Fig B-7). Once clicked, the window in Fig B-8 will appear.

The user has to simply enter the epoch he would like to get to and click **OK**. Once **OK** is clicked the data displayed in the main window will jump to the entered epoch value. Note that an error message will appear if an incorrect epoch number is entered. The epoch corresponding to the displayed data is always indicated in the green box of Fig B-7.

To view the frequency estimate of a segment within the current epoch, the user may click on the pull down window of the frequency estimate for the abdominal or ribcage signals (shown in the purple box of Fig B-7). The user must then select the time interval he/she desires in the pull down window. Once selected, the frequency estimate for that interval will be displayed under the pull down window. An example of the frequency estimate for the interval 0-5s for the abdominal signal and 10-20s for the ribcage signal is shown in Fig B-9.

Finally, once the user has finished using the tool he/she may save the analysis by clicking the **Save Analysis** button (brown box in Fig B-7).

Analyzed Data Storage

The analysis completed by a user is stored in a *.mat format (only if the user decides to save the data). Scored data is saved with the name offlineNAME.mat, where offline is always appended to the beginning to indicate that the file contains the analysis information. The NAME portion of the filename is identical to the patient identification that is used to identify the LABDAT file containing the cardiorespiratory data (the *.DAT filename). An example is: For the ARC.DAT file, the file containing the scored data is named offlineARC.mat.

The visually scored data is stored into five MATLAB variables and three arrays: AsynchDetect, PauseDetect, MvtDetect, ThresPauseRC, ThresPauseAB, ThresAsynch, ThresMvtRC and ThresMvtAB. ThresPauseRC, ThresPauseAB, ThresAsynch, ThresMvtRC and ThresMvtAB are the thresholds used for each of the detectors in the analysis. While, AsynchDetect, PauseDetect and MvtDetect are logic arrays that are either 1 or 0 for each sample of the data. When any element of the arrays is one it indicates that the given detector (pause, asynchrony or movement) detected the event at the given sample.

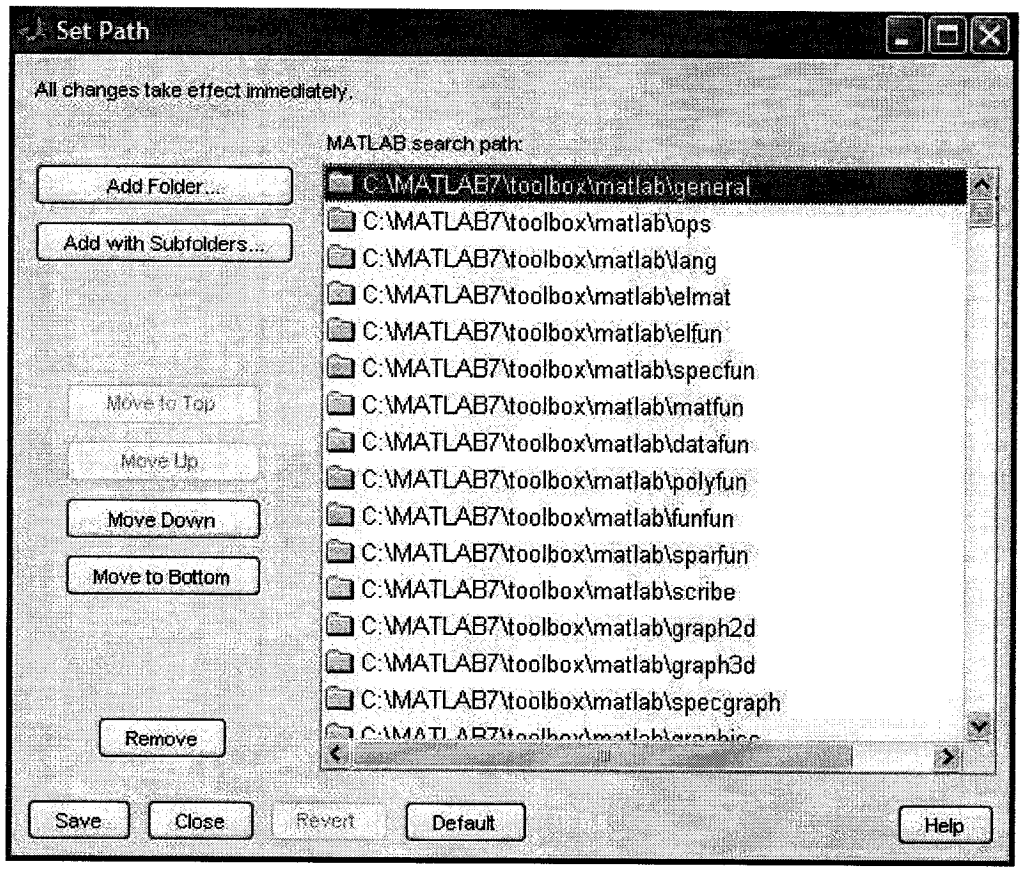

Figure B-1: Matlab set path window.

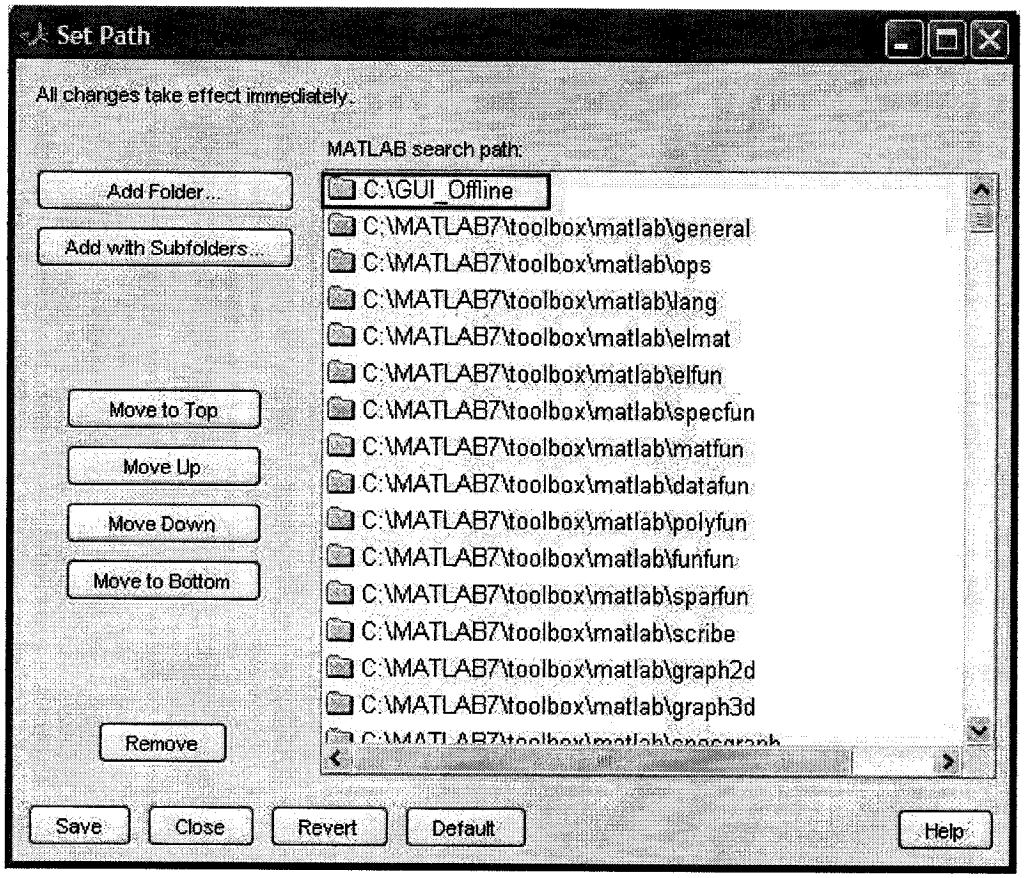

Figure B-2: Example of adding the file 'C: GUI_Offline' in the Matlab set path window.

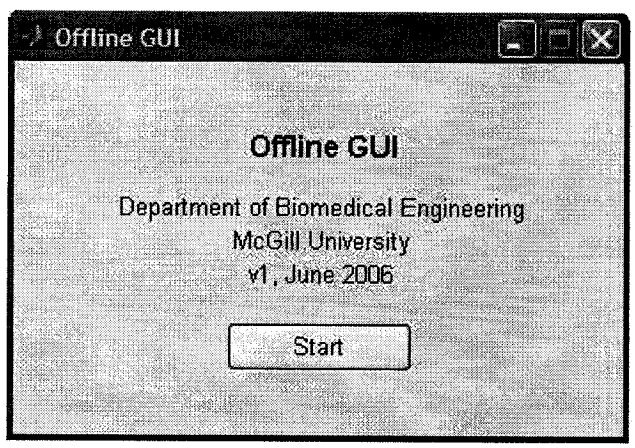

Figure B-3: Opening window of the Offline GUI.

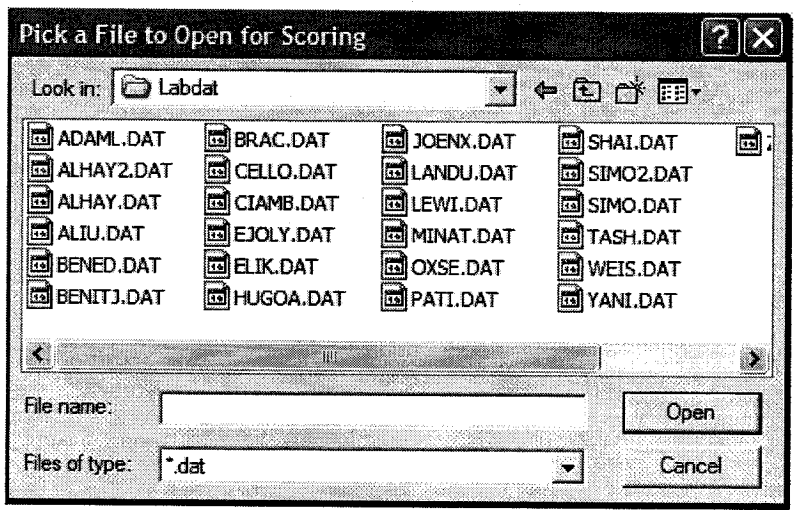

Figure B-4: Labdat file selection example.

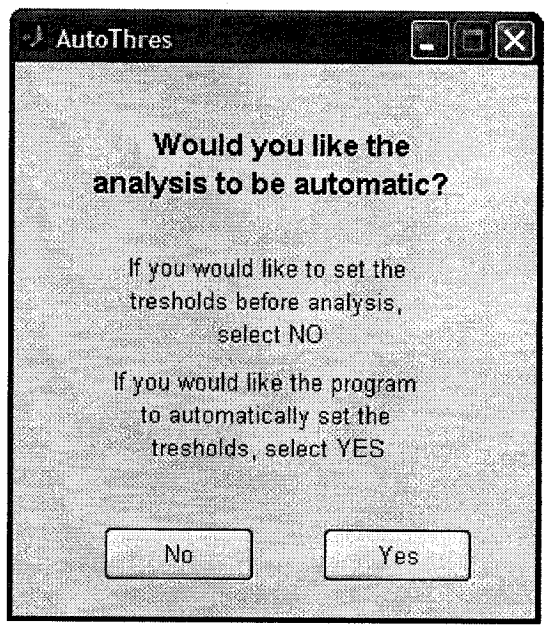

Figure B-5: Threshold selection decision window.

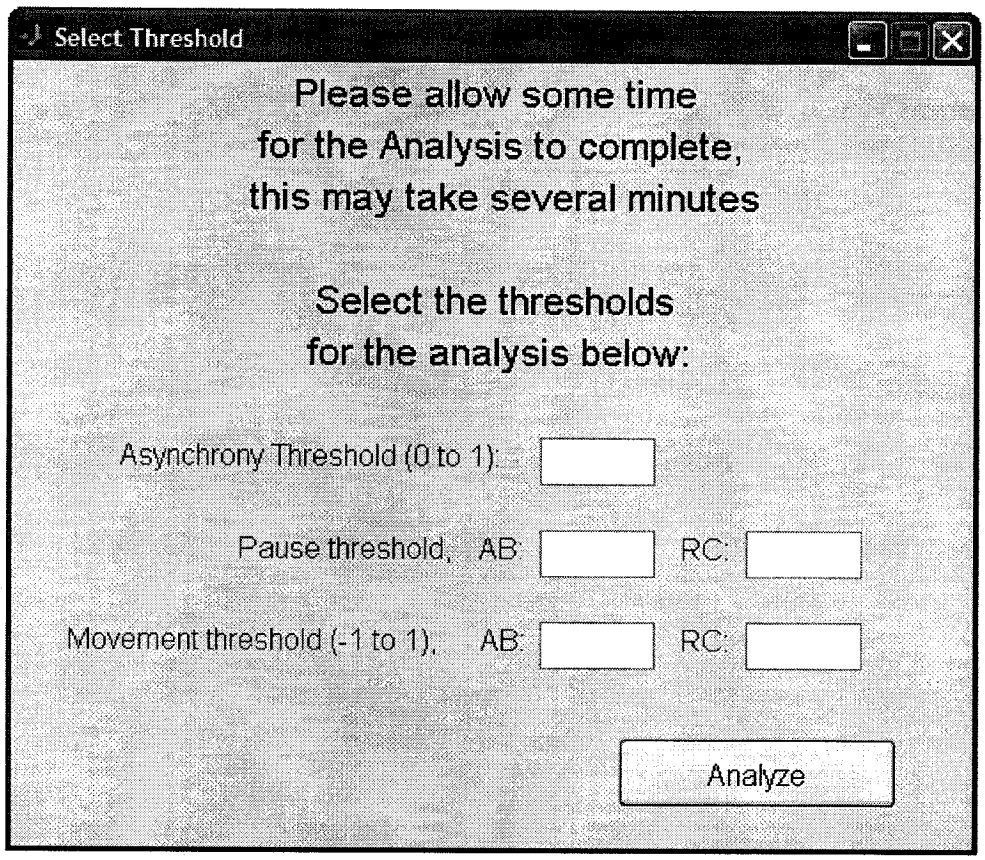

Figure B-6: Manual threshold selection window.

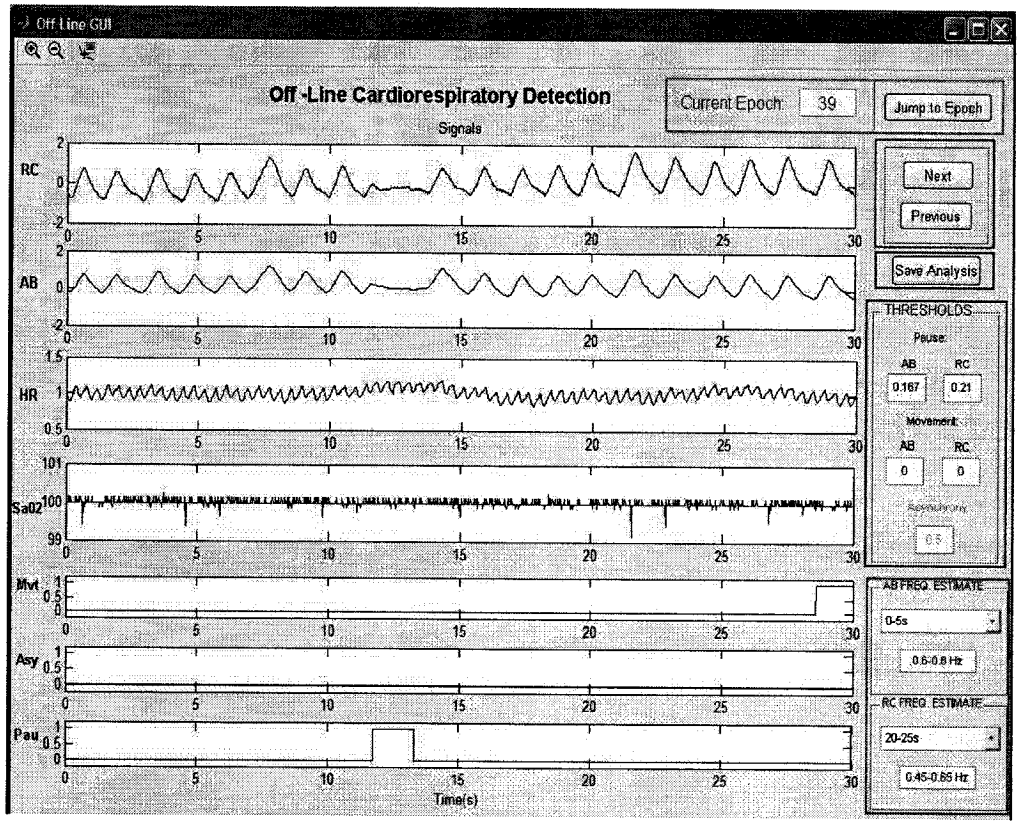

Figure B-7: Main Offline GUI window

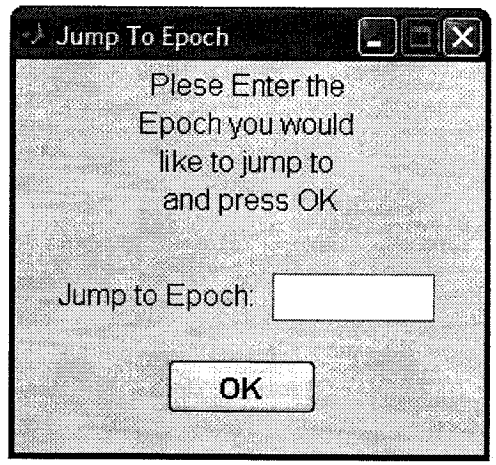

Figure B-8: Jumpto window of the Offline GUI.

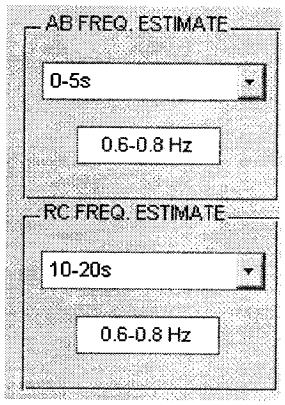

Figure B-9: Example frequency estimation for the Offline GUI.

Appendix C: Conference Paper

Power-Based Segmentation of Respiratory Signals Using Forward-Backward Bank Filtering

A. A. Aoude, A. L. Motto, H. L. Galiana, K. A. Brown and R. E. Kearney

C-1 Abstract

We present an automated method for the segmentation of ribcage and abdominal signals measured by noninvasive respiratory inductance plethysmography (RIP) into quiet breathing and artifact-corrupted segments. This procedure, which involves forward-backward filtering, is applicable to the automated off-line analysis of long records of respiratory signals. Examples of applications include home and sleep laboratory studies of cardiorespiratory data. The new procedure was successfully applied to the segmentation of cardiorespiratory signals acquired post-operatively from infants in the recovery room of the Montreal Children's Hospital (MCH).

C-2 Introduction

Signal processing procedures for marking the start and end times of "useful data segments" from a given record of respiratory and sleep data, or a subset thereof, have an important role in the diagnosis of clinically significant abnormalities. The term "useful data segment" is used here to designate any time interval of respiratory inductance plethysmography (RIP) signals that has a sufficiently high signal-to-noise ratio. A low signal-to-noise ratio arises when either or both ribcage and abdominal channels are corrupted by non-respiratory-induced movements, occurring, for example, when the subject is moving or being moved. For illustration, Fig. C-3a provides a representative segment of an abdominal excursion signal measured by RIP in the recovery room of the Montreal Children's Hospital (MCH) [7]. The first 20-second period shows no apparent artifact whereas the following 11-second period is corrupted by artifact. This paper presents a signal processing procedure for the off-line, automated partitioning of RIP signals into segments either with or without artifacts.

The need for the automated segmentation of cardiorespiratory signals has been well recognized. Weese-Mayer *et al.* [75] reported that the performance of automated cardiorespiratory monitoring

procedures could be significantly improved if signal segments corrupted with artifacts could be systematically identified. In [5], we proposed an automated procedure for estimating the phase relation between thoracic and abdominal excursions measured by noninvasive RIP. We noted that the performance of the phase estimator could be improved if it was combined with an automated procedure for partitioning a realization of RIP signals into periods with and without artifact corruption. Such automated signal segmentation procedures would also be useful in the analysis of long records of off-line respiration and sleep data. Furthermore, assuming that the probability of apnea occurring while a subject is moving or being moved is negligibly small, this procedure could be used to reject the hypothesis "apnea present", thereby improving the detection performance of automated apnea detectors.

In [6], we showed that a Neyman-Pearson energy-based detector could be used for the automated detection of artifacts. Reference [6] was mainly concerned with the on-line detection of artifacts whereas the present paper is concerned with the off-line detection and, therefore, uses forward-backward IIR (infinite impulse response) filters, producing an array of zero-phase filters with narrower pass bands and smaller transition bands. As a by-product, we obtain an estimate of the fundamental frequency of breathing up to a narrow band. The new method is aimed to be integrated into the cardio-respiratory monitor reported in [72].

C-3 Methods

We have developed a new method to allow for the automated segmentation of thoracic and abdominal signals into periods with artifact present and periods with artifact absent. From our previous study [5], it was observed that:

1. Quiet breathing signals are band limited with a given frequency.
2. The energy of sensor noise is negligible compared to quiet breathing components.
3. The energy of movement artifact is generally greater than that of quiet breathing and sensor noise with predominance at lower frequencies.

Using the above observations, we developed a method that uses a bank of IIR filters and average power to automatically segment respiratory data.

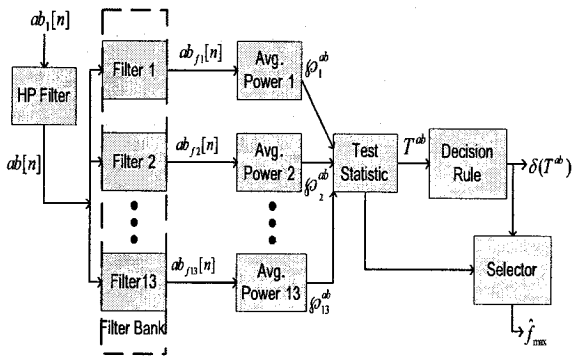

Figure C-1: Simplified diagram of proposed method for respiratory data segmentation. The figure depicts the process for the abdominal RIP signal ($ab_1[n]$). The same process is also applied to the ribcage RIP signal.

Fig. C-1 shows a block diagram of the proposed method. Next, we describe the main components of the method.

C-3.1 High Pass Filter

To remove offsets and exponential decays observed in real infant data, a high pass filter with cut off frequency equal to 0.05Hz was used. As shown in Fig. C-1, the original RIP signal is denoted $ab_1[n]$ and the high pass filtered signal is denoted $ab[n]$.

C-3.2 IIR Filter Bank

To estimate the fundamental frequency of the RIP signals, 13 filters were used to achieve little overlap between adjacent filter passband widths over [0, 2.0]Hz. The filters were chosen to span frequencies between 0 Hz and 2.0 Hz for two main reasons. Firstly, this range covers the range of fundamental frequencies of infant quiet breathing, as reported in [5]. Secondly, this range covers the low-frequency artifacts that are predominant in RIP signal corruption.

These filters were designed with a pass-band width of 0.2 Hz as well as specified pass-band and stop-band ripples (refer to Table I). Forward-backward filtering using IIR filters is used in the filter bank to perform zero-phase digital filtering and therefore not distort the phase between the thoracic and abdominal signals. The IIR filters were chosen to be elliptic or Cauer digital filters to obtain sharper roll offs and precise filter designs [77]. The optimal filter order was chosen using the

Table C-1: Design specification of IIR filters[1]

Filter number (i)	f_l (Hz)	f_h (Hz)	n	ω_p (dB)	ω_s (dB)
1	0	0.2	7	0.01	50
2	0.15	0.35	3	0.1	30
3	0.3	0.5	4	0.01	40
4	0.45	0.65	4	0.01	40
5	0.6	0.8	4	0.01	50
6	0.75	0.95	4	0.01	50
7	0.9	1.1	4	0.01	50
8	1.05	1.25	4	0.01	50
9	1.2	1.4	4	0.01	50
10	1.35	1.55	4	0.01	50
11	1.5	1.7	4	0.01	50
12	1.65	1.85	4	0.01	50
13	1.8	2.0	4	0.01	50

[1] f_l denotes the filters' low cut off frequency; f_h denotes the filters' high cut off frequency; n denotes the filter order; ω_p denotes the maximum pass-band ripple level; ω_s denotes the minimum stop-band ripple attenuation level.

elliptic low-pass filter order prediction formula described in [77, p.241] with the Signal Processing Toolbox of Matlab [8].

Table I enumerates the filters used and the specifications used to design them.

C-3.3 Average Power

The average power of the filtered RIP signals over a window length $2L+1$ was used to segment the signals. Let $\wp_i^{ab}[n, N]$ denote the average power value of the filtered abdominal signals over a window $N = 2L + 1$, then

$$\wp_i^{ab}[n, N] = \frac{1}{N} \sum_{k=n-L}^{n+L} ab_{fi}^2[k], \text{ for } i = 1, 2, ...13 \tag{6.1}$$

Where $ab_{fi}[n]$ represents the i^{th} filtered abdominal signal from the filter bank (refer to Fig. C-1). Note that the ribcage power, $\wp_i^{rc}[n, N]$ is similarly defined.

C-3.4 Test Statistic

Since it is assumed that infant quiet breathing is between [0.4, 2]Hz and that artifacts are at lower frequencies, let $\mathcal{I}$ and $\mathcal{J}$ denote the index sets of the IIR bandpass filters covering the the quiet breathing and artifact frequency ranges, respectively; that is $\mathcal{I} = \{3, 4, ..., 13\}$ and $\mathcal{J} = \{1, 2\}$.

Then, we can define the test statistic, T^{ab} as

$$T^{ab}[n] = \frac{\max\limits_{i}\{\wp_i^{ab}\}_{i\in\mathcal{I}} - \max\limits_{j}\{\wp_j^{ab}\}_{j\in\mathcal{J}}}{\max\limits_{i}\{\wp_i^{ab}\}_{i\in\mathcal{I}} + \max\limits_{j}\{\wp_j^{ab}\}_{j\in\mathcal{J}}}, \tag{6.2}$$

where we use the convention $\frac{0}{0} = 1$.

C-3.5 Decision Rule

The test statistic T^{ab} can then be used, together with a Neyman-Pearson threshold γ [78], for deciding

$$\delta(T^{ab}) = \begin{cases} 1, \text{if } T^{ab} \leq \gamma \\ 0, \text{if } T^{ab} > \gamma \end{cases} \tag{6.3}$$

The decision rule above states that we choose the hypothesis $\mathcal{H}_0$ if $T^{ab} \leq \gamma$ and we choose the hypothesis $\mathcal{H}_1$ if $T^{ab} > \gamma$. Where the hypotheses are: $\mathcal{H}_0$: *Artifact Absent* and, $\mathcal{H}_1$: *Artifact Present.*

C-3.6 Selector

The selector in Fig. C-1 yields an estimate of the breathing rate up to a narrow band, $\hat{f}_{max}$:

$$\hat{f}_{max}[n] = \delta[n] \min\{\arg\max_{i\in\mathcal{I}} \wp_i^{ab}[n]\}. \tag{6.4}$$

Equation (6.4) states that $\hat{f}_{max}[n] = 0$ if we decide *artifact present*; otherwise, $\hat{f}_{max}[n]$ is the index of a filter whose average power is maximum. The operation min ensures that $\hat{f}_{max}[n]$ is a singleton if more than one filter produces maximum average power.

C-4 Application to Simulated Data

C-4.1 Description of Simulated Data

The main concepts and derivations of the simulated breathing and additive noise signals used for this paper can be found in [5, pp.617-618]. In brief, these signals were composed of piecewise-linear frequency-modulated sinusoidal signals to model quiet breathing, white Gaussian noise to model sensor or electronic noises, and a stochastic diffusion process to model movement artifacts.

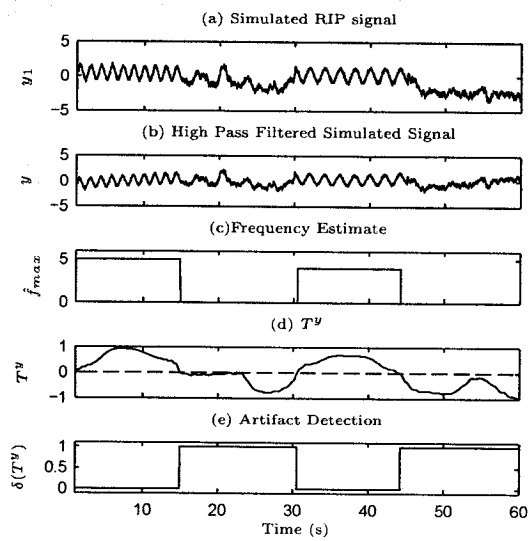

Figure C-2: Segmentation analysis of a 60s simulated segment of infant RIP signal. Note that for the simulated RIP signal a 0.7 Hz noise corrupted signal was used for the first 15s and a 0.5 Hz noise corrupted signal was used for time 30s to 45s. Time 15s to 30s and the last 15s of the simulated signal was predominantly composed of simulated movement artifact. (a) is the original signal, (b) is the high pass filtered signal, (c) is a plot of $\hat{f}_{max}$, (d) is a plot of the test statistic T^y (dashed line: $\gamma = 0$), and (e) is the decision $\delta(T^y)$. As expected, the method detect the artifact corrupted segments ($\delta(T^y) = 1$).

C-4.2 Analysis of Simulated signals

To assess the effectiveness of our method, a simulated RIP signal was generated. This signal was composed of four segments. The first and third segments were normal breathing while, the second and fourth segments were predominantly composed of movement. All segments also had additive electronic noise.

Fig. C-2 shows that our method correctly detects the artifact corrupted segments as well as the normal breathing segments in data with uncorrelated noise. In fact, the breathing segments are labeled with $\hat{f}_{max}$ values equal to 5 and 4 which are the expected values since they correspond to breathing frequencies anywhere in [0.6, 0.8]Hz and [0.45, 0.65]Hz respectively (the simulated frequencies were 0.7Hz and 0.5Hz respectively).

C-5 Application to Infant Data

C-5.1 Description of Data

We now consider segmentation in breathing periods from 8 infants aged 44 ± 5 weeks, weighing 4.9 ± 1 kilograms. This data was previously reported by Brown *et al.* [7] as part of another study with appropriate ethics approval. This provided a convenient initial database for the validation of the proposed method. The observed continuous-time ribcage and abdominal signals (NIMS^{TM}, Respitrace Plus, North Bay Village, Florida), were amplified and filtered with 15Hz 8-pole Bessel filters (Frequency Devices, Haverhill, MA), and sampled at 50 Hz with a 12-bit analog-to-digital converter (Data Translation, Marlborough, MA). This data was stored on a computer using LABDAT^{TM} data acquisition software (RHT-InfoDat, Montreal). No attempt was made to calibrate the signals in absolute terms.

C-5.2 Analysis of Infants' Data

Since there does not exist a widely accepted and exact mathematical definition of normal breathing and artifact corrupted segments, the visual scoring of 8 infant data sets consisting of over 46 hours of data was considered. Thus, to asses the effectiveness of the method in segmenting the off-line data, the data acquired in [7] was visually scored by K. A. Brown (MD) in accordance to approved practice at the MCH. A comparison between the segmentation obtained using the automated method and the segmentation by visual scoring was used to determine the accuracy of the method.

Signal Segment Illustration

To illustrate the effectiveness of the method, Fig. C-3 shows a segment of real infant data consisting of normal breathing followed by artifact corruption. As expected the artifact corrupted segment had $\delta(T^{ab})$ values (e) equal to 1, while the breathing segment had $\delta(T^{ab})$ values equal to 0.

Note that Fig. C-2 and Fig. C-3 were generated using the threshold $\gamma = 0$ for illustration purposes and using a window length (N) equal to 251 samples or 5s.

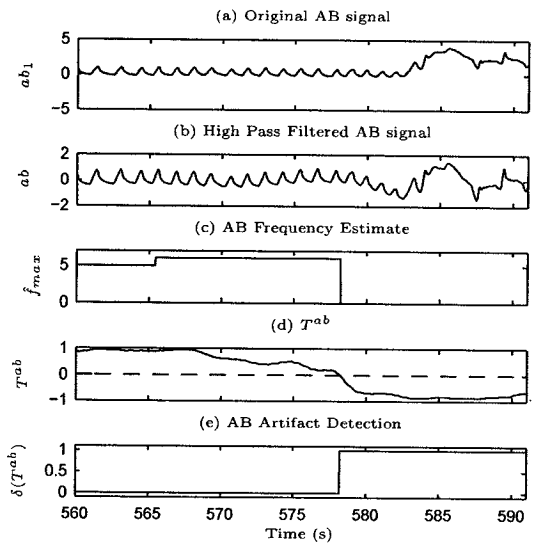

Figure C-3: Segmentation analysis of a 31s segment of abdominal ($ab_1[n]$) breathing excursions measured by inductance plethysmography of an infant (42 weeks old weighing 3.9 kg). Note that a quasi-sinusoidal breathing signal is observed for the first 20s followed by 11s of artifact corruption. (a) is the original RIP signal, (b) is the high pass filtered signal, (c) is a plot of $\hat{f}_{max}$, (d) is a plot of the test statistic T^{ab} (dashed line: $\gamma = 0$), and (e) is the decision $\delta(T^{ab})$. Note that for the time interval 577.5s to 582s the signal is composed of both, low frequency artifact and quiet breathing; since the power of the low frequency component is higher ($T^{ab} < 0$), the method labeled this segment as having artifact corruption.

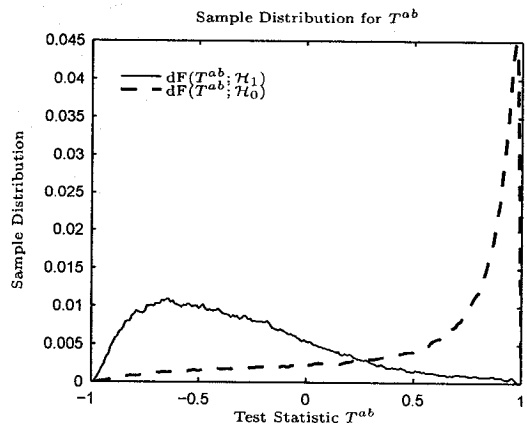

Figure C-4: Sample distributions of the test statistic T^{ab} for all 8 data files that have been visually scored by Dr. K. A. Brown. The plot shown was generated with N =251 (i.e. 5 seconds at 50 Hz), under the hypotheses $\mathcal{H}_0$ (movement artifact absent) and $\mathcal{H}_1$ (movement artifact present).

Comparison to Visual Scoring

Fig. C-4 shows the distribution of T^{ab} over periods of quiet breathing and gross body movement for all 8 infant files in the data base used; that is under $\mathcal{H}_0$ and $\mathcal{H}_1$, respectively. We derived T^{ab} from the visual scoring done by K. A. Brown.

The performance of the proposed off-line detector, based on the visual scoring, is summarized in the receiver operating characteristic (ROC) for the test statistic T^{ab} of equation (6.2). The ROC plot is presented in Fig. C-5, where P_{FA} denotes the probability of false alarm; that is, the probability of deciding *artifact present* when there is no artifacts and, where P_D denotes the probability of detection; that is, the probability of deciding *artifact present* when artifact is almost surely present.

Note that from the distribution shown in Fig. C-4, P_D and P_{FA} for a given threshold γ can be found by solving

$$P_D = \int_{-1}^{\gamma} dF(T^{ab}, \mathcal{H}_1),\ P_{FA} = \int_{-1}^{\gamma} dF(T^{ab}, \mathcal{H}_0) \tag{6.5}$$

The segmentation presented above could be improved by further processing $\delta(T^{ab})$. This processing removes any detection segments that are smaller than 5s and, combines any two consecutive detection segments separated by a gap smaller than 5s. For example, using the threshold of γ equal 0, we obtained the following probabilities of detection and false alarm for all 8 infants, $P_D = 80\%$

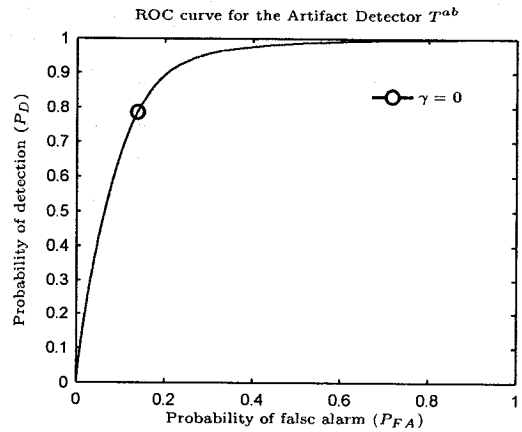

Figure C-5: Receiver operating characteristic for all 8 infants visually scored by Dr. K. A. Brown. The test statistic used was T^{ab} with N = 251 samples or 5 seconds. The circle indicates the probabilities for $\gamma = 0$.

and $P_{FA} = 15\%$. In comparison, after processing we obtained the following probabilities of detection and false alarm for all 8 infants, $P_D = 86\%$ and $P_{FA} = 11.25\%$. The results showed that it could prove useful to use T^{ab} as a decision criterion to segment real infant data.

C-6 Concluding Remarks

We have presented a new method to segment respiratory data into periods with or without movement artifact based on the frequency and energy content of RIP signals. The method is automated and used off-line to allow for segmentation of respiratory data. In addition, the method allows for repeatable analysis which is advantageous when compared to the inconsistencies of visual scoring.

Current studies are exploring the integration of the new procedure in the automated classification and detection of events such as obstructive and central apnea. The proposed procedure is fully automated and used off-line which will allow for less costly and more efficient analysis when compared to visual scoring.

Appendix D: Extended Results

The results for the three off-line detectors presented in chapter 5 are presented in this appendix on a file by file basis. For each patient file, an ROC curve representing each detector's effectiveness relative to Dr. K. A. Brown's visual scoring is presented. The distribution of the number segments and their respective length as scored by Dr. K. A. Brown and as obtained with the automated methods are also presented.

6.7 ROC Curves for the Off-Line Movement Artifact Detector

Figures D-1a to D-1c show the results for the off-line movement artifact detection method for each patient file. The plots shown were generated using N = 251 sample (i.e. 5 s at 50Hz).

6.8 ROC Curves for the Off-Line Pause Detector

Figures D-2a to D-2c show the results for the off-line pause detection method for each patient file. The plots shown were generated using $N_1 = 51$ sample (i.e. 1 s at 50Hz).

6.9 ROC Curves for the Off-Line Asynchrony Detector

Figures D-3a and D-3b show the results for the off-line asynchrony detection method for each patient file. The plots shown were generated using N = 251 sample (i.e. 5 s at 50Hz). Note that only 16 out of the 21 infants had asynchronous breathing episodes which explains the fewer number of plots in Figures D-3a to D-3b.

6.10 Number of Events Versus Duration

Figures D-4 and D-5 show the results for the automated off-line pause and movement detection methods. The figures show the distribution of the number of segments versus their respective length as obtained with the automated method and as scored by the Dr. K. A. Brown. For the movement detector, a value of $\gamma = 0$ and N = 251 samples or 5 s was used. For the pause detector, the thresholds were chosen using the automated threshold selection technique described in chapter 5 and using $N_1 = 51$ samples or 1 s. The distribution for asynchronous breathing is omitted since it is assumed that the automated phase estimation technique presented in this thesis is less biased than asynchrony detection by visual scoring.

The following number of segments were obtained for each method, considering segments of all lengths:

Movement: 2760 segments (Visual scoring) and 2945 segments (Automated method)

Pause: 2399 segments (Visual scoring) and 3256 segments (Automated method)

In comparison, the following number of segments were obtained for each method, considering segments greater than 4 seconds long:

Movement: 2668 segments (Visual scoring) and 2945 segments (Automated method)

Pause: 1602 segments (Visual scoring) and 1847 segments (Automated method)

From the results presented in this appendix and the chapters of this thesis, we can conclude that the automated processes for asynchrony, movement artifact and pause detection produce results that are comparable to visual scoring.

Recall that the visually scored data obtained with the ApneaScore tool was scored in 30 s epochs and then processed to combine events that spanned more than one epoch. This concatenation considered events that had gaps smaller that 2 s between consecutive epochs. Therefore, the peaks for the visual scoring at 30 s, 60 s and 90 s in Fig. D-4 can be attributed to the effect of this processing as well as visual scoring inconsistencies.

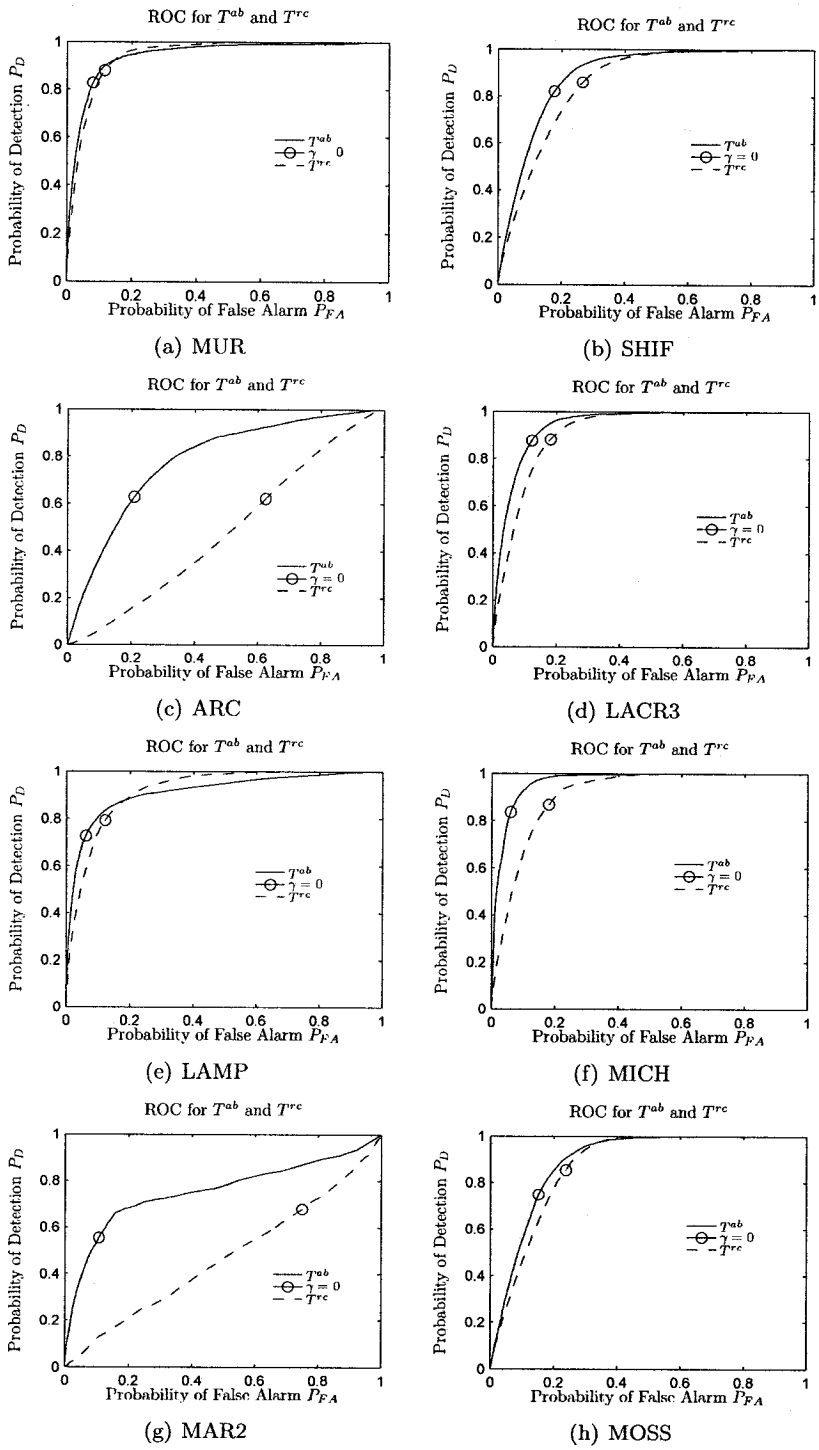

(a) MUR (b) SHIF

(c) ARC (d) LACR3

(e) LAMP (f) MICH

(g) MAR2 (h) MOSS

Figure D-1a: ROC curves for Movement detection in the abdominal and ribcage RIP signals of eight infant patient data records (Montreal Childrens Hospital Study ID: (a) MUR, (b) SHIF, (c) ARC, (d) LACR3, (e) LAMP, (f) MICH, (g) MAR2 and (g) MOSS)

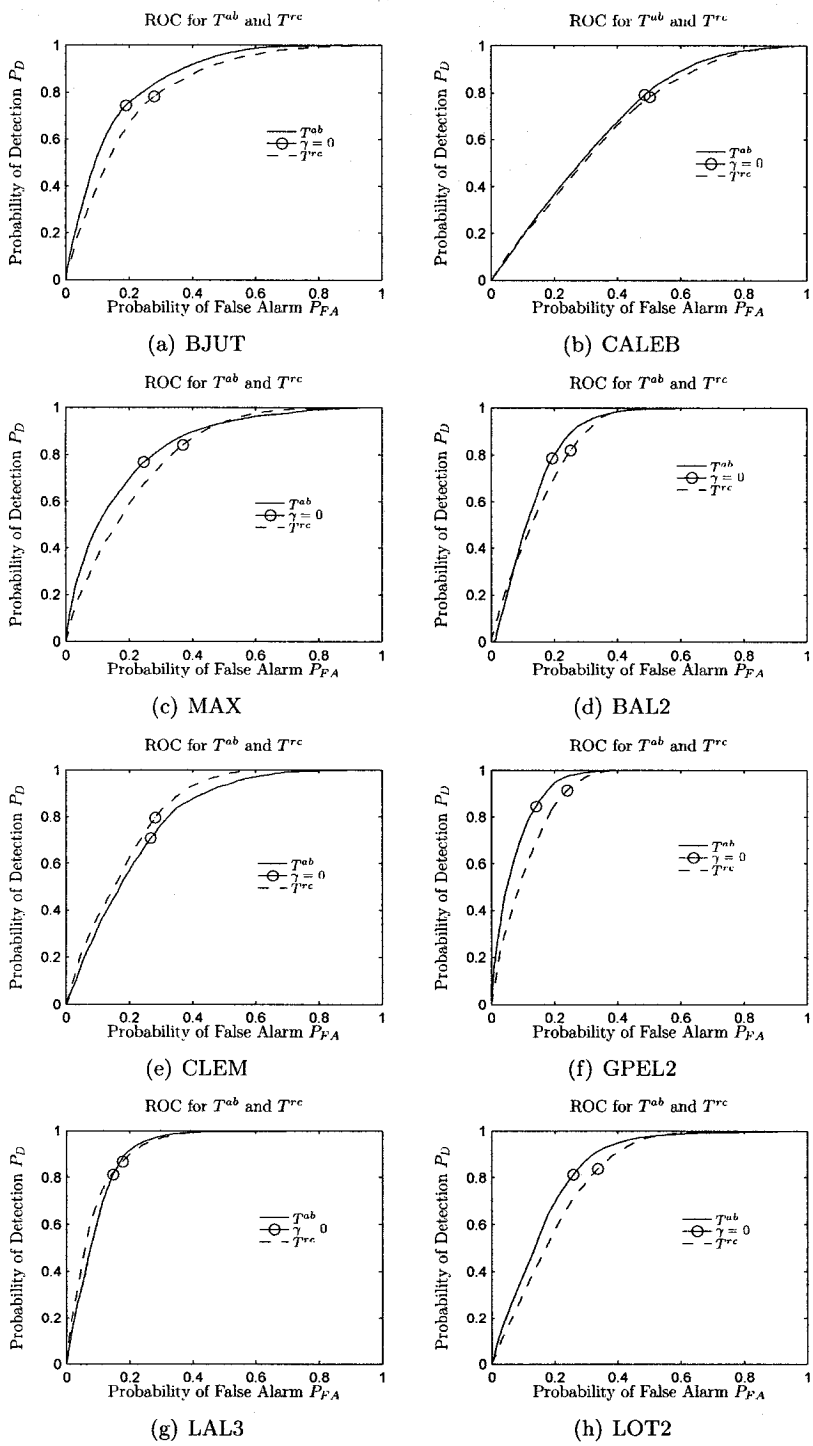

(a) BJUT (b) CALEB

(c) MAX (d) BAL2

(e) CLEM (f) GPEL2

(g) LAL3 (h) LOT2

Figure D-1b: ROC curves for Movement detection in the abdominal and ribcage RIP signals of eight infant patient data records (Montreal Childrens Hospital Study ID: (a) BJUT, (b) CALEB, (c) MAX, (d) BAL2, (e) CLEM, (f) GPEL2, (g) LAL3 and (h) LOT2)

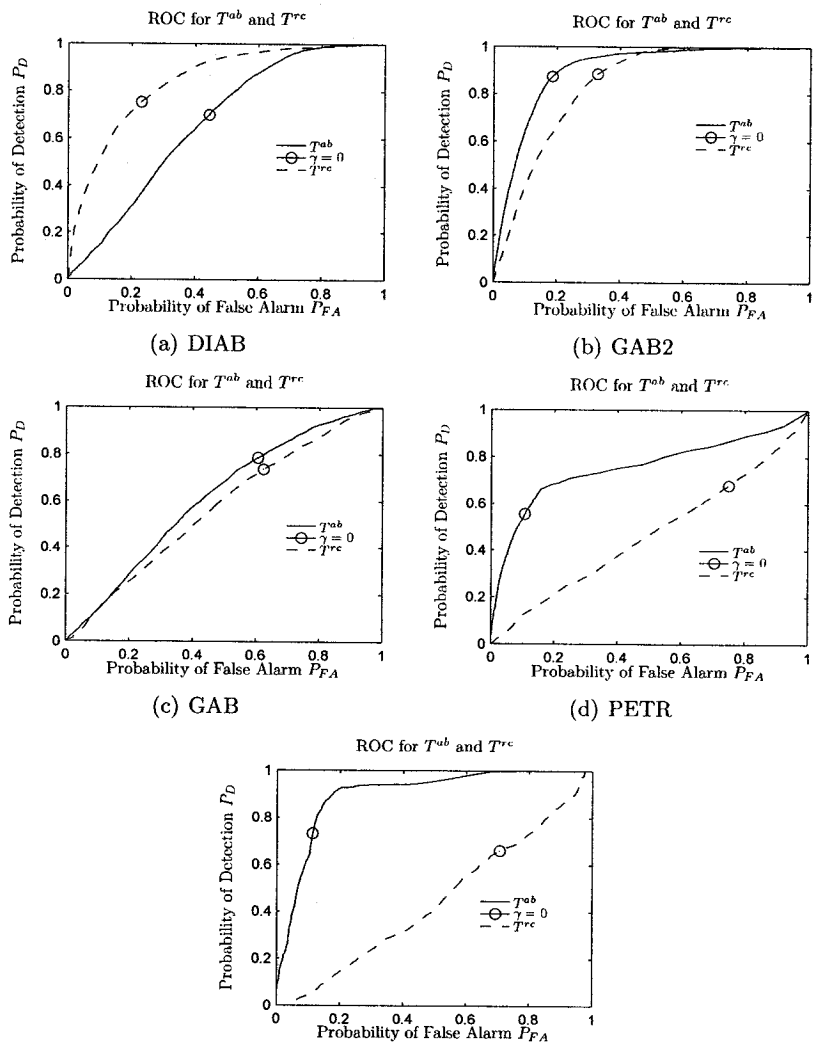

(a) DIAB

(b) GAB2

(c) GAB

(d) PETR

(e) MART3

Figure D-1c: ROC curves for Movement detection in the abdominal and ribcage RIP signals of six infant patient data records (Montreal Childrens Hospital Study ID: (a) DIAB, (b) GAB2, (c) GAB, (d) PETR, and (e) MART3)

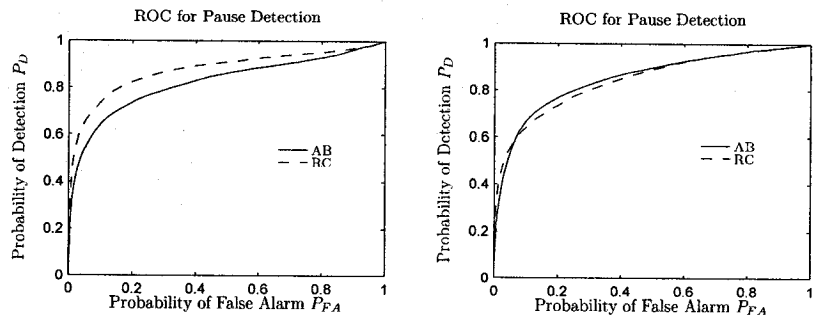

(a) MUR

(b) SHIF

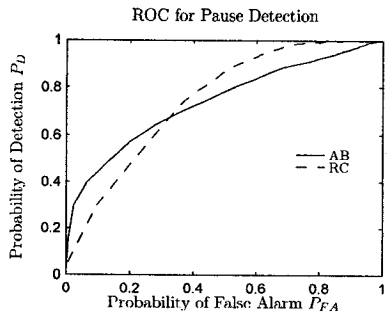

(c) ARC

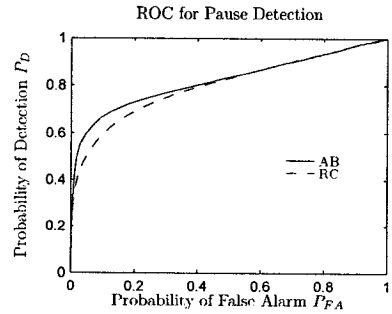

(d) LACR3

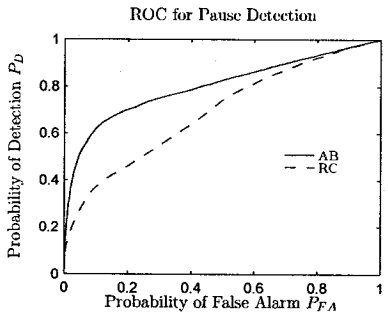

(e) LAMP

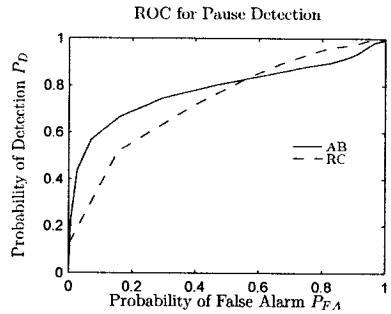

(f) MICH

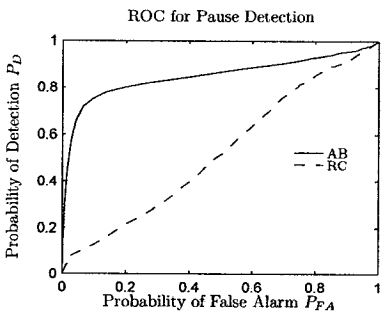

(g) MAR2

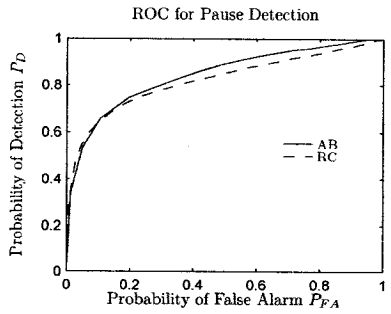

(h) MOSS

Figure D-2a: ROC curves for Pause detection in the abdominal and ribcage RIP signals of eight infant patient data records (Montreal Childrens Hospital Study ID: (a) MUR, (b) SHIF, (c) ARC, (d) LACR3, (e) LAMP, (f) MICH, (g) MAR2 and (g) MOSS)

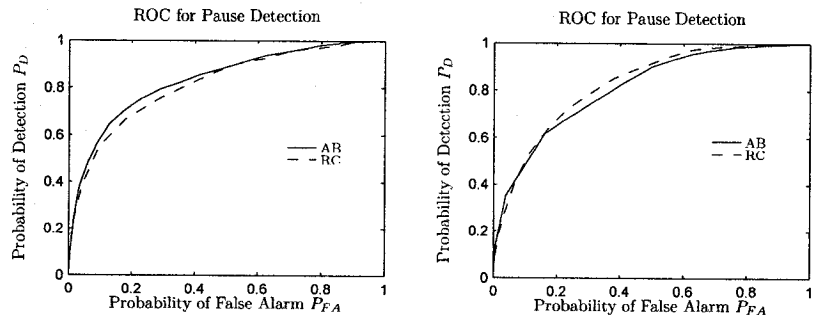

(a) BJUT

(b) CALEB

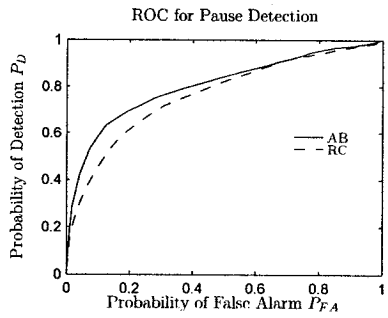

(c) MAX

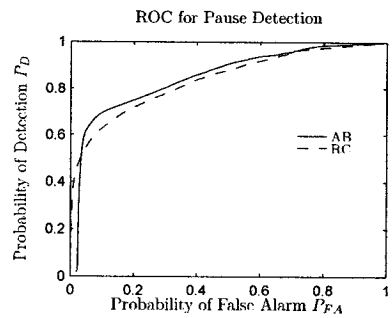

(d) BAL2

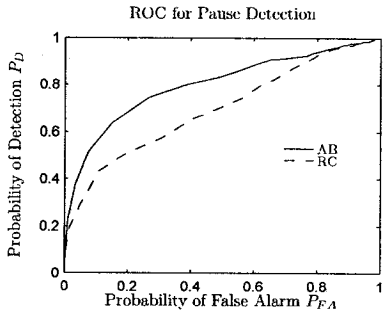

(e) CLEM

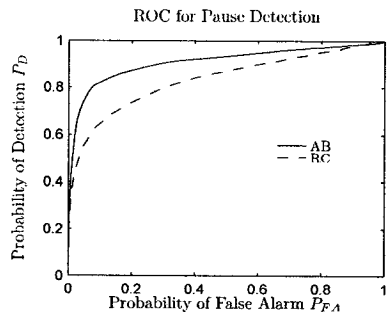

(f) GPEL2

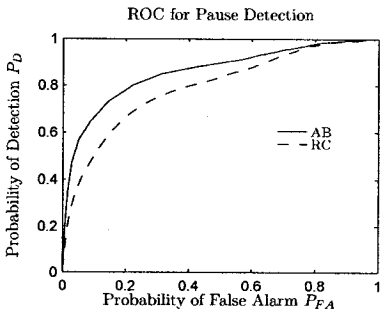

(g) LAL3

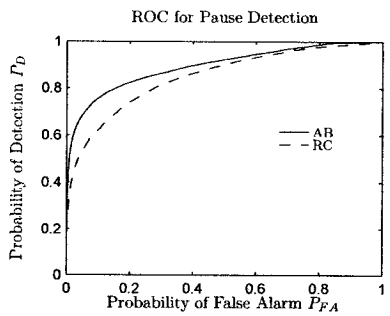

(h) LOT2

Figure D-2b: ROC curves for Pause detection in the abdominal and ribcage RIP signals of eight infant patient data records (Montreal Childrens Hospital Study ID: (a) BJUT, (b) CALEB, (c) MAX, (d) BAL2, (e) CLEM, (f) GPEL2, (g) LAL3 and (h) LOT2)

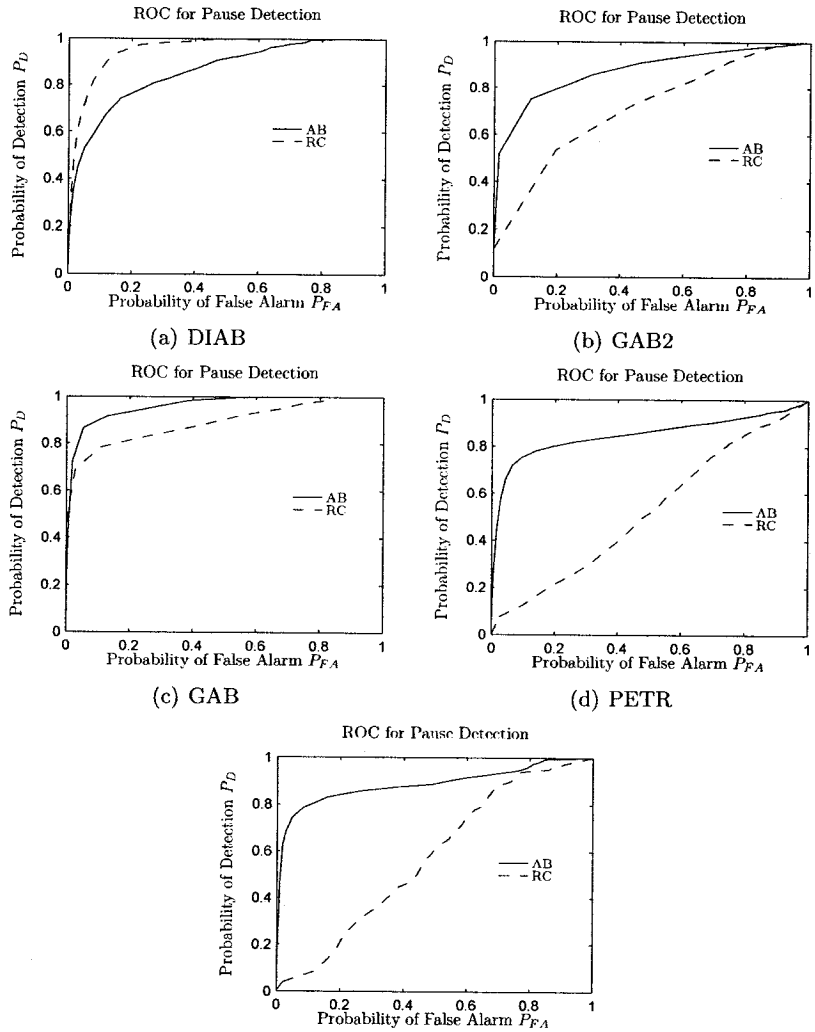

Figure D-2c: ROC curves for Pause detection in the abdominal and ribcage RIP signals of six infant patient data records (Montreal Childrens Hospital Study ID: (a) DIAB, (b) GAB2, (c) GAB, (d) PETR, and (e) MART3)

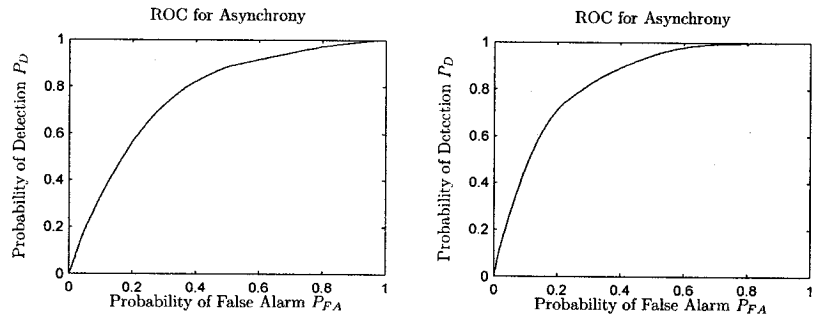

(a) ARC

(b) BJUT

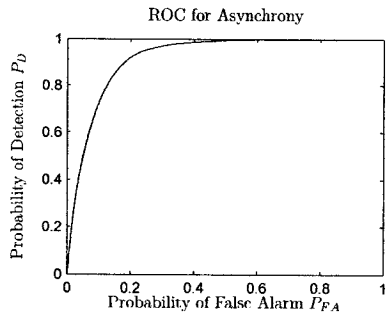

(c) LACR3

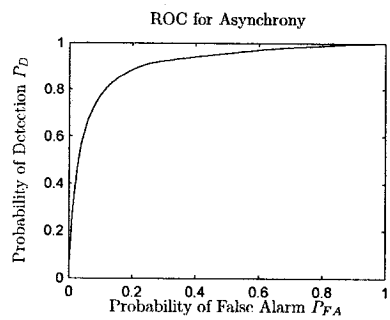

(d) LAMP

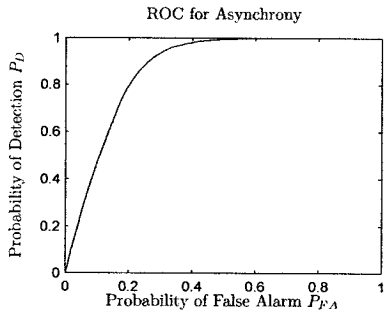

(e) MOSS

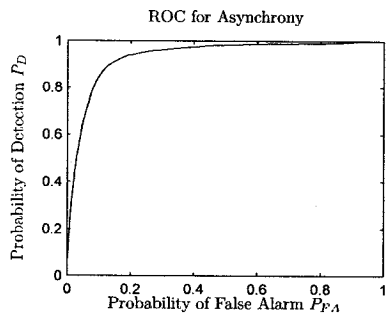

(f) MUR

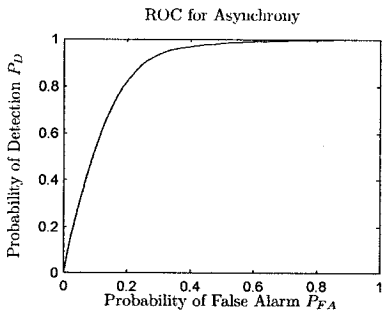

(g) SHIF

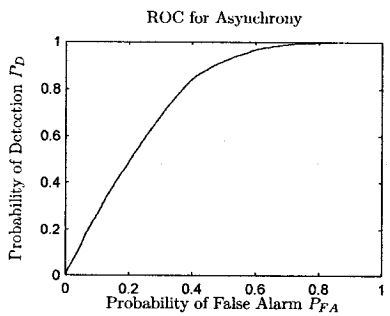

(h) MAX

Figure D-3a: ROC curves for Asynchrony detection in eight infant patient data records (Montreal Childrens Hospital Study ID: (a) ARC, (b) BJUT, (c) LACR3, (d) LAMP, (e) MOSS, (f) MUR, (g) SHIF and (h) MAX)

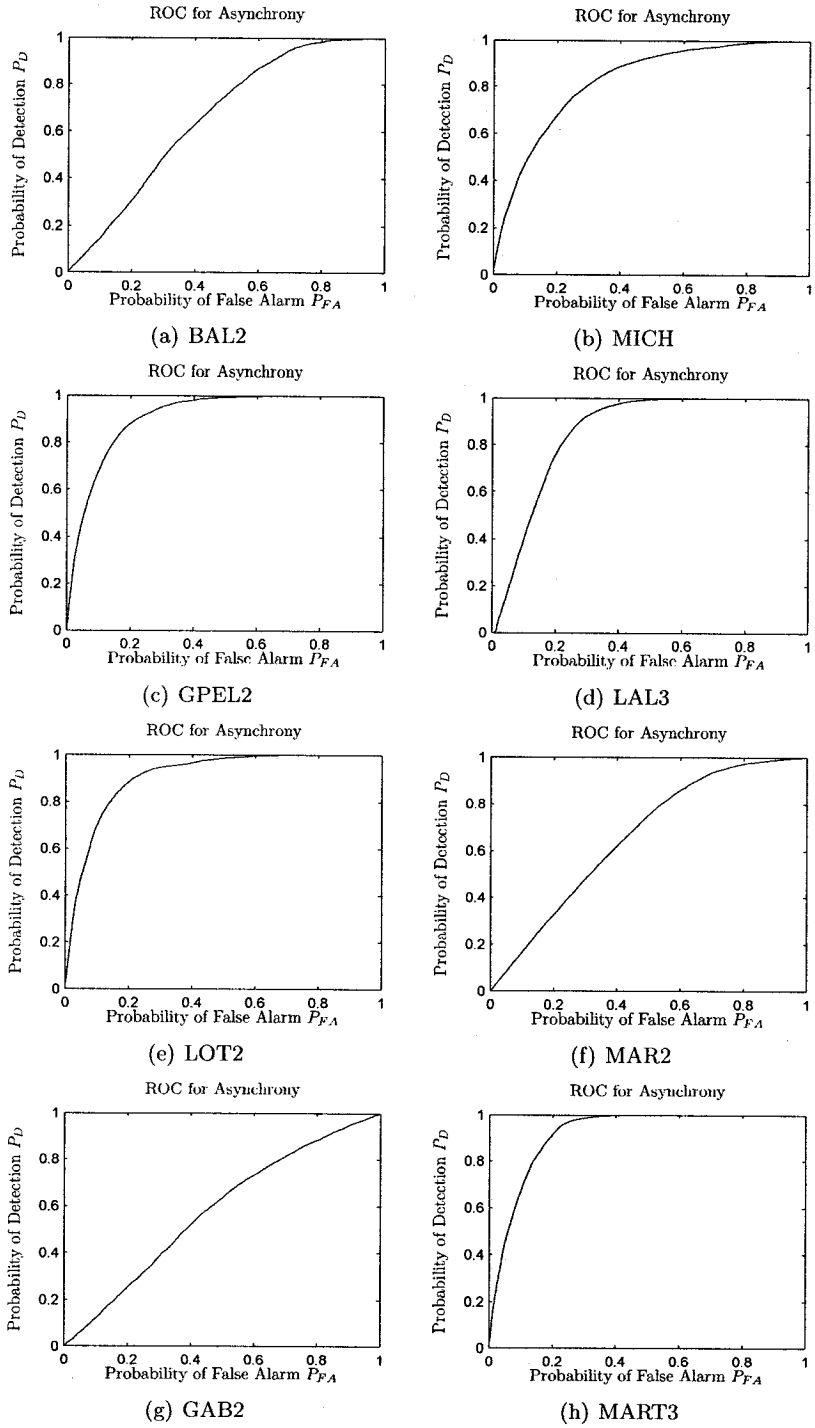

Figure D-3b: ROC curves for Asynchrony detection in eight infant patient data records (Montreal Childrens Hospital Study ID: (a) BAL2, (b) MICH, (c) GPEL2, (d) LAL3, (e) LOT2, (f) MAR2, (g) GAB2 and (h) MART3)

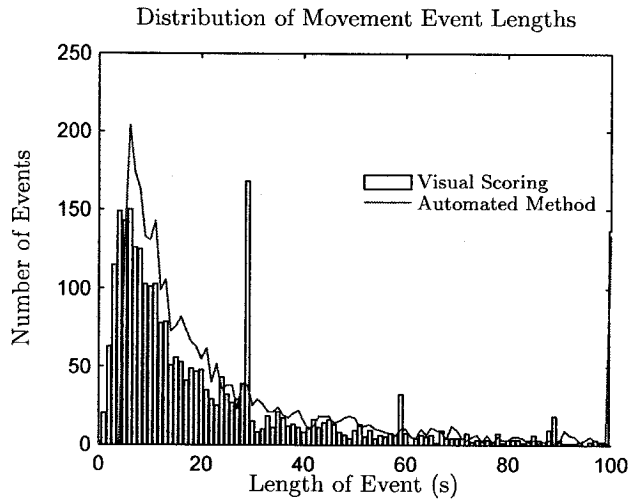

Figure D-4: Distribution of movement events versus their respective lengths, as scored by the clinician, and as determined by the automated method for all 21 infant files.

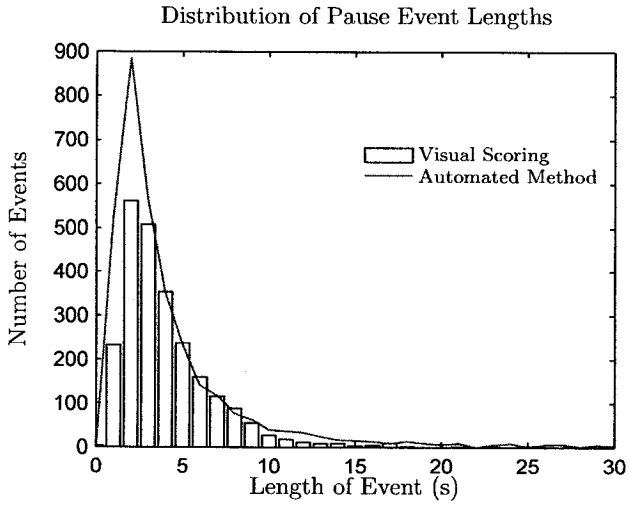

Figure D-5: Distribution of pause events versus their respective lengths, as scored by the clinician, and as determined by the automated method for all 21 infant files.

REFERENCES

[1] T. Machen and J. Forte, "Respiratory physiology (mcb-136 course slides)," accessed: April 12 2006. [Online]. Available: http://mcb.berkeley.edu/courses/mcb136/topic/Respiration/SlideSet1/Resp1.pdf

[2] T. M. St.John, "Chapter 1: The lungs and respiratory system," accessed: April 12 2006. [Online]. Available: http://www.lungcancerguidebook.org/LCGuidebook%20Aug05/Ch1_0605.pdf

[3] G. Ritchison, "Human physiology: Respiration (bio-310 course notes)," accessed: April 12 2006. [Online]. Available: http://www.nda.ox.ac.uk/wfsa/html/u12/u1211_01.htm

[4] "Chater 12: The respiratory system (slides)," accessed: April 12 2006. [Online]. Available: http://www.recreation.ucsb.edu/ess/ess40/downloads/chap12.pdf

[5] A. L. Motto, H. L. Galiana, K. A. Brown, and R. E. Kearney, "Automated estimation of the phase between thoracic and abdominal respiratory movement signals," *IEEE Transactions on Biomedical Engineering*, vol. 52, no. 4, pp. 614–621, Apr. 2005.

[6] ——, "Detection of movement artifacts in respiratory inductance plethysmography: Performance analysis of a Neyman-Pearson energy-based detector," in *Proceedings of the 26th Annual International Conference of the IEEE Engineering in Medicine and Biology Society*, vol. 1, San Francisco, CA, Sep. 1–5 2004, pp. 49–52.

[7] K. A. Brown, R. Platt, , and J. H. T. Bates, "Automated analysis of paradoxical ribcage motion during sleep in infants," *Pediatric Pulmonology*, vol. 33, pp. 38–46, 2002.

[8] The MathWorks. (2004, Jun.) Signal processing toolbox user's guide. [Online]. Available: http://www.mathworks.com/access/helpdesk/help/toolbox/signal/

[9] A. A. Aoude, A. L. Motto, H. L. Galiana, K. A. Brown, and R. E. Kearney, "Power-based segmentation of respiratory signals using forward-backward bank filtering," in *Proceedings of the 28th Annual International Conference of the IEEE Engineering in Medicine and Biology Society*, New York, NY, Aug. 30–Sept 3 2006.

[10] "Standards and indications for cardiopulmonary sleep studies in children," *Am J Respir Crit Care Med*, vol. 153, pp. 866–878, 1996.

[11] "Clinical practice guideline: diagnosis and management of childhood obstructive sleep apnea syndrome," *Pediatrics*, vol. 109, pp. 704–712, 2002.

[12] J. D. Kennedy and K. A. Waters, "Investigation and treatment of upper-airway obstruction: childhood sleep disorder i," *Medical Journal of Australia*, vol. 182, no. 8, pp. 419–423, 2005.

[13] C. M. Nixon and R. T. Brouillette, "Diagnostic techniques for obstructive sleep apnoea: Is polysomnography necessary?" *Pediatric Respiratory Reviews*, vol. 3, pp. 18–24, 2002.

[14] Khann, D. Blum, E. Rebuffat, M. Sottiaux, J. Levitt, A. Bochner, M. Alexander, J. Grosswasser, and M. F. Muller, "Polysomnographic studies of infants who subsequently died of sudden infant death syndrome," *Pediatrics*, vol. 2, pp. 721–727, 1988.

[15] "Infantile apnea and home monitoring," National Institute of Health, Tech. Rep., 1987.

[16] J. E. Yount, "Technical problem in recognizing and monitoring infant apnea," *Proceedings of the IEEE Engineering in Medicine and Biology Society 11th Annual Conference.*

[17] N. J. Ali, D. Pitson, and J. R. Stradling, "Snoring, sleep disturbance, and behavior in 4-5 year olds," *Arch Dis Child*, vol. 68, pp. 360–366, 1993.

[18] T. Gislason and B. Benediktsdottir, "Snoring, apneic episodes, and nocturnal hypoxemia among children 6 months to 6 years old. an epidemiologic study of lower limit of prevalence," *Chest*, vol. 107, pp. 963–966, 1995.

[19] C. L. Rosen, E. K. Larkin, L. Kirchner, J. L. Emancipator, S. F. Bivins, and S. A. Surovec, "Prevalence and risk factors for sleep disordered breathing in 8 to 11 year old children: association with race and prematurity," *J Pediatr*, vol. 142, pp. 383–389, 2003.

[20] S. Redline, P. V. Tishler, M. Schluchter, J. Aylor, K. Clark, and G. Graham, "Risk factors for sleep-disordered breathing in children. associations with obesity, race, and respiratory problems," *Am J Respir Crit Care Med*, vol. 159, pp. 1527–1532, 1999.

[21] F. Roberts, "Respiratory physiology," accessed: April 12 2006. [Online]. Available: http://www.nda.ox.ac.uk/wfsa/html/u12/u1211_01.htm

[22] J. F. Nunn, *Applied Respiratory Physiology*, 2nd ed. London-Boston: Butterworths, 1977.

[23] S. Sovik, "Quantifying infant respiratory variability: how to capture complexity," *Acta Paediatr*, vol. 89, pp. 1401–1407, 2000.

[24] D. P. White, "Central sleep apnea," *Med Clin N America*, vol. 69, pp. 1205–1219, 1985.

[25] S. S. Semienchuk, "A portable monitor for automated, on-line cardiorespiratory state classification," Master's thesis, McGill University, 2004.

[26] M. S. Schechter, "Technical report: diagnosis and management of childhood obstructive sleep apnea syndrome," for the Section on Pediatric Pulmonology, Subcommittee on Obstructive Sleep Apnea Syndrome, Tech. Rep., 2001.

[27] J. Chan, J. C. Edman, and P. J. Koltai, "Obstructive sleep apnea in children," *American Family Physician*, vol. 69, no. 5, pp. 1147–1154, 2004.

[28] D. Gozal and L. M. O'Brien, "Snoring and obstructive sleep apnoea in children: Why should we treat?" *Pediatric Respiratory Reviews*, vol. 5(suppl A), pp. S371–S376, 2004.

[29] M. G. Lind and B. P. Lundell, "Tonsillar hyperplasia in children. a cause of obstructive sleep apneas, co2 retention, and retarded growth," *Arch Otolaryngol*, vol. 108, pp. 650–654, 1982.

[30] J. L. Carroll, S. A. McColley, and C. L. Marcus, "Inability of clinical history to distinguish primary snoring from obstructive sleep apnea syndrome in children," *Chest*, vol. 108, pp. 610–618, 1995.

[31] Y. K. Wing, S. H. Hui, and W. M. Pak, "A controlled study of sleep related disordered breathing in obese children," *Arch Dis Child*, vol. 88, pp. 1043–1047, 2003.

[32] K. Chau, D. K. Ng, and C. K. Kwok, "Clinical risk factors for obstructive sleep apnoea in children," *Singapore Med J*, vol. 44, pp. 570–573, 2003.

[33] E. Hulcrantz, B. Lofstrand-Tidestrom, and J. Ahlquist-Rastad, "The epidemiology of sleep related breathing disorder in children," *Int J Pediatr Otorhinolaryngol*, vol. 6(suppl), pp. S63–S66, 1995.

[34] A. M. Ferreira, V. Clemente, D. Gozal, A. Gomes, C. Pissarra, H. Cesar, I. Coelho, C. F. Silva, and M. H. P. Azevedo, "Snoring in portuguese primary school children," *Pediatrics*, vol. 106, pp. e64–e69, 2000.

[35] A. M. Li, E. Wong, J. Kew, S. Hui, and T. F. Fok, "Use of tonsil size in the evaluation of obstructive sleep apnoea," *Arch Dis Child*, vol. 87, pp. 156–159, 2002.

[36] R. C. Wang, T. P. Elkins, and D. Keech, "Accuracy of clinical evaluation in pediatric obstructive sleep apnea," *Otolaryngol Head Neck Surg*, vol. 118, pp. 69–73, 1998.

[37] N. J. Ali, D. Pitson, and J. R. Stradling, "Sleep disordered breathing: effects of adenotonsillectomy on behaviour and psychological functioning," *Eur J Pediatr*, vol. 155, pp. 56–62, 1996.

[38] B. C. Freidman, A. Hendeles-Amitai, and E. Kozminsky, "Adenotonsillectomy improves neurocognitive function in children with obstructive sleep apnea syndrome," *Sleep*, vol. 26, pp. 999–1005, 2003.

[39] J. S. Suen, J. E. Arnold, and L. J. Brooks, "Adenotonsillectomy for treatment of obstructive sleep apnea in children," *Arch Otolaryngol Head Neck Surg*, vol. 121, pp. 525–530, 1995.

[40] P. Nieminen, U. Tolonen, and H. Lopponen, "Snoring and obstructive sleep apnea in children: a 6-month follow-up study," *Arch Otolaryngol Head Neck Surg*, vol. 126, pp. 481–486, 2000.

[41] J. L. Alen, M. R. Wolfson, K. McDowell, and T. H. Shaffer, "Thoracoabdominal asynchrony in infants with airflow obstruction," *Am Rev Respir Dis*, vol. 141, pp. 337–342, 1990.

[42] M. J. Corwin, G. Lister, J. M. Silvestri, M. Peucker, L. J. Brooks, Davidson, S. L. Ward, C. E. Hunt, M. R. Neuman, D. H. Crowell, T. Colton, and the CHIME study Group, "Agreement among raters in assessment of physiologic waveforms recorded by a cardiorespiratory monitor for home use," *Pediatr Res*, vol. 44, pp. 682–690, 1998.

[43] Y. Sivan, T. W. Deakers, and C. J. Newth, "Thoracoabdominal asynchrony in acute upper airway obstruction in small children," *Am Rev Respir Dis*, vol. 142, pp. 540–544, 1990.

[44] A. D. Groote, J. Groswasser, H. Bersini, P. Mathys, and A. Kahn, "Detection of obstructive apnea events in sleeping infants from thoracoabdominal movements," *J Sleep Res*, vol. 11, pp. 161–168, 2002.

[45] K. A. Brown, "Pattern of ventillation during halothane anaesthesia in infants less than two months of age," *Can J Anaesth*, vol. 43, pp. 121–128, 1996.

[46] D. M. Fisher, "When is the ex-premature infant no longer at risk of apnea?" *Anesthesiology*, vol. 82, pp. 807–808, 1995.

[47] A. J. Lipton and D. Gozal, "Treatment of obstructive sleep apnea in children: do we really know how," *Sleep Med Rev*, vol. 7, pp. 61–80, 2003.

[48] A. M. Li, D. F. Y. Chan, T. F. Fok, and Y. K. Wing, "Childhood obstructive sleep apnoea: an update," *Hong Kong Med J*, vol. 10, no. 6, pp. 406–413, 2004.

[49] H. D. Goldberg and M. I. G. (Inventors), "Deformable pick-up coil and cooperating magnet for measuring physical quantities, with means for rendering coil output independent of orientation," US Patent 3,731,184, Tech. Rep., Jan 1973.

[50] P. Martinot-Lagarde, R. Sartene, and M. Mathieu, "What does inductance plethysmograph realy measure?" *J Appl Physiol*, vol. 64, pp. 1749–1756, 1988.

[51] P. Y. Carry, P. Baconnier, A. Eberhard, P. Cotte, and Benchetrit, "Evaluation of repiratory inductive plethysmography: accuracy for analysis of respiratory waveforms," *Chest*, vol. 11, pp. 910–915, 1997.

[52] H. L. Watson, D. A. Poole, and M. A. Sackner, "Accuracy of repiratory inductive plethysmographic cross-sectional areas," *J Appl Physiol*, vol. 65, pp. 615–620, 1983.

[53] I. Kato, P. Franco, J. Groswasser, I. Kelmanson, H. Togari, and A. Kahn, "Frequency of obstructive and mixed sleep apneas in 1023 infants," *Sleep*, vol. 23, 2000.

[54] M. Folke, L. Cernerud, M. Ekstrom, and B. Hok, "Critical review of non-invasive respiratory monitoring in medical care," *Med Biol Eng Comput*, vol. 41, pp. 377–383, 2003.

[55] S. Gothberg, "Lung volume recruitment in lambs during high-frequency oscillatory ventilation using respiratory inductive plethysmography," *Pediatr Res*, vol. 49, pp. 38–44, 2001.

[56] K. Konno and J. Mead, "Measurement of the separate volume changes of ribcage and abdomen during breathing," *J Appl Physiol*, vol. 22, pp. 407–422, 1967.

[57] T. S. Chadha, H. Watson, and S. Birch, "Validation of respiratory inductance plethysmography using different calibration procedures," *Am Rev Respir Dis*, vol. 125, pp. 644–649, 1982.

[58] M. A. Sackner, H. Watson, and A. S. Belsito, "Calibration of respiratory inductance plethysmograph during natural breathing," *J Appl Physiol*, vol. 66, pp. 410–420, 1989.

[59] R. Sartene, J. Dartus, and J. L. Bernard, "Comparison of thoracoabdominal calibrition methods in normal human subjects," *J Appl Physiol*, vol. 75, pp. 2142–2150, 1993.

[60] K. A. Brown, C. Aun, E. Jackson, A. Mackersie, and J. Stocks, "Validation of respiratory inductive plethysmography using the quanlitative diagnostic calibration method in anaesthetized infants," *Eur Respir J*, vol. 12, pp. 935–943, 1998.

[61] S. Lord, "Interrater reliability of computer-assisted scoring of breathing during sleep," *Sleep*, vol. 12, pp. 550–558, 1989.

[62] D. E. Weese-Mayer, M. J. Corwin, M. R. Peucker, J. M. D. Fiore, D. R. Hufford, L. R. Tinsley, M. R. Neuman, R. J. Martin, L. J. Brooks, S. L. D. Ward, G. Lister, M. Willinger, and the CHIME study Group, "Comparison of apnea identified by respiratory inductance plethysmography with that detected by end-tidal co2 or thermistor," *Am J Crit Care Med*, vol. 162, pp. 471–480, 2000.

[63] R. T. Brouillette, S. K. Fernbach, and C. E. Hunt, "Obstructive sleep apnea in infants and children," *J Pediatr*, vol. 100, pp. 31–40, 1982.

[64] A. Kahn, J. Grosswasser, E. Rebuffat, M. Sottiaux, D. Blum, M. Foerster, P. Franco, A. Bochner, M. Alexander, A. Bachy, P. Richard, M. Verghote, D. LePolain, and J. L. Wayenberg, "Sleep and cardiorespiratory characteristics of infant victims of sudden death: a prospective case-control study," *Sleep*, vol. 15, pp. 287–292, 1992.

[65] T. Al-Ani, Y. Hamam, R. Fodil, F. Lofaso, and D. Isabey, "Sleep apnea syndrome identification using hidden markov models," *Simulation Modelling Practice and Theory 12*, pp. 117–128, 2004.

[66] P. M. Macey, J. S. J. Li, and R. P. K. Ford, "Expert system for the detection of apnoea," *Engineering applications of artificial intelligence*, vol. 11, pp. 425–438, 1998.

[67] F. Steimann and K. P. Adlassnig, "Clincal monitoring with fuzzy automata," University of Vienna," Technical report MES-2, 1993.

[68] J. E. Larsson, "A toolbox for fast model-based diagnosis," Knowledge Systems Laboratory, Stanford University, Technical Report KSL-95-06, 1995.

[69] B. S. Todd and D. C. Andrews, "The identification of peaks in physiological signals," *Comp Biomed Res*, vol. 32, pp. 322–335, 1999.

[70] B. H. Taha, "Automated detection and classification of sleep disordered breathing from conventional polysomnography data," *Sleep*, vol. 20, pp. 991–1001, 1997.

[71] Y. Sivan, W. S. Davidson, T. Deakers, T. G. Keens, and J. L. Newth, "Ribcage to abdominal asynchrony in children undergoing polygraphic sleep studies," *Pediatric Pulmonol*, vol. 11, pp. 141–146, 1991.

[72] S. S. Semienchuk, A. L. Motto, H. L. Galiana, K. A. Brown, and R. E. Kearney, "A portable, PC-based monitor for automated, on-line cardiorespiratory state classification," in *Proc. 27th Annual International Conference of the IEEE Engineering in Medicine and Biology Society*, Shangai, China, Sep. 1–4, 2005.

[73] C. L. Rosen, "Obstructive sleep apnea syndrome in children: controversies in diagnosis and treatment," *Pediatr Clin N Am*, vol. 51, pp. 153–167, 2004.

[74] J. P. L. Tang, C. L. Rosen, E. K. Larkin, J. M. Difiore, J. L. Arnold, S. A. Surovec, J. M. Youngblut, and S. Redline, "Identification of sleep-disordered breathing in children: variation with event detection," *Sleep*, vol. 1, pp. 72–79, 2002.

[75] D. E. Weese-Mayer, M. J. Corwin, M. R. Peucker, J. M. Di Fiore, D. R. Hufford, L. R. Tinsley, M. R. Neuman, R. J. Martin, L. J. Brooks, S. L. D. Ward, G. Lister, M. Willinger, and The CHIME Study Group, "Comparison of apnea identified by respiratory inductance plethysmography with that detected by end-tidal CO2 or thermistor," *American Journal of Respiratory and Critical Care Medicine*, vol. 162, pp. 471–480, 2000.

[76] T. Penzel, K. Kesper, V. Gross, H. F. Becker, and C. Vogelmeier, "Problems in automatic sleep scoring applied to sleep apnea," in *Proc. 25th Annual International Conference of the IEEE Engineering in Medicine and Biology Society*, Cancun, Mexico, Sep. 17–21, 2003.

[77] L. R. Rabiner and B. Gold, *Theory and Application of Digital Signal Processing.* Englewood Cliffs, NJ: Prentice-Hall, 1975.

[78] S. M. Kay, *Fundamentals of Statistical Signal Processing—Volume II: Detection Theory.* Englewood Cliffs, NJ: Prentice-Hall, 1998.

[79] W. L. Andrew, "Maximum likelihood estimation of generalized ito processes with discretely sampled data," *Econometric Theory*, vol. 4, pp. 231–247, 1988.

[80] "Cardiorespiratory sleep studies in children, establishment of normative data and polysomnographic predictors of morbidity," *Am J Respir Crit Care Med*, vol. 160, pp. 1381–1387, 1999.

[81] S. V. Jacob, A. Morielli, M. A. Mograss, F. M. Ducharme, M. D. Schloss, and R. T. Brouillette, "Home testing for pediatric obstructive sleep apnea syndrome secondary to adenotonsillar hyperthrophy," *Pediatric pulmonology*, vol. 20, pp. 241–252, 1995.

[82] C. J. Cote, A. Zaslavsky, J. J. Downes, D. Kurth, L. G. Welborn, L. O. Warner, and S. V. Malviya, "Postoperative apnea in former preterm infants after inguinal herniorrhaphy," *Anesthesiology*, vol. 82, pp. 809–822, 1995.

[83] J. R. norton, D. S. Ward, S. Karan, W. A. Voter, L. Palmer, A. Varlese, O. Rackovsky, and P. Bailey, "Difference between midazolam and propofol sedation on upper airway collapsibility using dynamic negative airway pressure," *Anesthesiology*, vol. 104, pp. 1155–1164, 2006.

[84] M. Suzuki, H. Saigusa, S. Chiba, T. Yagi, K. Shibasaki, M. H. band M. Suzuki, K. Moriyama, and K. Kodera, "Discrepansy in polysomnography scoring for a patient with obstructive sleep apnea hypopnea syndrome," *Tohoku J Exp Med*, vol. 206, pp. 353–360, 2005.

[85] H. Danker-Hopfe, D. Kunz, G. Gruber, G. Klosch, J. L. Lorenzo, S. L. Himanen, B. Kemp, T. Penzel, J. Roschke, H. Dorn, A. Schlogl, E. Trenker, and G. Dorffner, "Interrater reliability between scorers from eight european sleep laboratories in subjects with different sleep disorders," *J Sleep Res*, vol. 13(1), pp. 63–69, 2004.

[86] K. Kim, M. Kurachi, M. Horita, K. Matsuura, and Y. Kamikawa, "Agreement of visual scoring of sleep stages among many laboratories in japan: effect of a supplementary definition of slow wave on scoring of slow wave sleep," *Jpn J Psychiatry Neurol*, vol. 47(1), pp. 91–97, 1993.

[87] N. Schaltenbrand, R. Lengelle, M. Toussaint, R. Luthringer, G. Carelli, A. Jacqmin, E. Lainey, A. Muzet, and J. P. Macher, "Sleep stage scoring using the neural network model: comparison between visual and automatic analysis in normal subjects and patients," *Sleep*, vol. 19(1), pp. 26–35, 1996.

[88] R. G. Norman, I. Pal, C. Stewart, J. A. Walsleben, and D. M. Rapoport, "Interobserver agreement among sleep scorers from different centers in a large dataset," *Sleep*, vol. 23(7), pp. 901–908, 2000.

[89] W. W. Flemons, M. R. Littner, J. A. Rowley, P. Gay, W. M. Anderson, D. W. Hudgel, R. D. McEvoy, and D. I. Loube, "Home diagnosis of sleep apnea: a systematic review of the literature," *Chest*, vol. 124, pp. 1543–1579, 2003.

[90] R. Ferber, R. Millman, M. Coppola, J. Fleetham, C. F. Murray, C. Ibera, V. McCall, G. Nino-Murcia, M. Sanders, K. Strohl, B. Votteri, and A. Williams, "Portable recording in the assessment of obstructive sleep apnea," *Sleep*, vol. 17(4), pp. 378–392, 1994.